Pia Gruber, BSc

Comparison and optimization of matrix materials for CO_2 sensors

Masterarbeit

zur Erlangung des akademischen Grades

Master of Science MSc

in Chemie

eingereicht an der

Technischen Universität Graz

Betreuer

Univ.-Prof. Dipl.-Chem. Dr.rer.nat Ingo Klimant

Institut für Analytische Chemie und Lebensmittelchemie

der Technischen Universität Graz

Graz, im März 2014

STATUTORY DECLARATION

I declare that I have authored this thesis independently, that I have not used other than the declared sources / resources and that I have explicitly marked all material which has been quoted either literally or by content from the used sources.

…… ……..
date (signature)

„It would have been nice to have unicorns."

- Tom Stoppard, *Rosencrantz and Guildenstern Are Dead*

Zusammenfassung

Optische Sensoren haben sich in den letzten Jahren als wichtige Instrumente für die Messung von CO_2 hervorgetan. Sie sind vor allem für marine Anwendungen von großer Bedeutung, da die Übersäuerung der Meere ein Problem darstellt, dessen Überwachung nicht trivial ist.
Als Standardmatrix für CO_2 Sensoren hat sich Ethylcellulose etabliert. Dieses Polymer zeigt jedoch eine starke Temperaturabhängigkeit, was einen Vergleich von Messungen bei verschiedenen Temperaturen schwierig macht.
Im Zuge dieser Masterarbeit wurden verschiedene Matrizes und Basen auf ihren Einfluss auf den Temperaturkoeffizienten der CO_2 Sensoren getestet.
Weiter wurden in einem Langzeitexperiment die Einflüsse besagter Matrizes und Basen auf die Haltbarkeit der Sensoren bestimmt. Im Zuge der Langzeitstabilitätstests wurden auch die Einflüsse einiger zusätzlicher Schutzschichten auf die Haltbarkeit der Sensoren getestet.

Abstract

Over the course of the last decade, optical sensors have been established as a promising analytical tool for the measurement of CO_2 in aqueous environment. They are especially useful for marine research, as the acidification of the oceans is a serious matter that isn't easily monitored. For this purpose ethyl cellulose has been the most commonly used matrix for optical CO_2 sensors, however, this polymer shows a strong temperature dependence. Measurements taken at different temperatures are therefore not easily comparable.

In this thesis the different polymers for matrices and different bases were compared to find a sensor that shows a better temperature coefficient than the standard ethyl cellulose matrix.

Furthermore, the long term stability of the ethyl cellulose and the new sensor materials was tested in combinations with the different bases. Additionally, various polymers were tested in an attempt to find a protective layer that would increase the long-term stability of the sensors.

Acknowledgement

I would like to cease this opportunity to thank Professor Ingo Klimant, who made this thesis possible by welcoming me into his research group. His constant supply of input and ideas kept the lab work interesting and helped me achieve my research goals and I really appreciate his friendly nature and good spirits.

I'd like to thank Susanne Schutting and Sergey Borisov for guiding and supervising me throughout my thesis work. Without their knowledge, expertise and support this thesis would not have been possible.

Of course, I also want to thank the entire ACFC research group. I really enjoyed working with and around them as the working climate was very friendly. I will never be able to have cake again without thinking of you guys.

Last, but definitely not least, I'd like to thank my family for supporting me both morally and financially through all these years. I would never have made it so far without them.

Thank you!

Content

1 Introduction

The detection of carbon dioxide is one of the most important lines of inquiry on the planet as the carbon dioxide level is a crucial parameter in medicine[1], biotechnology[2-3], food packaging[4], and oceanography[5-6].

The long-term measurement of CO_2 is one of the most important ambitions in oceanography as the acidification of the oceans has a great impact many aspects of the earth's ecosystem[7-8]. Therefore a stable, durable CO_2 sensor that isn't too sensitive to varying temperatures would be a valuable analytical tool for long-term monitoring. Optical sensors present a promising option for this application, however, direct optical sensing via infrared spectroscopy (IR) is not a suitable method for detecting dissolved CO_2[9]. Measuring CO_2 indirectly via the pH change it causes in a Mill's type sensor[10] is proving to be a good option.

In the field of optical CO_2 sensors based on the principle of pH change, ethylcellulose in combination with tetraoctyl ammonium hydroxide (TOAOH) has been established as a standard matrix. It is cheap, easy to work with, has a relatively low water uptake and shows a good permeability for CO_2[11].
However, this matrix shows a high temperature coefficient, which renders the comparability of measurements taken at fairly different temperatures (i.e. 5 and 37°C) less than ideal.
The aim of this work was to find a different matrix for CO_2 sensors that shows a lower temperature dependence as well as better long term stability.
Furthermore, the long-term stability of the potential sensor materials was to be tested and improved via the use of various types and combinations of protective layers.

2 Theoretical Background

2.1 Ocean acidification

It is estimated that the oceans have taken up a third of the anthropogenic carbon dioxide produced in the last two centuries[12]. Carbon dioxides residence time in the atmosphere is approximately 5 years[13], whereas its impact on aquatic systems is not as easily quantifiable.
The following equations depict the dissolving process of CO_2 in water[5], where the notations (g), (l) and (aq) refer to the chemical state of the components:

$$CO_2\,(g) \rightleftharpoons CO_2\,(aq)$$
$$CO_2\,(aq) + H_2O\,(l) \rightleftharpoons H_2CO_3\,(aq)$$
$$H_2CO_3\,(aq) \rightleftharpoons H^+\,(aq) + HCO^-\,(aq)$$
$$HCO^-\,(aq) \rightleftharpoons H^+ + CO_3^{2-}\,(aq)$$

The increased carbon dioxide concentration in the water has a variety of different effects on various parts of the eco system. The increase in CO_2 leads to an increasing acidification of the oceans, which in turn affects the marine flora and fauna. During the last two centuries the concentration of dissolved CO_2 has risen from 280 ppmv to 384 ppmv[12], causing the average pH of the oceanic surface to drop from 8.21 to 8.10[14]. According to the Intergovernmental Panel on Climate Change (IPCC) this value is going to drop by another 0.3-0.4 units by the end of the century[6].
Due to the following equilibria

$$CaCO_3 \rightleftharpoons CO_3^{2-} + Ca^{2+}$$
$$CO_2 + CO_3^{2-} + H_2O \rightleftharpoons 2\,HCO_3^-$$

the available amount of $CaCO_3$ in the oceans is decreased with an increase in dissolved carbon dioxide[6,12].

Consequently, organisms that depend on calcification, the secretion of $CaCO_3$-based skeletal structures for protection, such as corals, have shown a lower amount of calcification in correlation with an increased CO_2 concentration. Conversely, some species of planktonic calcifiers have shown an increase in their ability to achieve calcification[15].

The increase in acidity also affects the speciation of elements outside the carbonate cycle. Trace elements that are hydrolysed in water, form hydroxyl- or oxy-anion complexes, are strongly influenced by a pH shift in the water. The predicted decrease in pH that continued ocean acidification will lead to within the century will strongly impact the bioavailability of metal organic complexes for phytoplankton[16].

It is hard to predict how well marine organisms will adapt to this change in their environment. There has not yet been enough research conducted to present a clear picture of the impact that ocean acidification will have on the individual plant and animal species or the food chain as a whole[7].

One of the major problems hereby is the lack of long term monitoring systems for oceanic research. The continuous surveillance of the pCO_2 levels of water is especially challenging due to the fact that there is currently no system that allows for long-term measuring without drift or interferences.

2.2. Sensors

2.2.1 Definition of a sensor

The Oxford English Dictionary defines a sensor as:

"*A device which detects or measures a physical property and records, indicates, or otherwise responds to it*"[17]

In textbooks chemical sensors are described as miniaturized devices that convert a chemical state into an electronic signal as seen in Figure 2.2.1.1. [18, 19]

Figure 2.2.1.1: Principle of a chemical sensor

The term 'chemical state' can refer to different concentrations, partial pressures, or activity of the analyte. Different sensor types are distinguished by the analytes and the analytes' chemical state that they are used for.

Generally the analyte comes into contact with a receptor, which selectively reacts with the analyte. The basic setup can be optimized to achieve maximal accuracy, for example a protective layer or filter may be added to act as a barrier and reduce interferences with other species[18]. In a biosensor, the receptor is of natural origins, i.e. enzymes or antibodies, while the receptor of a chemosensor is synthetically manufactured[20].

In order for the sensor to be usable for long-term measurements the receptor must not be permanently –irreversibly- compromised by the interaction with the analyte. The reaction needs to be fully reversible. A variety of other requirements should be met by an ideal sensor, such as a small size, fast response, low manufacturing costs, lack of drift, and user-friendliness.

Other parameters simply need to be determined and listed. Examples for this are the following parameters summarized from source [18]:

2.2.1.1 Selectivity and cross-sensitivity

The selectivity of a sensor describes the accuracy at which a sensor interacts with the desired analyte as opposed to a different species, whereas the cross-sensitivity compliments this term by describing the interferences with other components of a system or parameters.

2.2.1.2 Sensitivity

This parameter describes the extent at which a sensor's output increases or decreases as the analyte concentration changes. A high sensitivity is especially desirable for the trace analysis of analytes, as a minor change still produces a quantifiable signal. For optical sensors the choice of dye usually has the greatest impact on the sensors' sensitivity.

2.2.1.3 Dynamic range

The operating range of a sensor is defined by the lowest detectable analyte concentration which is distinguishable over the noise of the sensor signal (see 'Limit of detection') and the highest detectable concentration at which no saturation effects occur.

2.2.1.4 Linearity

The linearity of a sensor describes the deviation of an experimentally determined calibration curve from an ideal linear calibration curve. Often, linearity applies over just a small portion of the dynamic range.

2.2.1.5 Limit of detection

Different texts define the limit of detection by different criteria such as three times the noise level + standard deviation of the signal, however, the most generally applicable -if vague- definition is that the limit of detection is the lowest distinguishable concentration at which the sensor generates a reliable signal.

2.2.1.6 Long-term stability

The long-term stability of a sensor describes both how long and how accurately a sensor remains functional when exposed to its target environment. It is especially relevant when the sensor is intended for unsupervised long-term monitoring of environmental parameters, such as CO_2 in water.

2.2.1.7 Lifetime/Shelf-life

The shelf-life of a sensor is especially relevant for sensors that are produced in bulk and/or intended to be user-friendly and calibration-free, such as glucose sensor strips for diabetics, as these sensors still need to function accurately after months of storage. Ideally, sensors for purposes like these should be free of instabilities and drifts.

2.2.1.8 Response time

The response time of a sensor is an important parameter to determine a sensor's suitability for certain applications. In this thesis, where new polymers were tested for their capability to function equally well under different conditions, this parameter played a particularly crucial role. Two of the most commonly listed characteristics concerning response time are t_{63} and t_{90} (Figure 2.2.1.8.1) of the sensor as they grant the user insight on the speed at which measurements can be taken with the sensor.

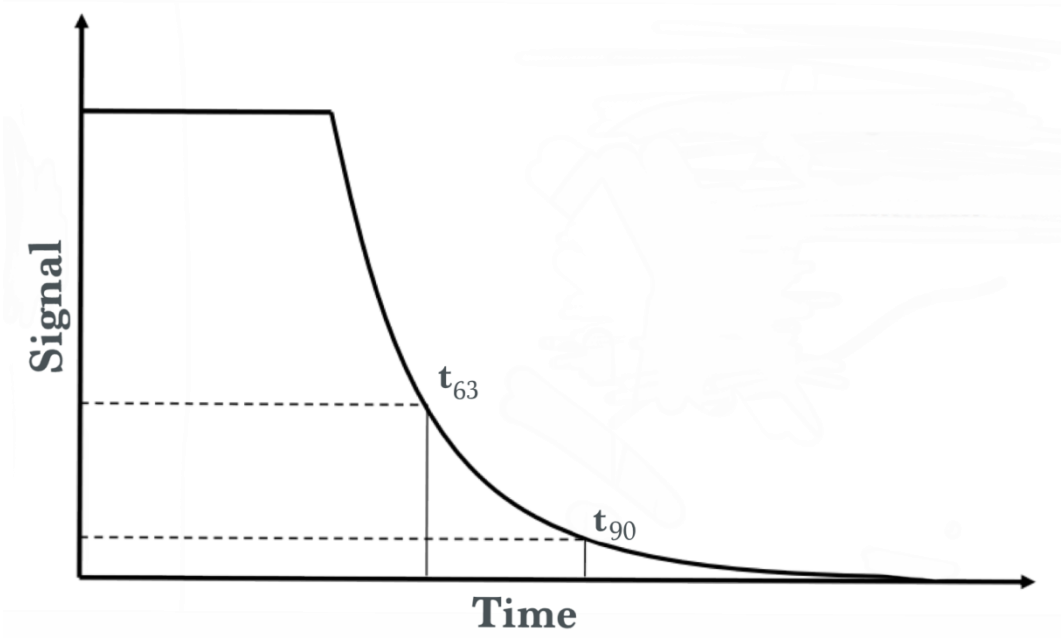

Figure 2.2.1.8.1: Important parameters regarding response time

This figure provides a depiction of the response time parameters t_{63} and t_{90}. t_{99} is another parameter of a sensor that is sometimes listed with the others as it provides a relevant insight into how long a full sensor response takes. As can be seen in the figure the last 10% of turnover can make up the bulk of the total response time.

2.3. Optical sensors

As optical sensors can be used to continuously measure the concentration of an analyte, they are suitable for a wide range of applications[21].
An aspect through which optical sensors can be classified is whether their signal output is the result of a direct or indirect reaction to the analyte. The terminology used for this factor is 'intrinsic' or 'extrinsic' sensor. Where an intrinsic sensor responds directly to an analytes optical properties, an extrinsic sensor produces a signal of its own in response to the interaction with the analyte[22].
The basic principles behind optical sensors will be summarized in this chapter.

2.3.1 Basic principles

The following chapters are based on [23]; other sources will be explicitly noted.

2.3.1.1. Absorption

As mentioned, the process of absorption consists of promoting an electron of a molecule from its ground state to an excited state, an unoccupied orbital, via the absorption of a photon. The molecule is then referred to as excited. The excited state is of the same energy the photon previously possessed.
The two most important orbitals in connection with both absorption and fluorescence are the Lowest Unoccupied Molecular Orbital (LUMO) and the Highest Occupied Molecular Orbital (HOMO), which describe the ground state of a molecule. Electrons can be excited from sigma, pi or non-bonding orbitals to excited sigma or pi orbitals in the following energy order:

$$n \rightarrow \pi^* < \pi \rightarrow \pi^* < n \rightarrow \sigma^* < \sigma \rightarrow \pi^* < \sigma \rightarrow \sigma^*$$

When an electron is excited from the ground state into a higher energetic state its spin remains the same. The light absorbance of an analyte is defined by the Beer-Lambert Law:

$$A = \log\left(\frac{I_0}{I}\right) = \varepsilon * c * d$$

A…. Absorption

I_0…. Light intensity before sample

I …. Light intensity after sample

ε …. Molar absorption coefficient

c …. Concentration of the analyte

d … Optical path length of sample

The instrument used to measure the absorption of CO_2 sensors investigated in this thesis was a UV/VIS spectrophotometer. The single ray photometer's xenon lamp produced the light beam that was guided through a monochromator to select the wavelength at which the sample should be scanned. The sample in each case was a piece of sensor foil fixed in a custom-made stainless steel cell with two glass windows that allowed the excitation light beam to pass through the cell and sample to the detector. A picture of the photometer's scheme can be found in Figure 2.3.1.2.1.

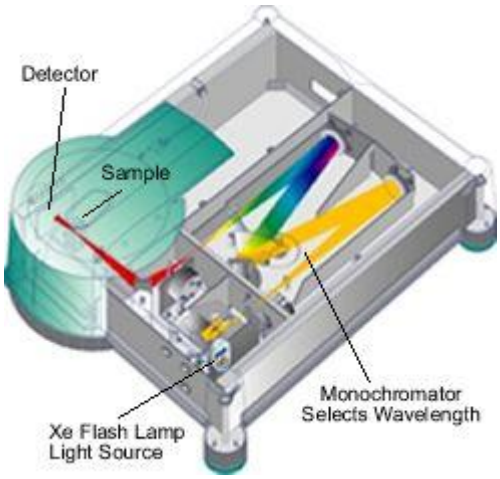

Figure 2.3.1.2.1: Spectrophotometer used for measurements[24]

2.3.1.2 Luminescence

The term luminescence encompasses the emission of ultraviolet, visible or infrared light from an electronically excited state of a species. The mode through which excitation is achieved in photoluminescence is the absorption of a photon. The excited state differs from the ground state exactly by the energy of the photon.

An excited molecule can return to its ground state by emitting the acquired energy through various ways, such as photochemical transformation, energy transfer, proton or electron transfer, conformational change or internal conversion. Fluorescence emission is possible if the relaxation is spin-allowed; if the relaxation is spin-forbidden it can be achieved through intersystem crossing which can either result in phosphorescence or delayed fluorescence.

These transitions from an excited state are summed up by the Jablonski diagram in figure 2.3.1.2.1. This will be briefly discussed since fluorescence based CO_2 sensors are important analytical tools with a wide range of applications.

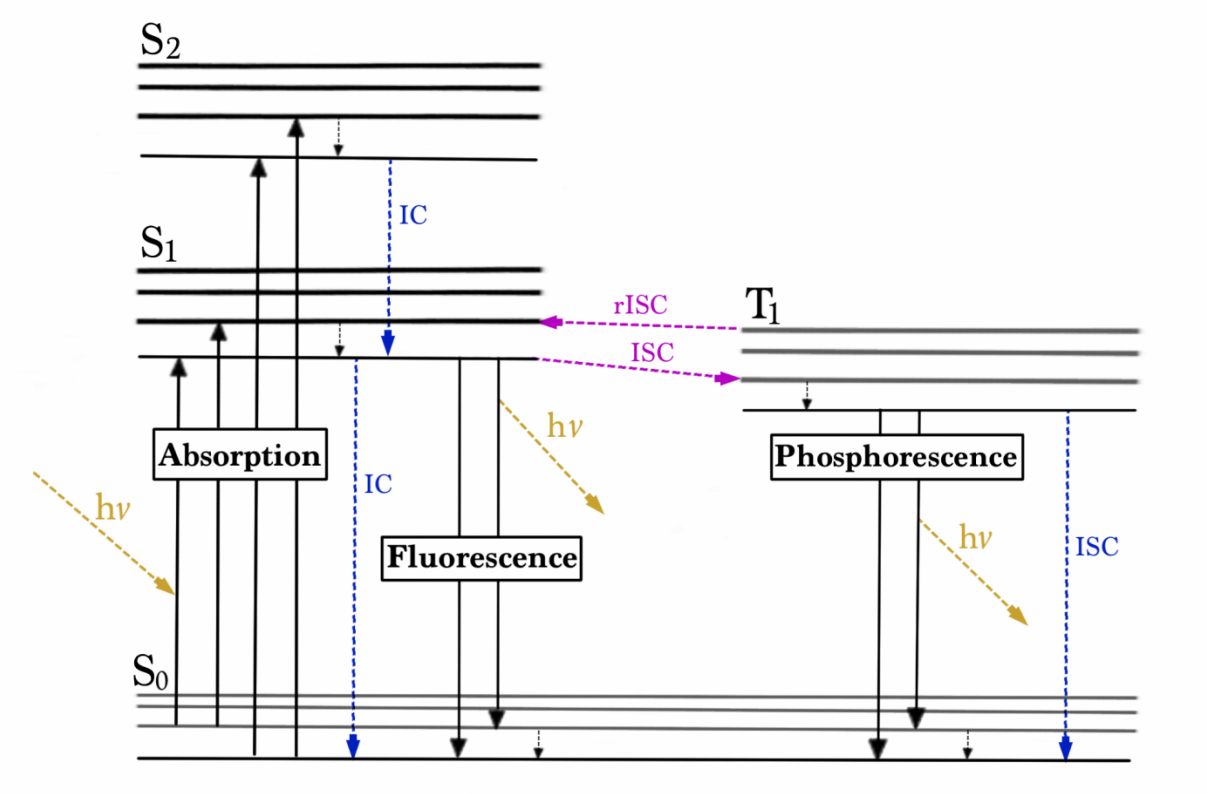

Figure 2.3.1.2.1: Jablonski diagram visualizes transitions between excited states and ground states. S_0 is the ground state, while S_1 and S_2 represent excited singlet states and T_1 describes an excited triplet state

This diagram is a useful tool for describing radiative and non-radiative deactivation processes.

2.3.1.3. Non-radiative Deactivation

As mentioned above two non-radiative transitions are represented in the Jablonski diagram and relevant to the radiative relaxations described above.

2.3.1.3.1 Internal conversion

This term describes a transition between two states of equal spin multiplicity, which is then followed by the vibrational relaxation to the ground state S_0. The larger the energy difference between the two states is, the less efficient the internal conversion becomes. While the conversion between two excited states like S_2 and S_1 can be as swift as 10^{-13}-10^{-11} seconds, the transition between S_1 and S_0 is less effective and other processes can take precedence, such as fluorescence or intersystem crossing followed by phosphorescence.

2.3.1.3.2 Intersystem crossing

Conversely to internal conversion, intersystem crossing deals with the transition between two states of different spin multiplicity i.e. the transition from a single state to a triplet state. This includes a forbidden spin change. However, the spin-orbit coupling may be large enough to enable the transition. This transition is fast enough to compete with other relaxation processes like fluorescence.

2.3.1.4. Radiative Deactivation

2.3.1.4.1 Fluorescence

Molecular fluorescence and phosphorescence are popular analytical phenomena due to their high sensitivity and selectivity. They occur due to the emission of a photon from an excited state. Fluorescence, phosphorescence and delayed fluorescence can be summed up with the term photoluminescence. The term fluorescence describes the resulting emission of a photon that occurs due to a relaxation from the S_1 to the S_0 state, this process is independent from the initial excitation wavelength. According to the Stokes rule the fluorescence emission always

occurs at a higher wavelength than the absorption due to energy loss through vibrational relaxation. Realistically the absorption and fluorescence emission spectra tend to overlap. The difference in the wavelength between the first absorption band and the fluorescence maximum is referred to as Stokes shift. Fluorescence is a fast process, the usual lifetime is about 10^{-10} to 10^{-8} seconds

2.3.1.4.2 Phosphorescence

Phosphorescence occurs due to the relaxation from the T_1 state to the S_0 state and can only occur after intersystem crossing from the S_1 state to the T_1 state. The process is comparatively slow at 10^{-6} to ~1 second. Since the T_1 state is energetically lower than the S_1 state phosphorescence occurs at a higher wavelength than fluorescence.

2.3.1.4.3 Delayed fluorescence

The process of delayed fluorescence is a phenomenon that occurs as a result of emission from the excited singlet state S_1 to the ground state S_0. The delay consists of intersystem crossing from S_1 to T_1 followed by reversed intersystem crossing from the T_1 state back to S_1. The reverse intersystem crossing is an occurrence that necessitates high temperatures as the energy difference between the T_1 state and the S_1 state needs to be breached and this can only happen when the electrons are energetic enough.

2.4. Common methods to measure CO_2

The most common method of measuring carbon dioxide outside of optical CO_2 sensors is via non-dispersive infrared gas analysis.

For this method a sample of gas, in which the analyte is present, is transferred into a gas sampling chamber while another reference chamber remains free of the analyte. Infrared light of a wavelength suitable to the analyte gas is guided through those chambers into a separate detector cell that is filled with the analyte gas. This detector cell is parted in the middle by a diaphragm. The analyte molecules in the gas sampling chamber absorb some of the light that is guided through the cell, causing fewer molecules on the gas sampling chamber's side of the detector cell to become excited, than on the reference side, where all the light passes through the cell unabsorbed. The gas on the reference side of the detector cell expands further than the gas on the other side, pressing against the diaphragm which produces an electrical signal. From this signal the analyte concentration in the sample can be calculated.[25]

Alternatively, a simpler setup can be used that consists of an IR light source, a sample chamber, and an optical detector on the other side, which detects the light that isn't absorbed by the CO_2, and the concentration is determined via that signal. This method is primarily used for gas samples, and shows a great cross-sensitivity with H_2O. It is also unsuitable for measurement of liquid samples and is therefore not usable to monitor ocean acidification.

Further methods exist that can be used to determine the CO_2 concentration in beverages via temperature and pressure variations on the sample[26], but these methods are also not suited for the subject matter of this thesis.

GC-MS and field transistors also present measurement possibilities for carbon dioxide; however, both require expensive equipment and active supervision.

Optical CO_2 sensors are a more promising tool for long-term unsupervised measurements of CO_2 in seawater, but as the next parts of the thesis will show they have their own upsides, downsides and challenges.

One of the most established methods of measuring CO_2 optically is with the Severinghaus electrode, which was first described by John W. Severinghaus in 1958[27] and later developed into an opt(r)ode, as well as the solid state sensors (also called Mills' type sensors) which are based on the same principle as the Severinghaus electrode. These sensors and other relevant optical CO_2 measurement concepts will be described in the following chapter.

2.5. Optical CO_2 chemosensors

Since the basic principles have now been reviewed, the following chapter will describe the current methods for measuring CO_2 via optical chemical sensors and the materials used for them. As mentioned earlier, the carbon dioxide measurement via infrared spectroscopy is prone to interferences from both humidity and CO[28].
There are various principles with which carbon dioxide can be measured optically. This part of the chapter will be used to show the diversity of approaches possible and describe some of the most important options available.

2.5.1. Viscosity sensors[29]

CO_2 sensors that measure the carbon dioxide concentration via the change in viscosity of the polymer that makes up the sensor are a creative concept in the field of optical CO_2 detection. These sensors consist of an aqueous solution of hydrophobic associative polymers that are arranged in the shape of a four armed star. The centre consists of a water-soluble polyacrylamide core and poly(N,N-diethylaminoethyl methacrylate) side chains.
These polymers are highly viscous in the absence of CO_2. An increase in CO_2 leads to a change in charge on the ends of the polymer chain, making the chains repel each other. This leads to a decrease in viscosity as the chains expand instead of sticking together.
A visual representation of this process is shown in figure 2.5.1. The viscosity of the polymer is then measured using a rotational viscometer.
The downside of these sensors is that the presence of electrolytes also affects the viscosity of the polymers. Electrolytes screen the charges on the ends of the polymers that previously kept said ends apart when CO_2 is present and strengthen the hydrophobic association of the chains when CO_2 is absent. The presence of electrolytes in combination with CO_2 causes the polymer chains to assume random positions. This affects the viscosity of the polymers, making their use in marine research problematic.

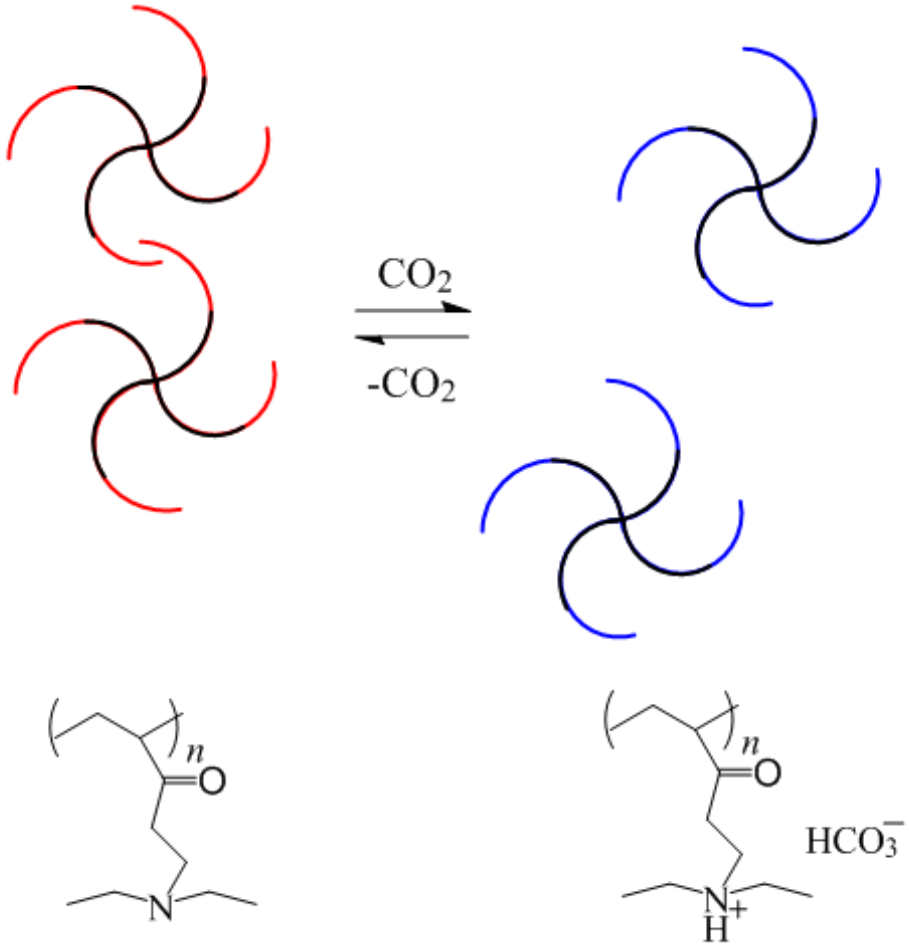

Figure 2.5.1.1: Effect of CO_2 in hydrophobic associative polymer matrix. The polyacrylamide core is presented in black while the poly(N,N-diethylaminoethyl methacrylate) side chains are shown in red when CO_2 is absent and blue in the presence of CO_2

2.5.2. Polarity sensors[30]

A polarity sensor allows the measurement of the polarity in a matrix around the indicator dye. For this purpose an amidine additive is used in the matrix to bind CO_2 according to the following reaction:

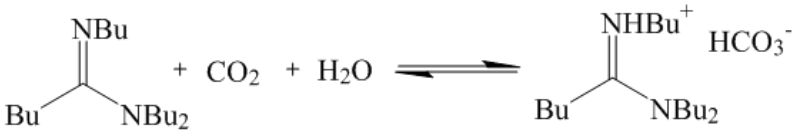

Figure 2.5.2.2: Binding of CO_2 via hydrophobic amidine

The polymer used for these sensors is typically ethylcellulose, while Nile Red is used as an indicator. The change in the dye can be detected both solvatochromatically and via fluorescence spectroscopy. The structure of Nile Red can be found in the figure 2.5.2.1.

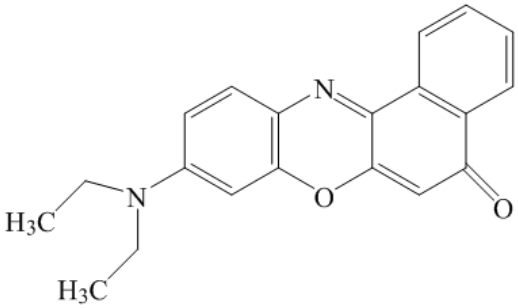

Figure 2.5.2.2: Structure of Nile Red indicator dye

This sensor shows no cross-sensitivity corresponding to the pH of its environment.
A downside to these sensor types is their response time which ranges from 3-25 minutes, and the setup of the measurement unit, which requires a digital camera and is therefore not so easily automatable.
A different take on this principle is the use of aggregation-induced emission, in which a dye that shows no emission when in solution, like the molecule shown in figure 2.5.2.3, becomes capable of emission when in an amine solution that is bubbled through with CO_2. As the aggregates form the dye becomes capable of emitting light[31].

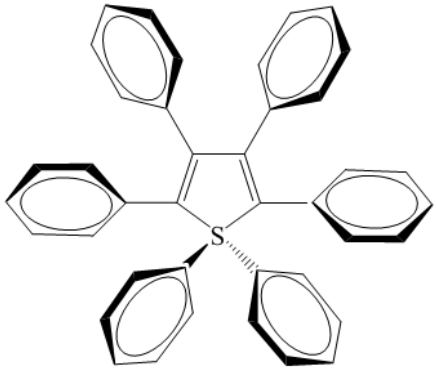

Figure 2.5.2.3: Structure 1,1,2,3,4,5-Hexaphenylsilole (HPS); Adapted from [31].

2.5.3 pH-sensitive CO_2 sensors

The sensors that are subject to this thesis are optical CO_2 sensors that function on the principle of a pH change within the sensor when the sensor is in contact with CO_2. This change in pH is detected via the use of an indicator dye. These sensors can be divided into two types: Severinghaus type sensors[27], and dry concept/solid state sensors as described by Mills[10].
A Severinghaus type CO_2 sensor consists of a thin film of bicarbonate solution, a Teflon membrane that is impermeable to ions but allows CO_2 to pass to the bicarbonate solution.

$$CO_2 + H_2O \rightarrow HCO_3^- + H^+$$

This design was also adapted from a carbon dioxide electrode[27]. This type of sensor is useful at higher CO_2 concentrations as it shows linearity between 1 and 11 kPa, but not at the levels that are relevant for marine research, as the levels in sea water are in the range of 0.04 kPa[9].
It is also a very slow sensor, as it takes a long time for the equilibrium in the buffer to be established. The influence of osmotic pressure also poses a problem for oceanic applications, as it causes the sensor to drift.
Meanwhile, a Mills type sensor is made up of polymer matrix, a base, which forms an ion pair with the pH-sensitive indicator dye. The sensor needs to be kept humid in order to function properly, because the water molecules allow the pH sensitive dye to function as an indirect indicator for the CO2 concentration through a bicarbonate equilibrium[10].

$$Q^+Ind^- * H_2O \leftrightarrow Q^+HCO_3^- * H_2O * HInd$$

Q^+ …. Quartanary ammonium ion
Ind … Indicator dye

In contrast to the Severinghaus electrode this sensor is very fast and sensitive. Osmotic pressure has little effect on the system.
Depending on the materials and dye used in these sensors they show a much higher sensitivity as will be discussed in the next section. The dry concept of these sensors, sometimes referred to as Mill's type sensors, were the subject of this thesis.

The indicator dye forms an ion pair with the base in the sensor. Various concepts for possible bases are known, the most common one being the use of a quaternary ammonium ion as a base.[32,33].
The most popular being tetraoctylammonium hydroxide or shorter chained equivalents. Hexadecyltrimethylammonium hydroxide has also been used for this purpose[34, 35].
Alternatives to these ions will be briefly explained in the following paragraphs:

- A possible modification for sensing CO_2 is the use of ionic liquids encapsulated in a silicone polymer matrix. The detection of carbon dioxide happens via absorption or emission based pH-sensitive dyes like thymol blue or HPTS. The use of a second reference indicator dye with fluorescent properties is possible in these sensors. Furthermore, inorganic salts can be used for the formation of ion pairs with the indicator molecules instead of the standard quaternary ammonium ions mentioned earlier[36].

- In solid state CO_2 sensors with lipophilic bases the customary quaternary ammonium ion has been replaced by a neutral phosphazene base. The base in combination with residual water inside the sensor acts as a buffer, which is also the cause of the sensor's downside: It shows a distinct cross-sensitivity towards the humidity contained by analyte gases. Humidity decreases the sensor's sensitivity towards carbon dioxide. However, the functionality of standard sensors containing quaternary ammonium ions as a base also suffers under decreased humidity, as the sensor requires water to protonate the indicator dye[37].

- Cs^+ ions can also be used to replace the base in CO_2 sensors. As all the other previously mentioned sensors do, this sensor too consists of a polymer matrix, such as ethylcellulose, and a pH-sensitive indicator dye on either absorption or emission basis. The function of the base is carried out by a metal cation, a metal ionophore complex, or a metal ligand complex. The purpose of this alteration is to improve the sensors lifetime, which decreases rapidly in standard sensors containing quaternary ammonium ions as base when stored under ambient air[38].

As mentioned previously, the choice of dye has a great effect on the sensitivity of a sensor. Mills *et al.* conducted a study on the influence of a dye's acid dissociation constant on the sensor's sensitivity. The study proved the theory that, the higher the pK_a value of a dye, the higher the sensitivity of the sensor. This is due to the fact that the protonation of the dye in correlation to the CO_2 concentration is more notable[39].

A number of different polymers and dyes have been used for CO_2 sensors. The following sections will sum up the most common dyes and polymers used for carbon dioxide sensing. For this purpose the dyes have been divided into absorption based and emission based indicators.

2.5.3.1 Absorption-based CO_2 sensor dyes

The following table lists some of the most common components for absorption based optical carbon dioxide sensors. m-cresol purple was used for the sensors discussed in this thesis and will be shown in the materials and methods section.

Table 2.5.3.1.1: Common dyes used in absorption based carbon dioxide sensors

Dye	Abbreviation	Source
m-cresol purple	MCP	[10]
Phenol red	PR	[21]
Cresol red	CR	[39]
Thymol blue	TB	[39]

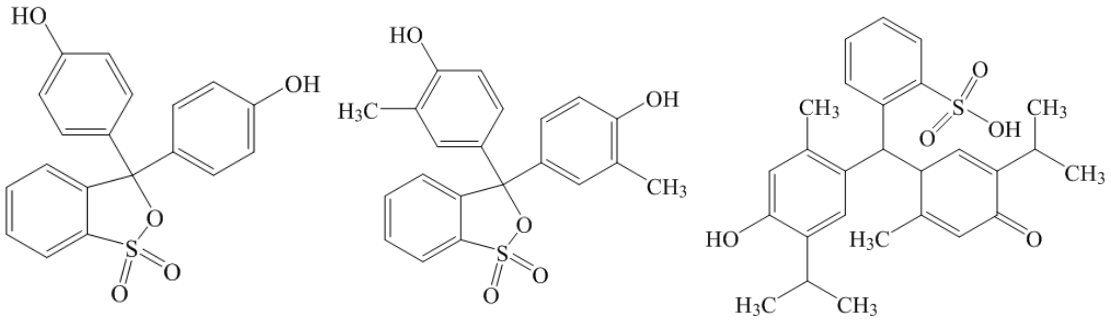

Figure 2.5.3.2.1: Common indicator dyes for absorption based carbon dioxide sensors

2.5.3.2. Emission-based CO_2 sensors

The following table shows some of the most common dyes used for fluorescence based carbon dioxide sensors.

Table 2.6.1: Common dyes used in fluorescence based carbon dioxide sensors

Dye	Abbreviation	Source
Diketopyrrolopyrrols	-	[9]
8-Hydroxy-1,3-pyrene-tris-sulphoic acid	HPTS	[9, 21, 40]
Nile Red	NR	[30]
Seminaphtho-rhodafluor derivates	SNARF	[41]

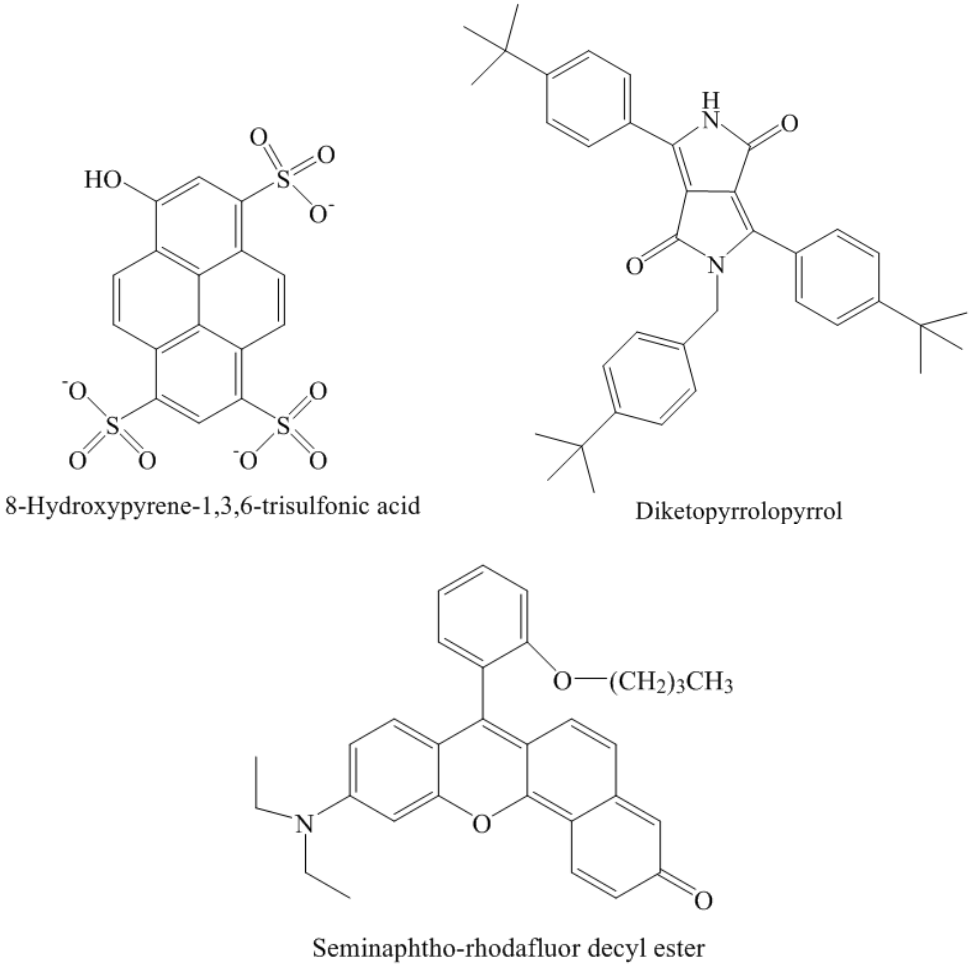

Figure 2.5.3.2.1: Common indicator dyes for emission based carbon dioxide sensors, the diketopyrrolopyrrol and SNARF derivate depicted are examples for their groups of dyes, which can be varied via the use of different organic substituents

Combinations of two fluorescent dyes can result in a single-layer dual sensor or two layer system[42]. The variation of dyes influences the sensitivity of the sensor. In a single-dye system the dye is first reacted with a quaternary ammonium cation in order to form an ion pair before it is dispersed in the sensor's polymer matrix[32,33].

The following table lists polymers that have been used in combination with optical carbon dioxide sensors.

Table 2.5.2: Common polymers used in carbon dioxide sensors

Polymer	Abbreviation	Source
Polystyrene	PS	[21, 22]
Polyvinylchloride	PVC	[21, 22]
Polymethyl methacrylate	PMMA	[21, 22]
Ethylcellulose	EC	[21, 22]
Hydrogels	D4, D7 etc.	[21, 30]

Not all of the above mentioned polymers and dyes are suitable for the application of monitoring ocean acidification. It is of paramount importance that the polymers don't expand too much in an aquatic setting, which i.e. eliminates certain hydrogels from being used for this purpose. For oceanic measurements, ethylcellulose has been the state of the art matrix in the past decade; however, due to its large temperature coefficient ethylcellulose has proven to be less than ideal for measurements in aquatic settings. Measurements at locations that greatly differ in temperature pose a problem, as the matrix effects that occur in correspondence to the ambient temperature have to be mathematically compensated for in order to allow comparison between measurements.

This is why the results presented in this thesis are relevant to the current research done towards optical sensing methods for carbon dioxide.

3 Materials and methods

3.1. Materials

3.1.1. Dye

m-Cresol purple was used as a dye in all the sensors mentioned in this thesis.

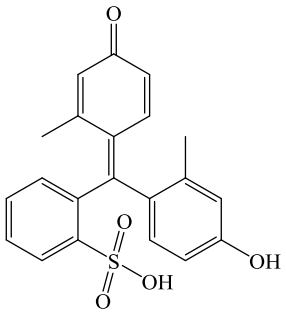

Fig. 3.1.1: Structure of m-Cresol purple

3.1.2. Polymers

The polymers used were selected for their availability and different properties regarding water retention, polarity, and permeability towards gases.

3.1.2.1. Ethylcellulose

Ethylcellulose with an ethoxyl content of 49% was used at a concentration of 5% in a mixture of 38% ethanol and 57% toluene. The ethoxyl content of the polymer can be used to regulate the sensitivity of a sensor in combination with some dyes[41].

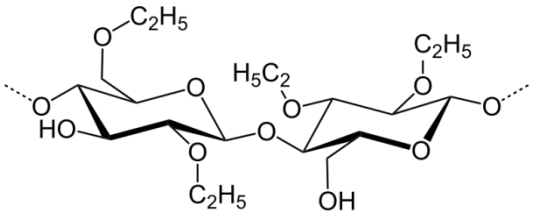

Figure 3.1.2.1: Structure of ethylcellulose

3.1.2.2 HydroMed D4 and HydroMed D7

Both HydroMed D4 and Hydromed D7 from AdvanSource were used at a concentration of 10% in tetrahydrofuran. They are ether-based hydrophilic polyurethanes with specially tailored water absorption capacities, 50% for D4 and 30% for D7[43]. D7 had to be washed before it could be used in a sensor as it contained acidic contaminants.

3.1.2.3 HydroThane

Hydrothane is a hydrophilic polyurethane elastomer; in the tests described in this thesis the variation that can contain up to 5% of water was used. The polymer from CT BIOMATERIALS was used at a concentration of 5% in 9.5% Ethanol and 85.5% tetrahydrofuran. This mixture requires a day of stirring to completely solubilize the hydrothane.

3.1.3. Bases

3.1.3.1. Tetraoctyl ammonium hydroxide (TOAOH)

Tetraoctyl ammonium hydroxide, referred to as TOAOH from this point is the standard base used in optical CO_2 sensors based on the principle of pH change. It was used in the sensors at a concentration of 0.04 mmol per 100 mg polymer.

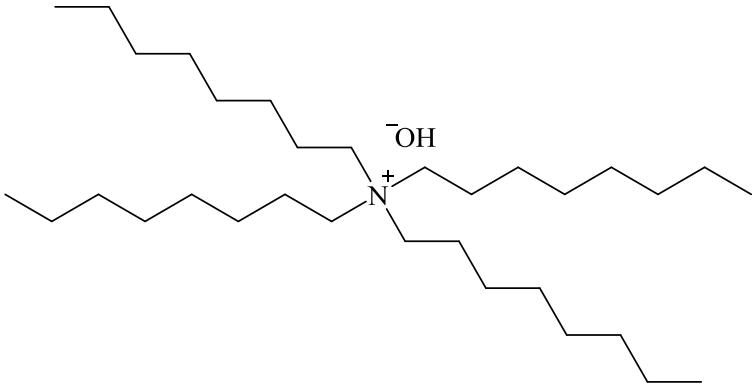

Fig. 3.1.3.1: Structure of tetraoctyl ammonium hydroxide

3.1.3.2. Tetrabutyl ammonium hydroxide (TBAOH)

Tetrabutyl ammonium hydroxide, referred to as TBAOH from this point is a smaller alternative to TOAOH. It was used in a concentration of 0.04 mmol per 100 mg polymer for the matrix optimization process and 0.15 mmol per 100 mg polymer for the long term stability test.

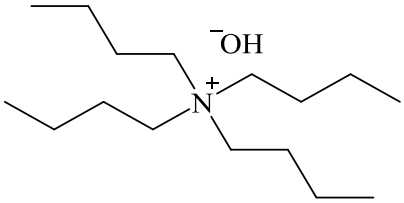

Fig. 3.1.3.2: Structure of tetrabutyl ammonium hydroxide

3.1.3.3. Hexadecyltrimethyl ammonium hydroxide (CTAOH)

Hexydecyltrimethyl ammonium hydroxide, or rather cetyltrimethyl ammonium hydroxide as it is commonly referred to in literature [34, 35], will be referred to as CTAOH from this point.

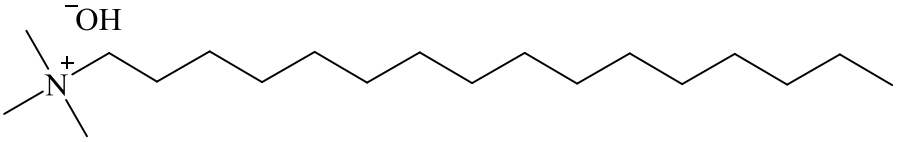

Fig 3.1.3.3: Structure of cetyltrimethyl ammonium hydroxide

All sensors were produced via knife-coating and the aid of a 3 Mil knife. Spacers were used when necessary.

3.1.4. Protective layers

3.1.4.1. Silicone rubber

The silicone rubber layer as it will be referred to throughout the thesis is a four component system in which a polymerisation is triggered via catalyst. The composition of the silicone matrix is as follows:

- 1000 mg Polydimethylsiloxane
- 2000 mg n-hexane
- 40 µL (25-35% Methylhydrosiloxane)-dimethylsiloxane copolymer
- 2.5 µL 1,3,5,7-Tetravinyl-1,3,5,7-tetramethylcyclotetrasiloxane
- 5 µL Platinum-divinyltetramethyldisiloxane complex

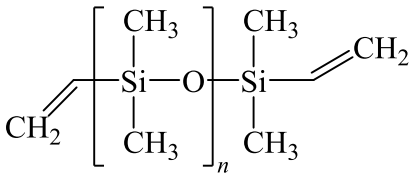

Figure 3.1.4.1.1: Structure of polymer polydimethylsiloxane

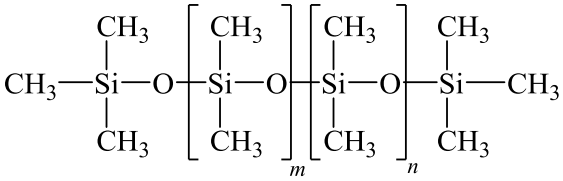

Figure 3.1.4.1.2: Structure of (25-35% Methylhydrosiloxane)-dimethylsiloxane copolymer

3.1.4.2. Hyflon® AD 60

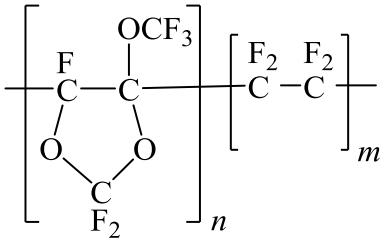

Figure 3.1.4.2: Structure of Hyflon® AD 60

Hyflon was suggested as a possible protective layer as its permeability to gases is more limited than that of silicone rubber. Due to its polyfluorinated chains it is meant to filter polar substances before they reach the sensor layer. A 6% solution in perfluorodecaline was used to coat the sensor films.

3.1.4.3. Polyhydroxyethylmethacrylate (PolyHEMA)

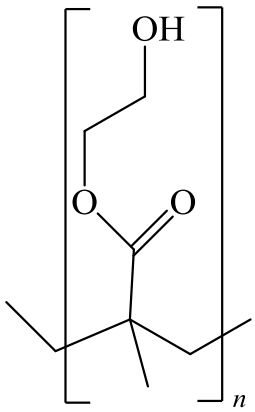

Figure 3.1.4.3: Structure of Polyhydroxyethylmethacrylate

PolyHEMA was tested as 5% solution in 9.5% distilled water and 85.5% ethanol.

3.1.4.4. Polyvinylalcohol

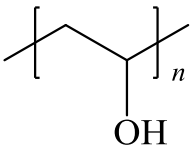

Figure 3.1.4.4: Structure of polyvinylalcohol

Polyvinylalcohol was suggested as a protective layer to be washed off before using the sensors due to its impermeability to gas.

3.2. Methods

3.2.1. Absorption

Absorption measurements were performed in the 300 to 800 nm range using a 'Varian Cary 50 Conc' UV/VIS spectrophotometer by Varian, Palo Alto, United States (www.varianinc.com). The measurements were taken at 'Fast' scan rate using baseline correction. A piece of Mylar® foil was used as a blank. The CO_2 measurements were done in a custom-made stainless steel flow-through cell.

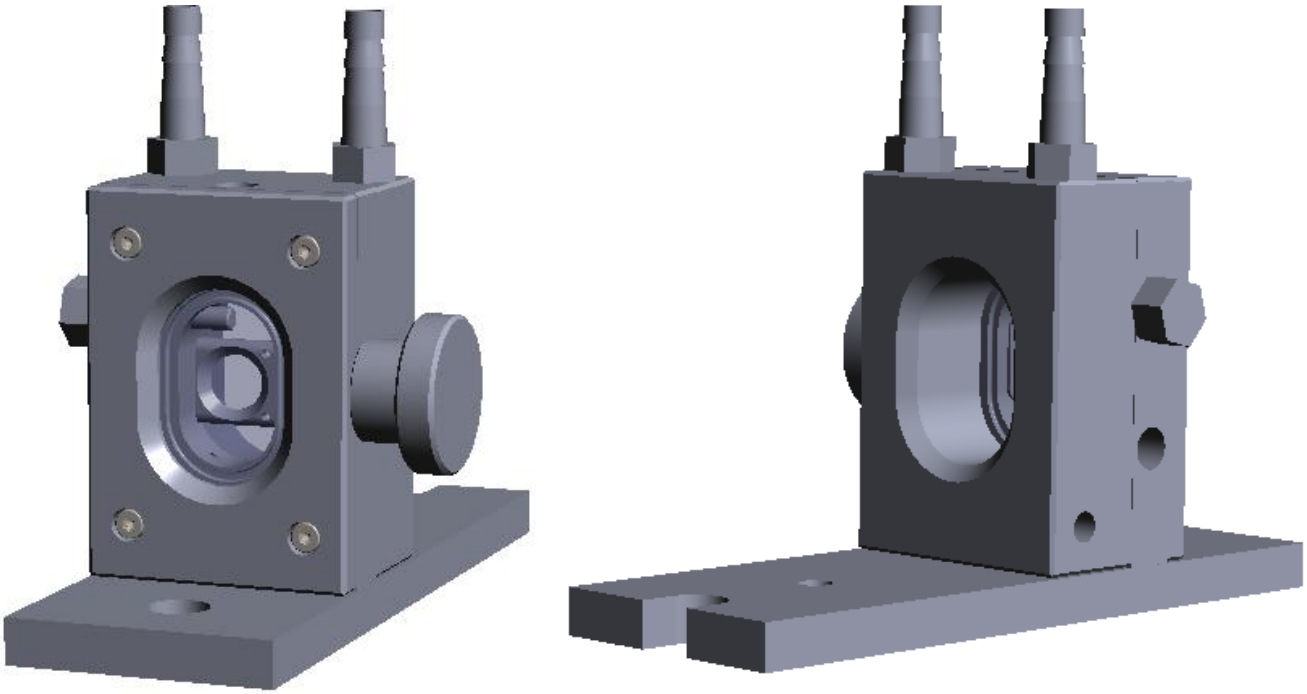

Figure 3.2.1: Stainless-steel measurement cell

4 Experimental Part

4.1. Matrix optimization

The main objective of this thesis was to optimize the matrix of CO_2 sensors to minimize the temperature dependence of CO_2 measurements for marine research. For this purpose four polymers in combination with three bases were tested for their suitability.

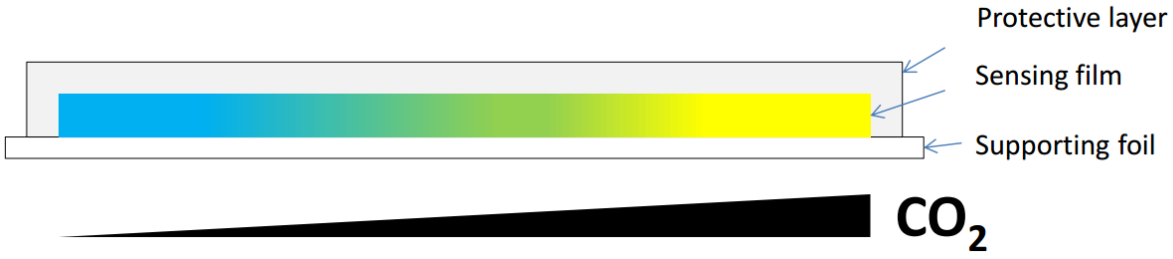

Figure 4.1.1: Composition of an optical CO_2 sensor with m-cresol purple as indicator dye

For this purpose sensor layers were knife coated on Mylar® foil with a 3 Mil knife. The measurement set up consisted of an MKS MassFlow® control gas mixing device with which concentrations of 0%, 0.5%, 1%, 2.5% and 5% CO_2 were achieved using nitrogen (5.0) and 5.01 % CO_2 in nitrogen from Linde. A CO_2 concentration of 10% was achieved with medical grade (100%) carbon dioxide and nitrogen. The sensor responses were measured at 0, 1, 2.5, 5, 10 and 100% CO_2 from 300 to 800 nm at a FAST scan speed. To compare the sensor responses at different temperatures the sensors were tested at 5°C, 25°C and 37°C. The measurement cell, the humidifier as well as the gas mixture was heated using a Julabo thermostat.

As the sensors need to be moistened to ensure a proper response the gas was channelled through a glass humidifier which was filled with silica. To ensure constant humidity the silica was moistened with a saturated potassium chloride solution which sets the humidity of the gas at a constant 85%. The humid gas is channelled through a gas spiral which is immersed in the thermostat to adjust the gas to the temperature in the custom-made stainless steel

measurement cell. The cell's temperature is monitored via a temperature sensitive FireStingO_2 compatible Submersible Temperature Sensor TSUB21 PT100[44] and kept within 0.3 °C of the desired measurement temperature.

The combinations of polymers and bases noted in Table 4.1.1 were measured at all temperatures to determine which combination was the most promising in regards of low temperature dependency.

Tab. 4.1.1: Combinations of polymers and bases that were investigated for their temperature dependence

	TOAOH	TBAOH	CTAOH
Ethylcellulose	✓	✓	✓
Hydromed D4	✓	✓	-
Hydromed D7	✓	✓	-
Hydrothane 5%	✓	✓	-

For this purpose all bases were added at the same concentration while ethylcellulose and hydrothane made up 5% of their respective cocktail and the Hydromed polymers were used at 10%.

4.2. Long term stability

4.2.1. Influence of different polymers and bases

To test the influence of different polymer and base combinations on the long-term stability of CO_2 sensors the following combinations of polymers and bases were knife coated on Mylar® foils in 3.75 µm (Ethylcellulose and HydroThane) and 7.5 µm (Hydromed D4 and D7) thick films.

Tab. 4.2.1.1: Sensor combinations without a protective silicone rubber layer used for long-term stability test

	TOAOH	TBAOH	CTAOH
Ethylcellulose	✓	✓	✓
Hydromed D4	✓	✓	-
Hydromed D7	✓	✓	-
Hydrothane 5%	✓	✓	-

Tab. 4.2.1.1: Sensor combinations with a protective silicone rubber layer used for long-term stability test

	TOAOH	TBAOH	CTAOH
Ethylcellulose	✓	✓	-
Hydromed D4	-	-	-
Hydromed D7	✓	✓	-
Hydrothane 5%	✓	-	✓

The sensors were measured via absorption spectrometry every 7 days via triple determination at 0.04% CO_2 (air) and 2.5% CO_2.

The triple determination was done via pre-cut stripes that were stored by being taped to a piece of Mylar® foil to prevent them from coming in contact with anything but the surrounding atmosphere. A large piece of the original planar sensor was stored alongside the stripes for each polymer/base combination to observe the aging of a larger sensor piece. A slide tray was used to keep the sensors from sticking to each other and their surroundings.

Figure 4.2.1: Example of a large piece of sensor foil and three pre-cut stripes as they were stored for every sensor type (Left) Example for a box containing a set of sensors (Right)

The 15 polymer/base combinations were stored in four different conditions to observe the aging behaviour under various conditions. One set of sensors stored in a desiccator at 5-8°C under CO_2 atmosphere, which is as close to an ideal storage condition as possible. The other sets of sensors were stored in shoeboxes with slits that allowed for air exchange, but shielded the sensors from direct contact with wind, light or dust. One of those boxes was placed

outside in a semi-protected location where the sensors wouldn't be disturbed or be directly subjected to the weather conditions. Another box was stored in a synthesis laboratory at 22°C to see if the chemically polluted air would affect the sensors quickly. The final box was stored in an office at an average of 25°C. The purpose of this test was to show the impact the incorrect storage of sensors has on the resulting measurements.

4.2.2. Influence of different protective layers

To test how different layers of protective polymers influence the stability of CO_2 sensors the following polymers were used as protective layers:

- Silicone rubber
- Hyflon® AD 60
- Silicone rubber + Hydromed D7
- Silicone rubber + Polyvinylalcohol
- Silicone rubber + Polyhydroxyethylmethacrylate (PolyHEMA)
- Hyflon® AD 60 + Ethylcellulose with 0.04 mmol/100 mg TBAOH + Hyflon® AD 60

These polymers were knife-coated over a CO_2 sensitive layer consisting of m-cresol purple, 5% ethylcellulose and tetraoctylammoniumhydroxide (0.04 mmol per 100 mg polymer) in a 3.75 µm film.
The sensors were measured via absorption spectrometry every 7 days via triple determination at 0.04% CO_2 (air) and 2.5% CO_2. The sensors were stored in an office at 25°C as this proved to be the setting in which the sensors were affected the quickest.
Additionally a sensor that consisted of 5% ethylcellulose with TOAOH and an equal amount of t-octyl phenol, covered in a protective layer of silicone rubber was added to the stability test to see if the addition of a different counter-ion affected the stability of the sensor.

4.3. Comparison of response time between ethylcellulose and HydroThane

As hydrothane seemed like an interesting candidate to replace ethylcellulose, its response time to CO_2 concentration changes was determined using Varian Cary 50 Conc's Kinetics software. For this purpose ethylcellulose and HydroThane sensors in combination with the bases TOAOH and TBAOH were measured at 5°C and 25°C. The concentrations between which the response time was measured were 1% and 3% since they are in the middle of the dynamic range of the sensor. The sensors responses were measured in the deprotonated maximum of the dye, m-Cresol purple at 600 nm. The measurements were done via triple determination.

4.4. Comparison of response time between protective layers of silicone rubber and Hyflon®

As Hyflon was proving to be a promising protective layer it was determined how long the response time of this polymer was compared to the standard layer of silicone rubber, since its permeability is 15.3 10^{-6} cm^3 (STP)/cm^2 sec cm Hg at 1 bar for CO_2[45]. For this purpose the sensors were measured at 5°C and 25°C in the dynamic range of 1% and 3% CO_2. The deprotonated maximum of m-Cresol purple at 600 nm was used to monitor the response time.

5 Results and discussion

5.1. Matrix optimization

5.1.1. The temperature accuracy of a measurement cell

In order to find a matrix that shows a lower temperature coefficient than ethylcellulose in combination with TOAOH, measurements were first attempted in the cell depicted in figure 5.1.1. The cell turned out to be insufficiently temperature controlled as there was no possibility to monitor the temperature inside the cells. Furthermore, the cell's glass walls were not insulated enough, causing condensation on those surfaces at 5°C and 37°C.

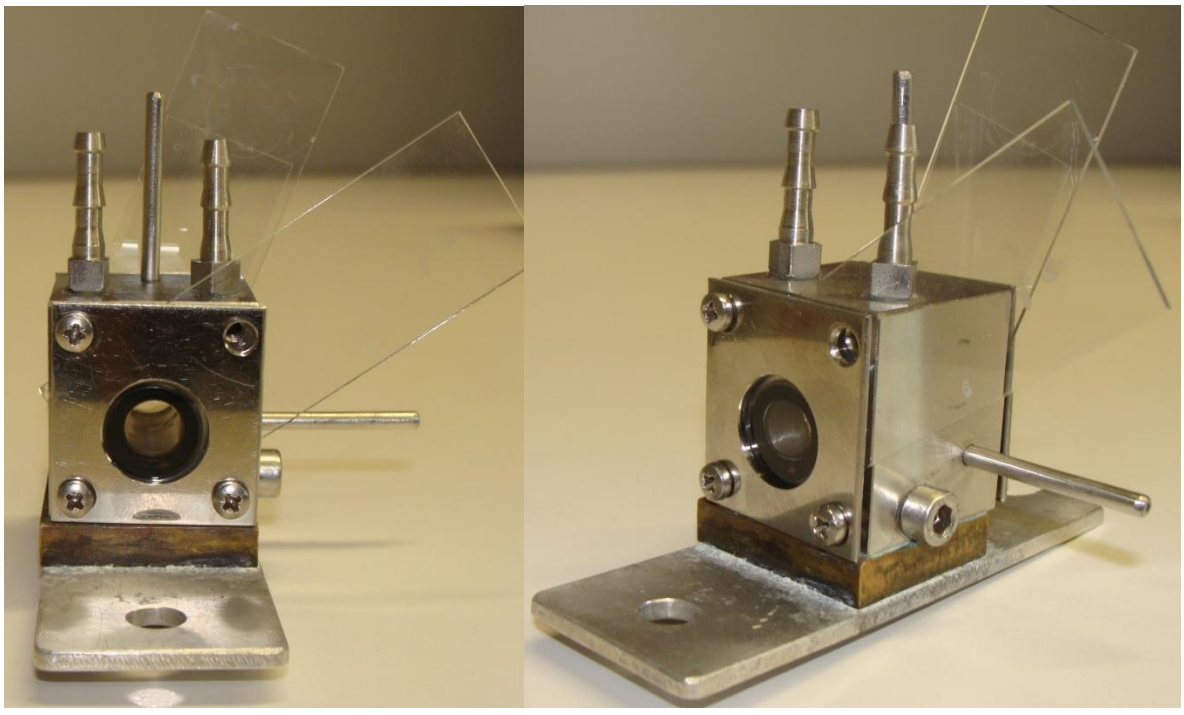

Fig 5.1.1: First measurement cell

After careful consideration a different cell was used for the measurement. This cell, shown in Figure 5.1.2., allowed for online temperature monitoring through a built-in sensor on the left side of the cell.

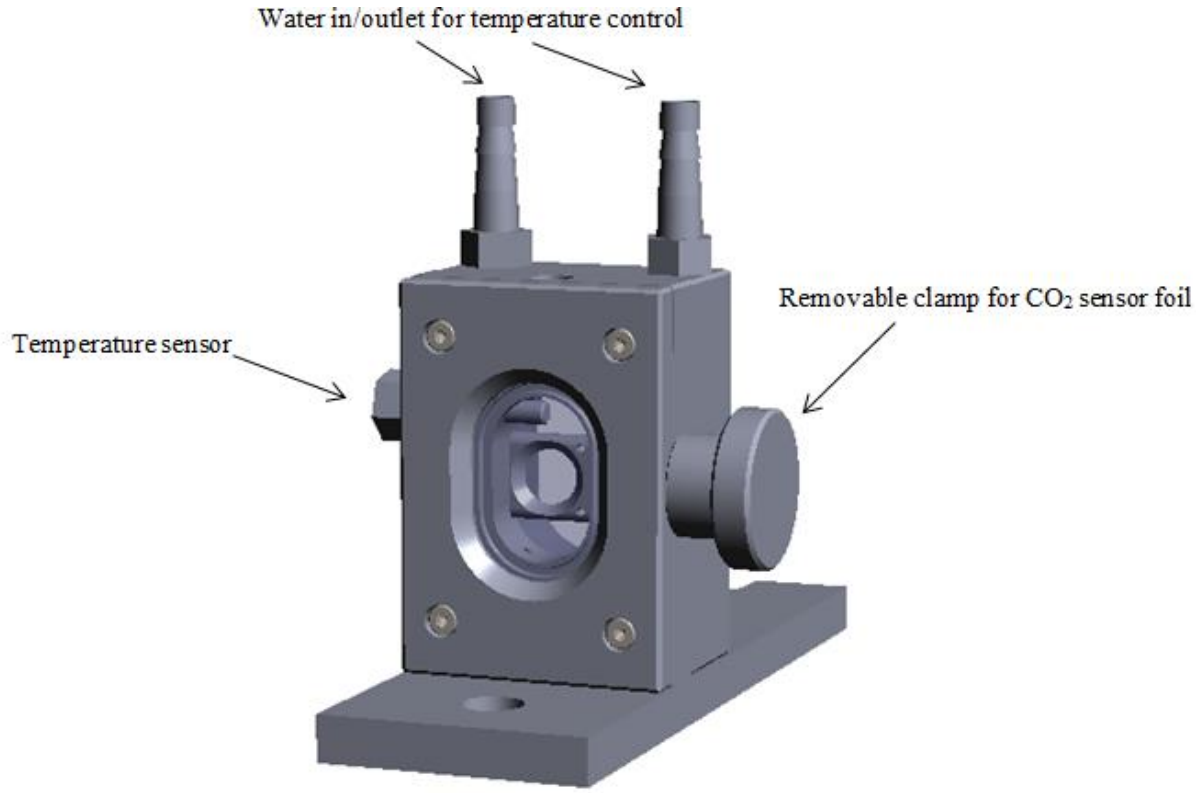

Fig. 5.1.2: Temperature controlled measurement cell

The sensor had to be replaced with a FireStingO_2 compatible Submersible Temperature Sensor TSUB21 PT100[44] as the built-in sensor showed an unquantifiable drift. With this cell the temperature of the measurement could be regulated to an accuracy of 0.3°C.

At 37°C the inside walls of the cell still showed significant condensation, which could only be resolved by replacing the silica in the humidifier that had previously been dampened by distilled water with silica that was moistened with a saturated potassium chloride solution. Saturated solutions of different salts set the humidity of a gas bubbled through them at a certain percentage. Potassium chloride regulates the humidity to 85%, which was enough to keep condensation at bay.

5.1.2. Temperature coefficient of the polymer and base combinations

The temperature dependence was determined by measuring the polymer/base combinations at 5, 25 and 37°C at the following partial CO_2 pressures:

Table 5.1.2.1: Partial pressures of CO_2 at different temperatures in [kPa]

Temperature	0% CO_2	0.5% CO_2	1% CO_2	2.5% CO_2	5% CO_2	10% CO_2	100% CO_2
5°C	0	0.50	1.00	2.51	5.02	7.25	100.43
25°C	0	0.49	0.98	2.45	4.91	7.08	98.13
37°C	0	0.48	0.95	2.38	4.75	6.85	94.98

The following combinations of polymers and bases were tested via this scheme:

Table 5.1.2.2: Combinations of polymers and bases that were tested for their temperature dependence

	Tetraoctyl ammmonium hydroxide (TOAOH)	Tetrabutyl ammonium hydroxide (TBAOH)	Cetyltrimethyl ammonium hydroxide (CTAOH)
Ethylcellulose	✓	✓	✓
Hydromed D4	✓	✓	-
Hydromed D7	✓	✓	-
HydroThane 5%	✓	✓	✓

CTAOH had to be excluded due to its lack of solubility in the matrices. Attempts were made to increase its solubility in the polymer using a various phenols such as t-octyl phenol, but the base continued to crystalize as the sensor dries, leading to formations such as the following:

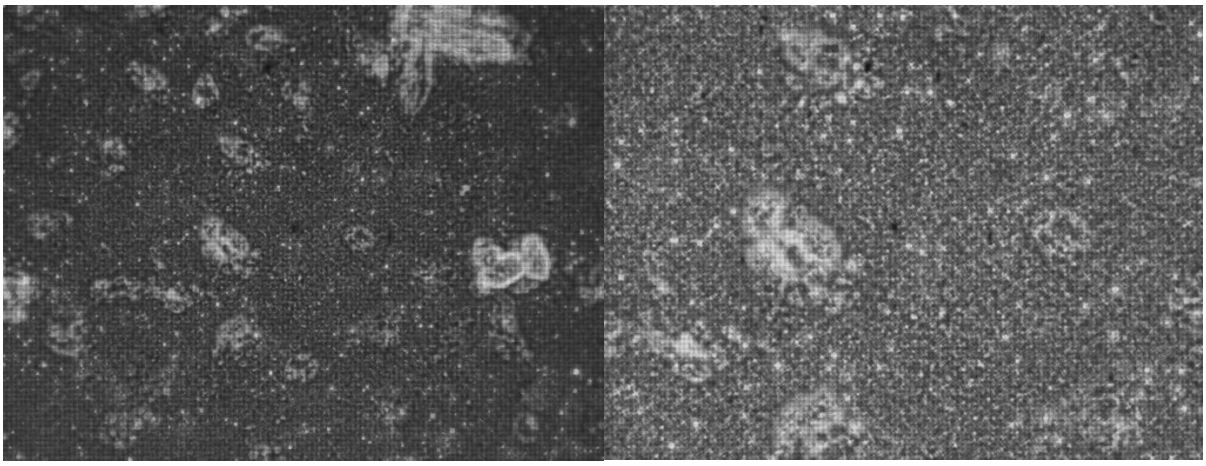

Figure 5.1.2.1: Microscopic picture capturing the crystallization of CTAOH in D7 ten times magnified (left) and twenty times magnified on the right

The following figures show the change of the absorption spectra of m-cresol purple in the different matrices at different temperatures in comparison to their ethylcellulose equivalent.

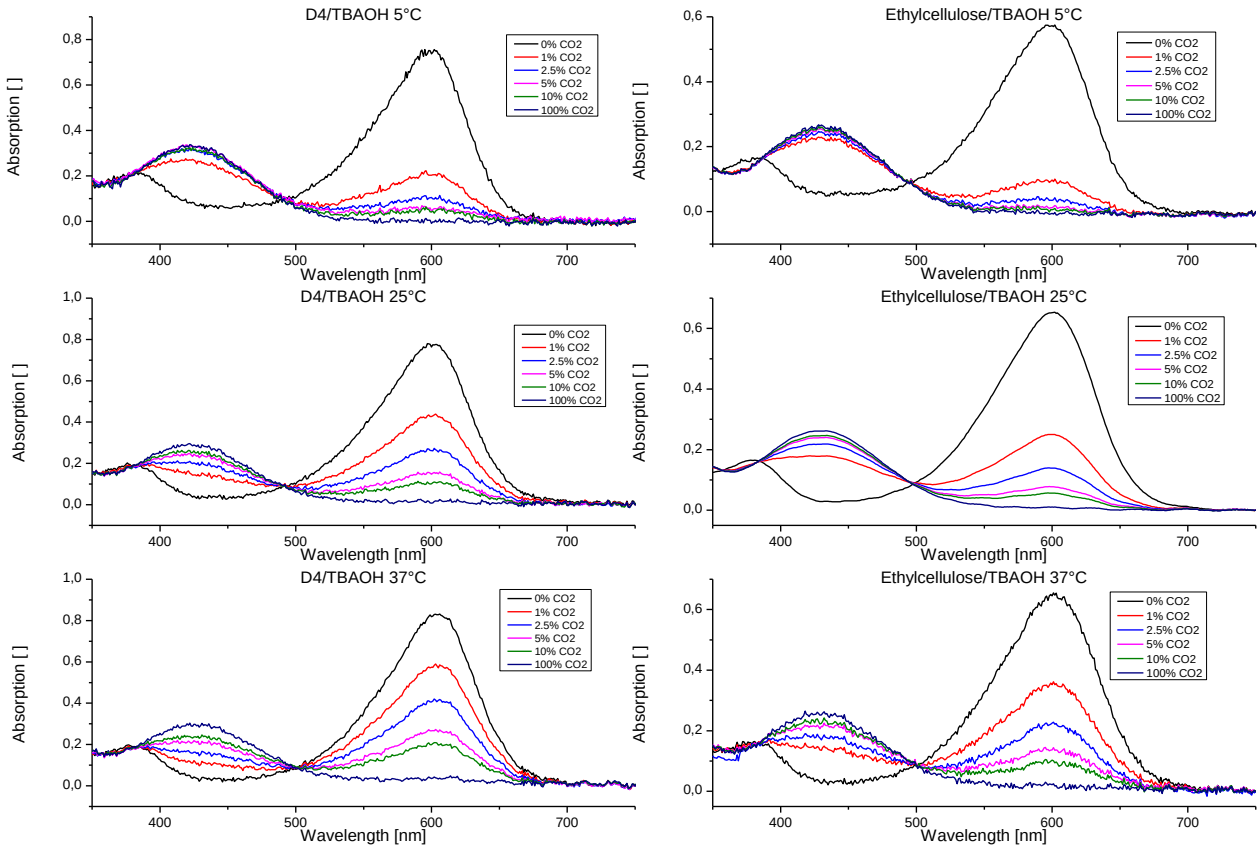

Figure 5.1.2.2: Hydromed D4 in comparison to standard matrix ethylcellulose with TBAOH as base

While Hydromed D4 shows a slightly lower temperature dependence than ethylcellulose the material had to be excluded as a possibility due to its too high water absorption capacity. D4's water absorption capacity is 50%. This does not only cause the material to swell too much in an aqueous environment but also makes the addition of protective polymer layers problematic. The standard silicone rubber protective layer does not dry on this material at all.

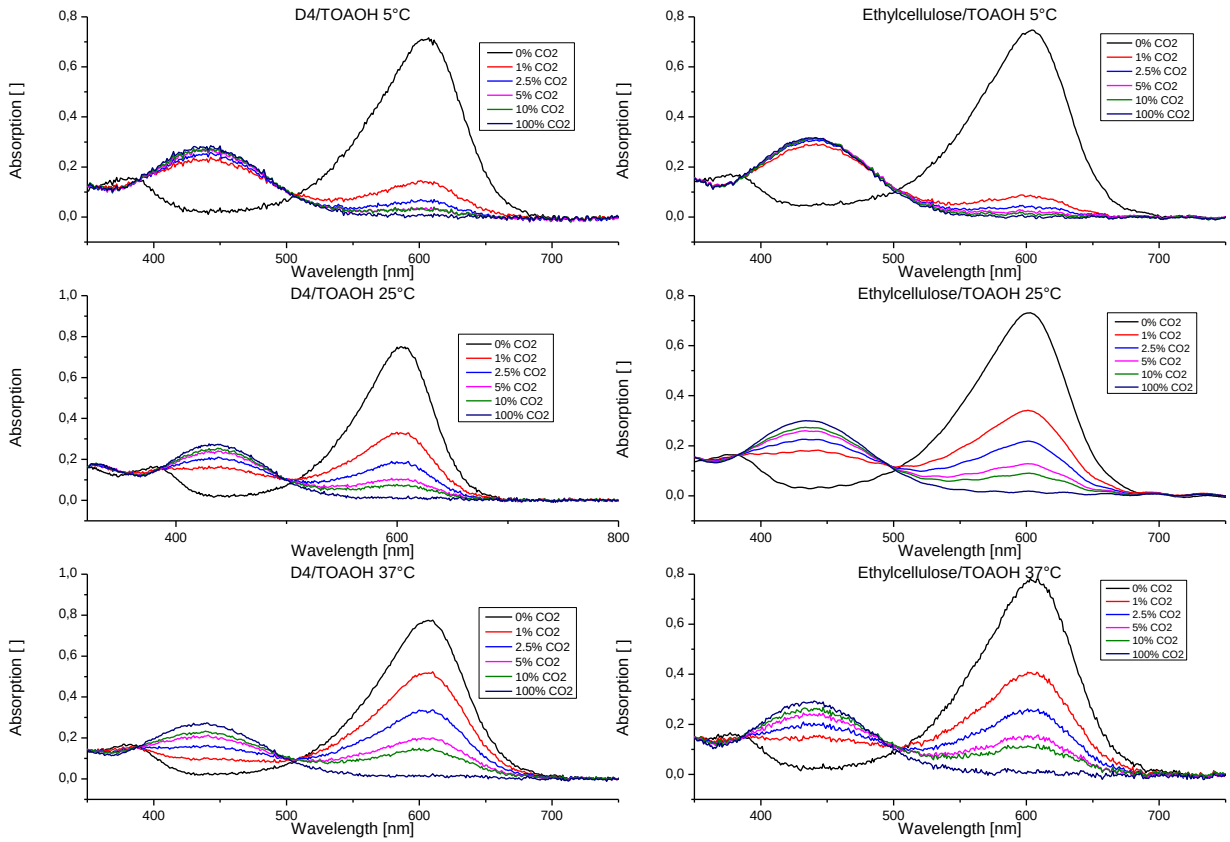

Figure 5.1.2.3: Hydromed D4 in comparison to standard matrix ethylcellulose with TOAOH as base

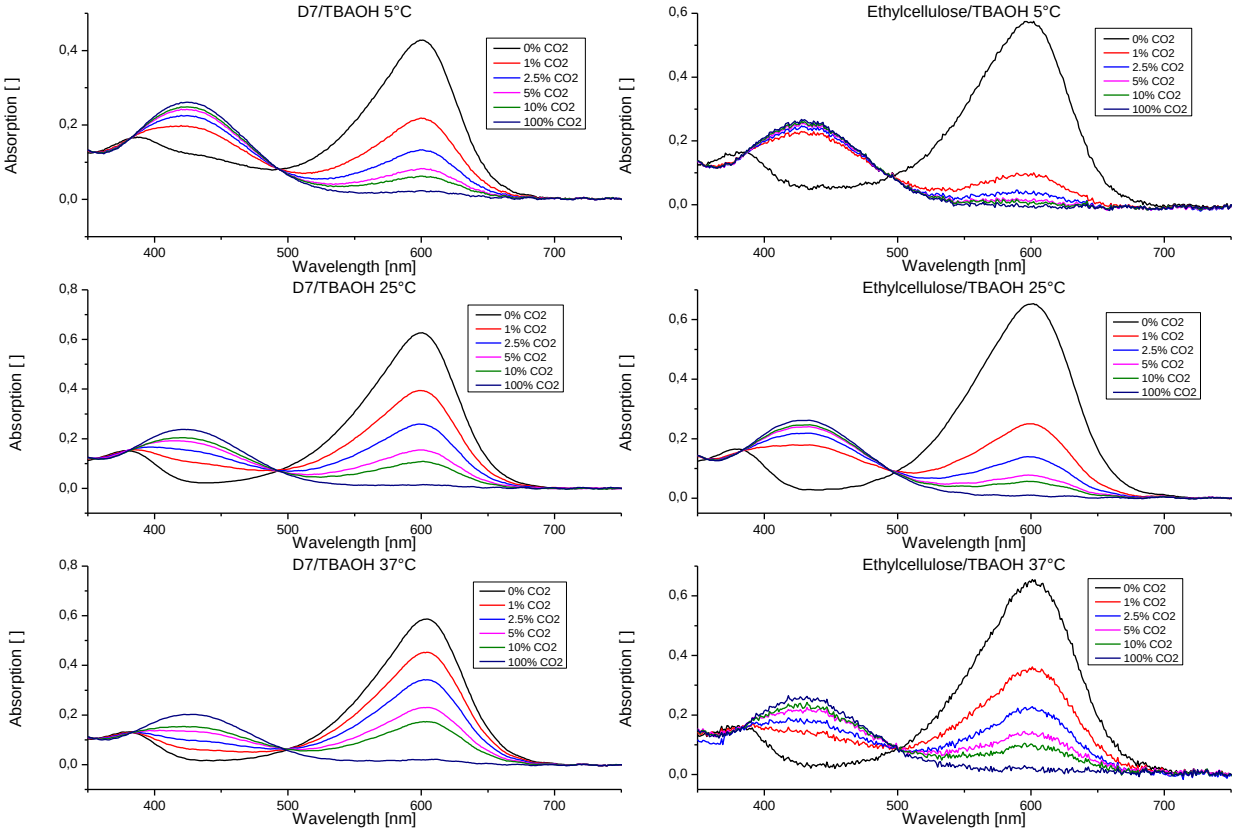

Figure 5.1.2.4: Hydromed D7 in comparison to standard matrix ethylcellulose with TBAOH as base

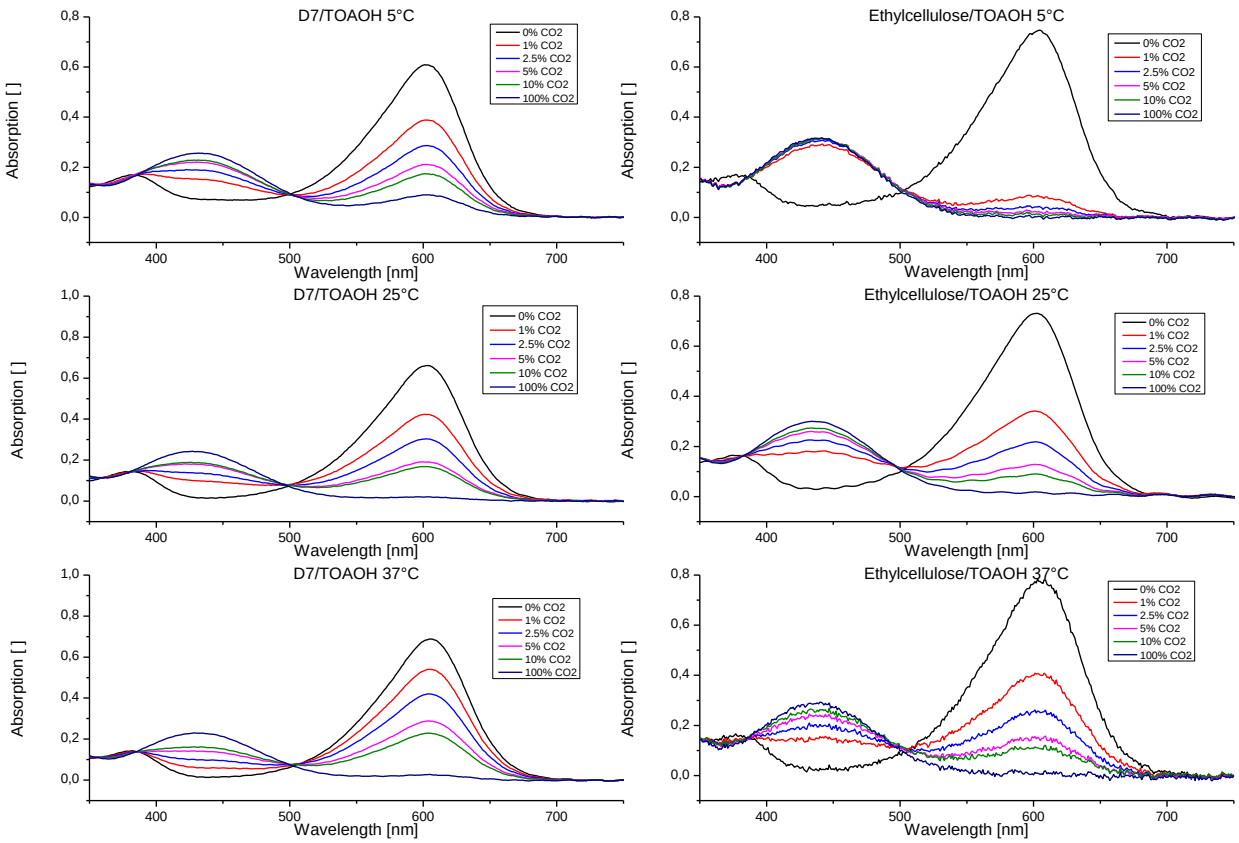

Figure 5.1.2.5: Hydromed D7 in comparison to standard matrix ethylcellulose with TOAOH as base

Hydromed D7 shows a very good temperature coefficient (Fig. 5.1.2.8 and 5.1.2.9). However, the material seems to lose the majority of its gas permeability at lower temperatures. The 5°C spectra in figures 5.1.2.4 and 5.1.2.5 were taken after 90 minutes of flushing the sensors with nitrogen. The spectra show that the indicator dye has not yet been completely deprotonated. This slow response time was the reason that Hydromed D7 had to be excluded as a possible matrix alternative.

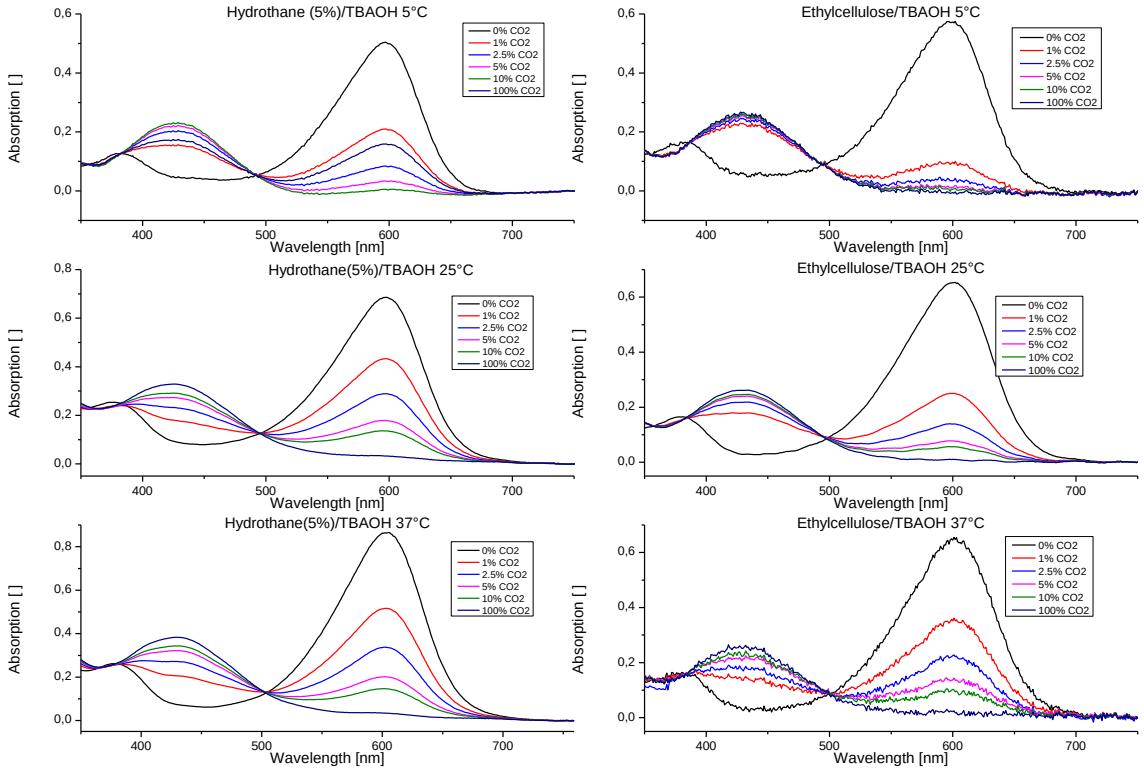

Figure 5.1.2.6: HydroThane in comparison to standard matrix ethylcellulose with TBAOH as base

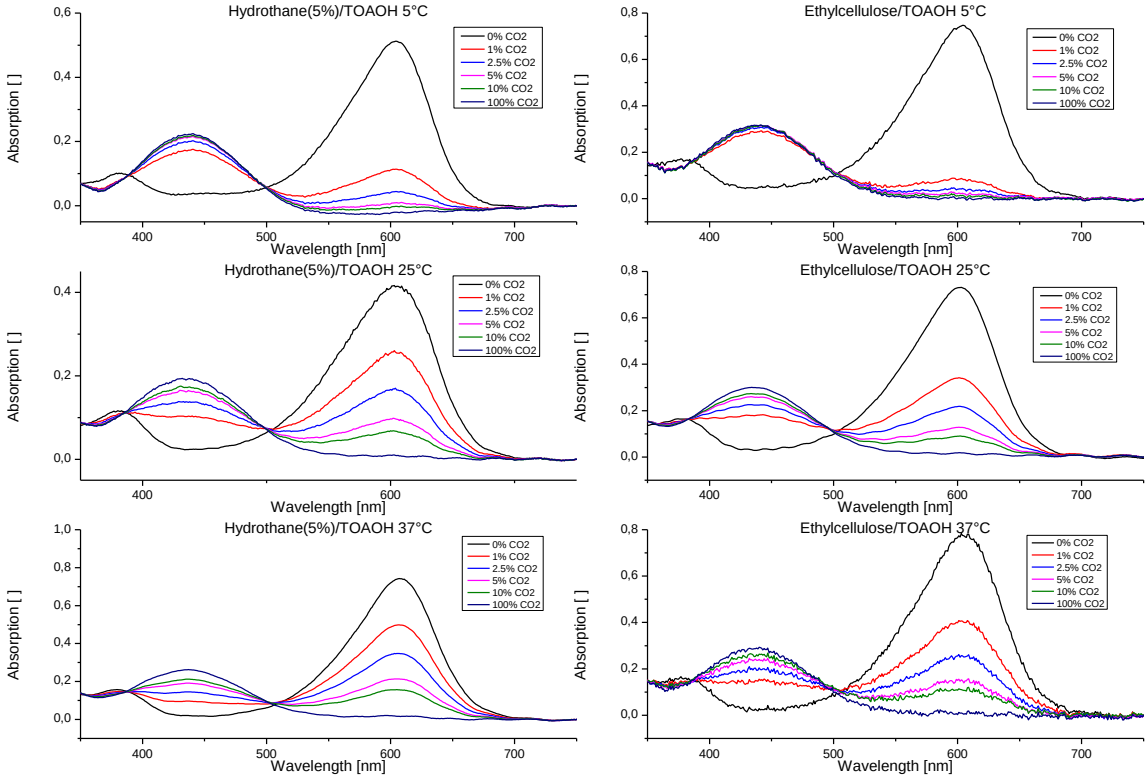

Figure 5.1.2.7: HydroThane in comparison to standard matrix ethylcellulose with TOAOH as base

In an attempt to quantify the difference in sensitivity between the polymers, the deprotonated maxima of the calibration curves at each temperature were plotted against the logarithmical partial pressure of CO_2. The resulting curves were fitted with a Boltzmann function as seen in Figure 5.1.2.8.

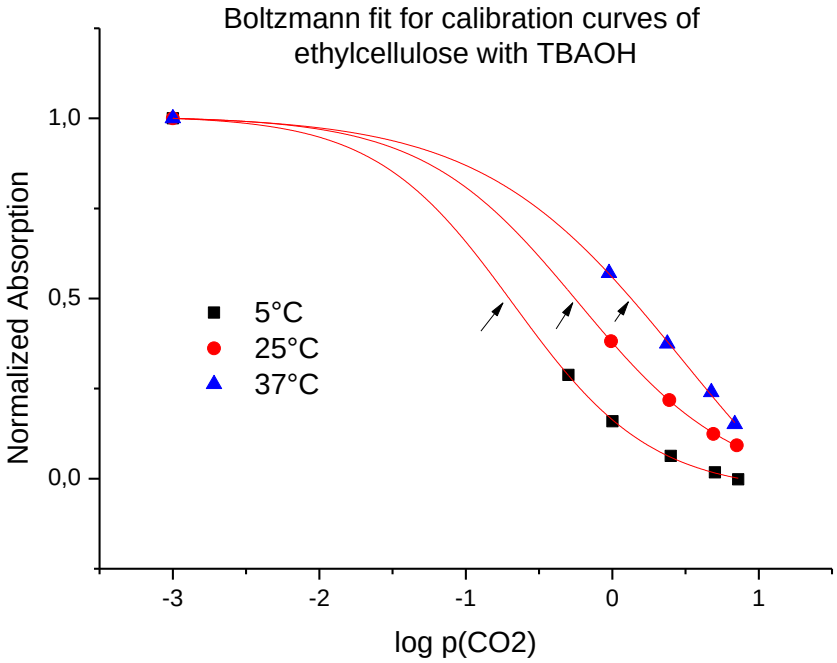

Figure 5.1.2.8: Boltzmann fit of the calibration points plotted against p(CO_2)

Afterwards the value at which half the sensor was protonated was determined for each temperature curve. The resulting values were called pK(CO_2) and plotted in the following diagrams to depict

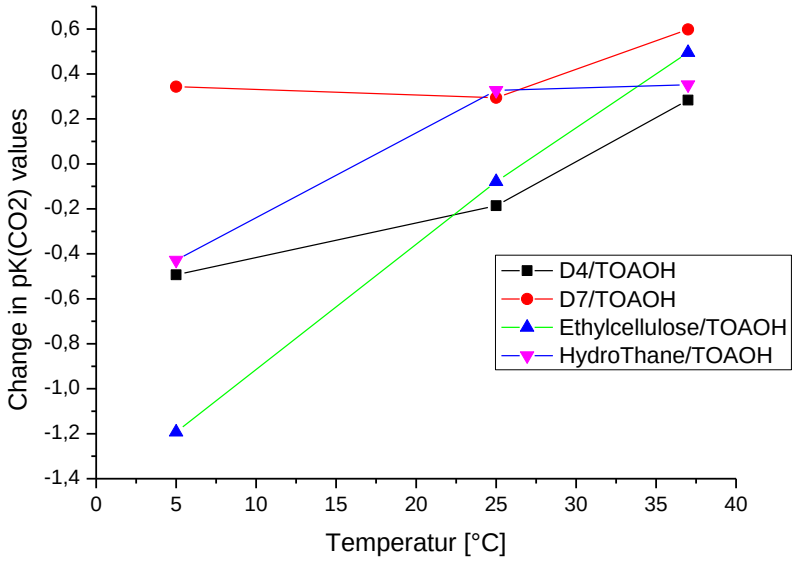

Figure 5.1.2.9: Change in pK(CO_2) values at different temperatures in the four polymers shown with TOAOH as a base

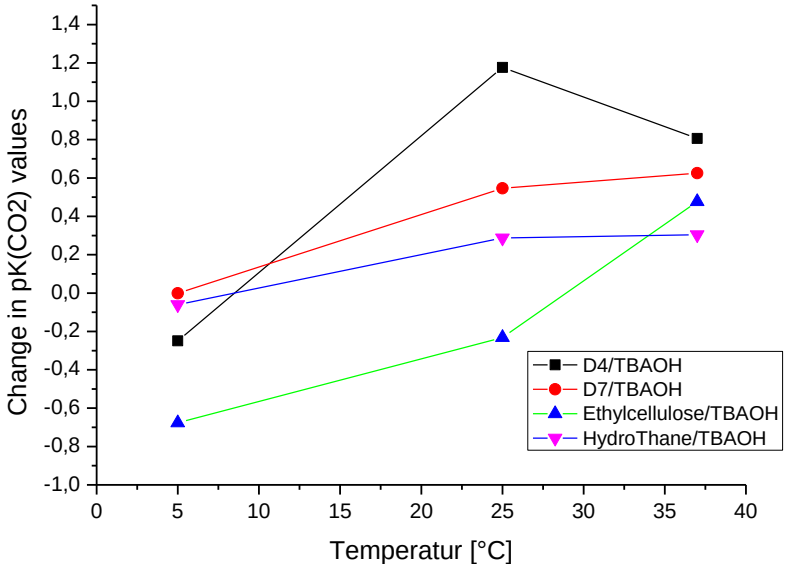

Figure 5.1.2.10: Change in pK(CO_2) values at different temperatures in the four polymers shown with TBAOH as a base

Figures 5.1.2.9 and 5.1.2.10 show the change in the pK(CO_2) value of the dye in the matrices for different bases at the different temperatures. The steeper the gradient between the temperatures becomes, the more temperature dependent the matrix is. A highly negative pK(CO_2) value suggests a high sensitivity. These figures further confirm the indications of the absorptions spectra and show that ethylcellulose has the greatest temperature dependency of the bases.

HydroThane shows a lower temperature dependency and reacts equally as fast as ethylcellulose at all temperatures as a measurement of the response times shows. The change the increasing CO_2 concentration had on the sensor was monitored via the deprotonated maximum at 600 nm. The resulting curve was fitted with the following equation – generated with TableCurve 2D - where a, b and c are independent coefficients and A is the measured absorption:

$$A = \frac{a + c * p(CO_2)}{1 + b * p(CO_2)}$$

The response times were calculated with the resulting p(CO_2) values of

$$p(CO_2) = \frac{-A + a}{A * b - c}$$

The response time measurement as described in section 4 of this thesis revealed that Hydrothane and ethylcellulose show a very similar response time at both 5°C and 25°C. The

response time parameters t_{63} and t_{90} of ethylcellulose and HydroThane with the bases TOAOH and TBAOH at 5°C and 25°C are shown in table 5.1.2.3 and 5.1.2.4.

t_{63} for the protonation describes the change in CO_2 concentration between 1% and 2.26% and 3% to 1.74% for deprotonation. t_{90} covers the concentration change between 1% and 2.8% for the protonation process and 3% to 1.2% of the deprotonation process.

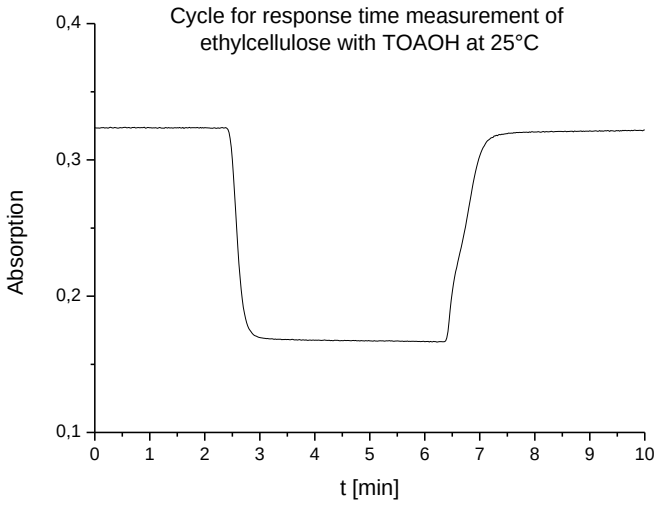

Figure 5.1.2.10: Example of a response time measurement cycle for an ethylcellulose/TOAOH sensor foil at 25°C

Table 5.1.2.3: Temperature dependence of HydroThane and ethylcellulose at 5°C

Polymer/Base combination	t_{63} protonated	t_{90} protonated	t_{63} deprotonated	t_{90} deprotonated
Ethylcellulose/TOAOH	28	48	30	58
Ethylcellulose/TBAOH	79	145	73	166
Hydrothane/TOAOH	19	29	29	58
Hydrothane/TBAOH	19	41	35	65

Table 5.1.2.3: Temperature dependence of HydroThane and ethylcellulose at 25°C

Polymer/Base combination	t_{63} protonated	t_{90} protonated	t_{63} deprotonated	t_{90} deprotonated
Ethylcellulose/TOAOH	18	24	20	35
Ethylcellulose/TBAOH	22	34	23	42
Hydrothane/TOAOH	19	26	25	41
Hydrothane/TBAOH	25	42	31	55

At this point it has to be noted that these values are not the absolute values for the measured sensors, but also include the response time of the cell and measurement setup itself, which is estimated to be about 12 seconds.

5.2. Long term stability of different polymer and base combinations

5.2.1. Laboratory storage conditions

The laboratory conditions were expected to be the most extreme of the four storage conditions, as it was expected that the solvent-heavy air would compromise the sensors faster than 'regular' air would.

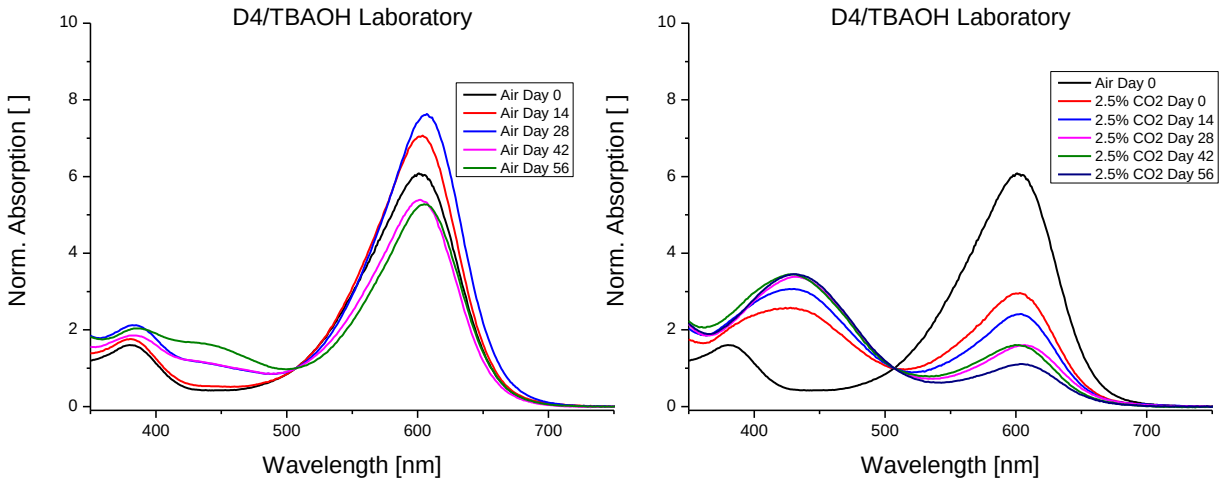

Figure 5.2.1.1: Hydromed D4 in combination with TBAOH kept under laboratory storage conditions

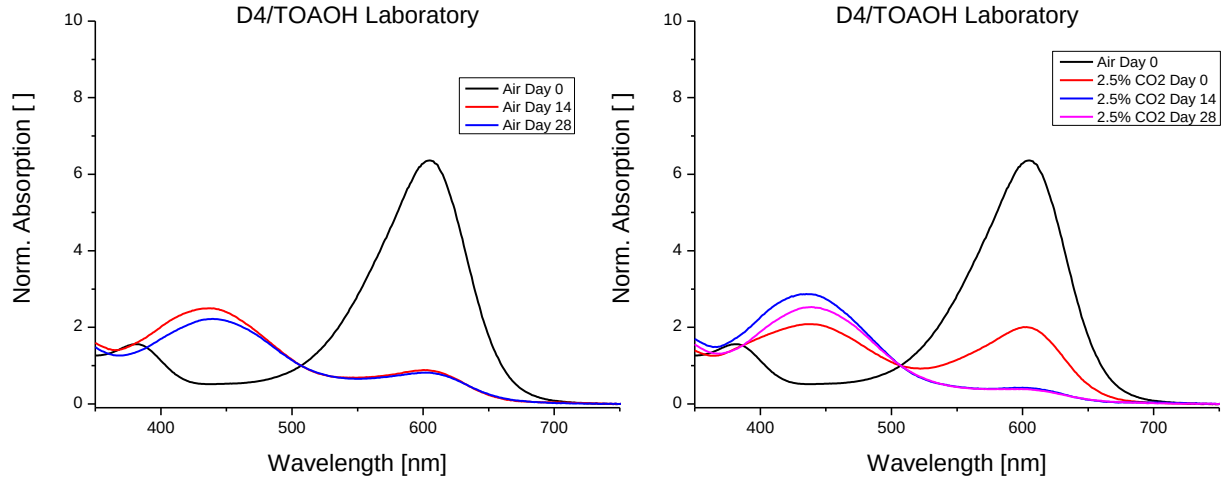

Figure 5.2.1.2: Hydromed D4 in combination with TOAOH kept under laboratory storage conditions

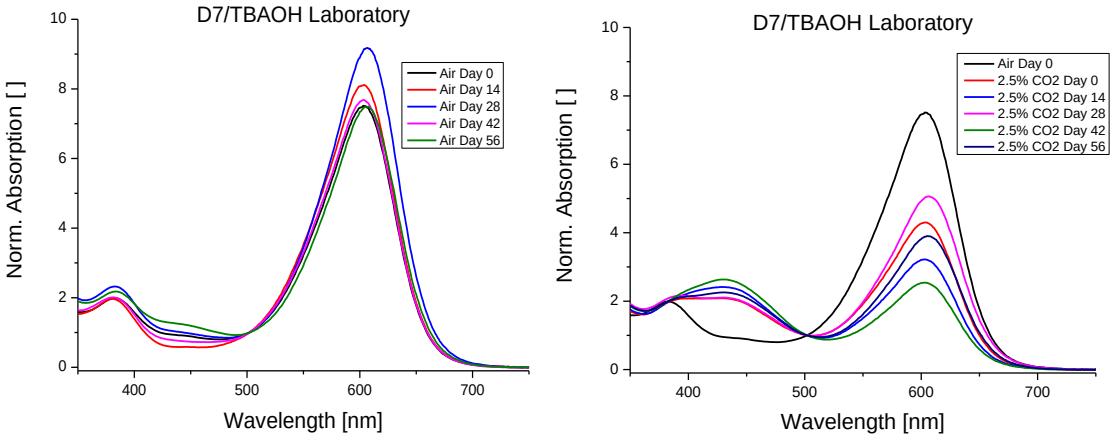

Figure 5.2.1.3: Hydromed D7 in combination with TBAOH kept under laboratory storage conditions

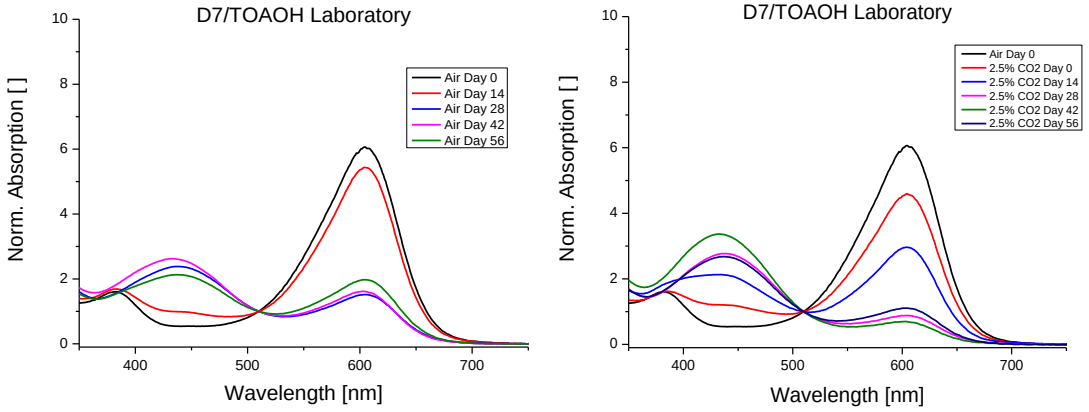

Figure 5.2.1.4: Hydromed D7 in combination with TOAOH kept under laboratory storage conditions

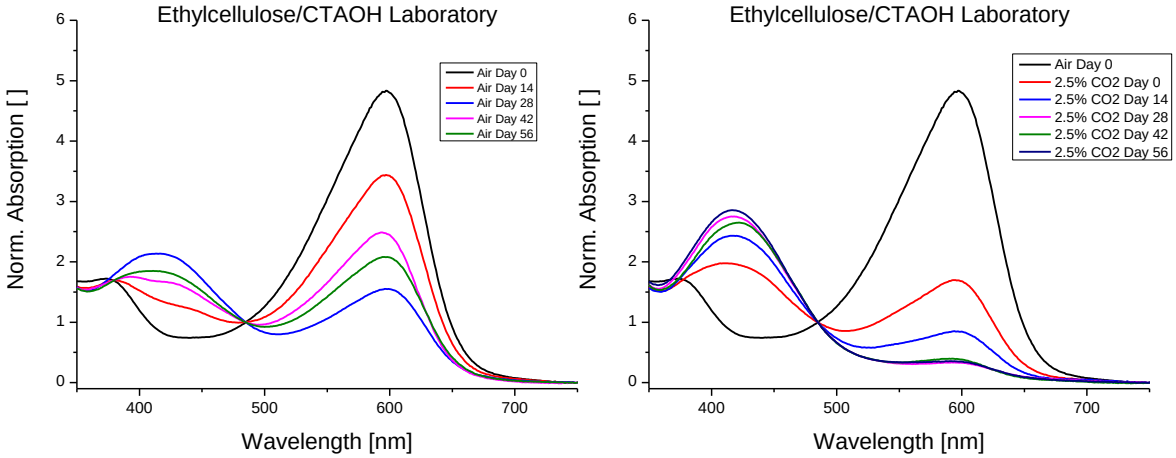

Figure 5.2.1.5: Ethylcellulose in combination with CTAOH kept under laboratory storage conditions

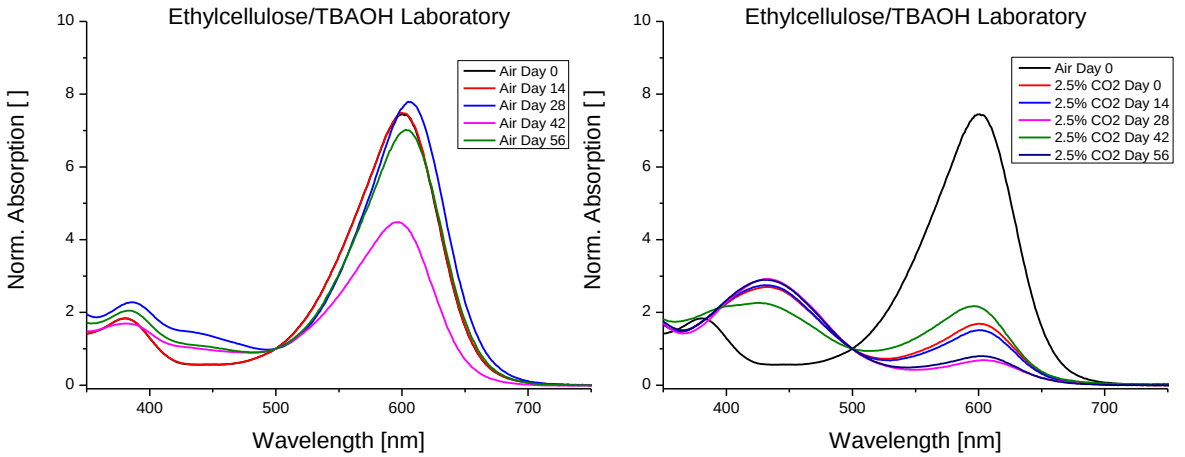

Figure 5.2.1.6: Ethylcellulose in combination with TBAOH kept under laboratory storage conditions

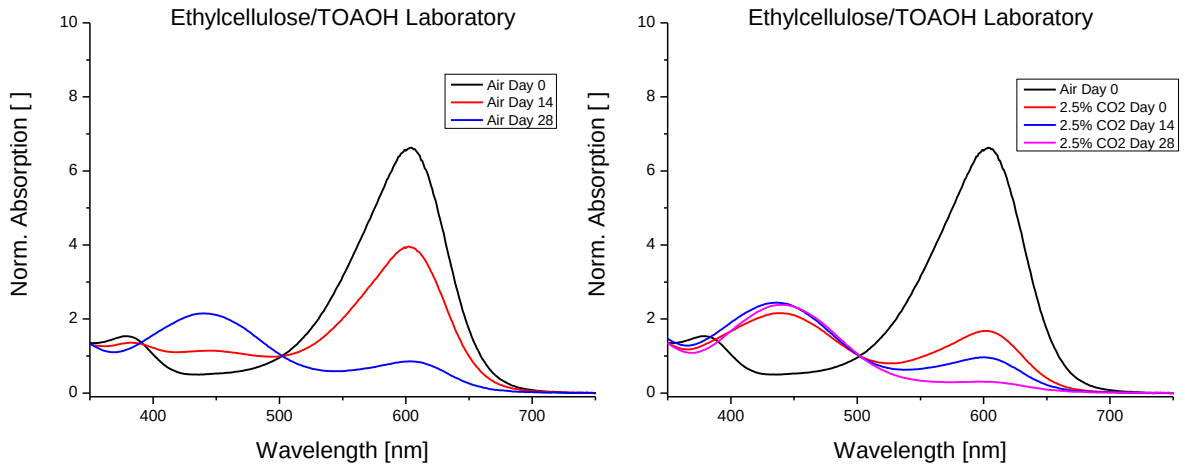

Figure 5.2.1.7: Ethylcellulose in combination with TOAOH kept under laboratory storage conditions

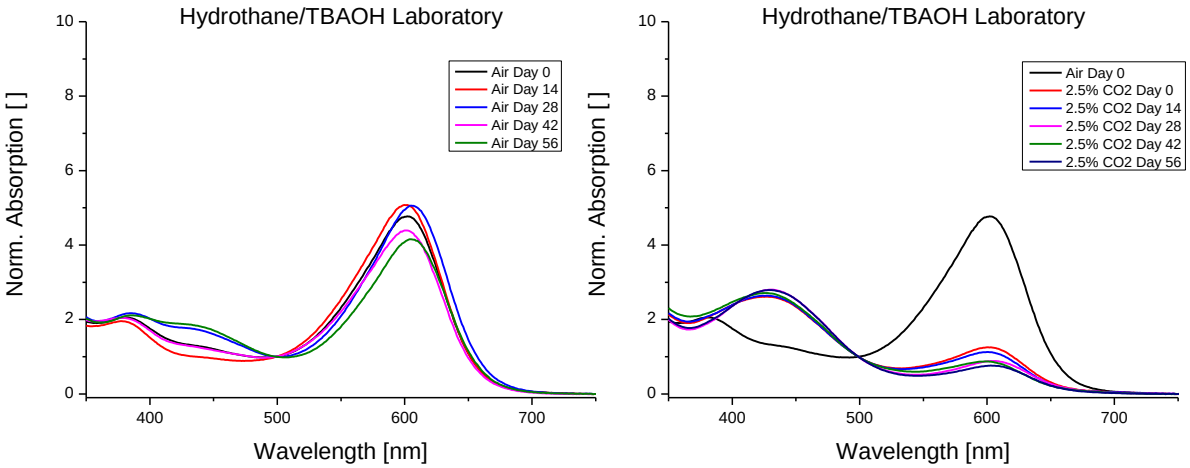

Figure 5.2.1.8: HydroThane in combination with TBAOH kept under laboratory storage conditions

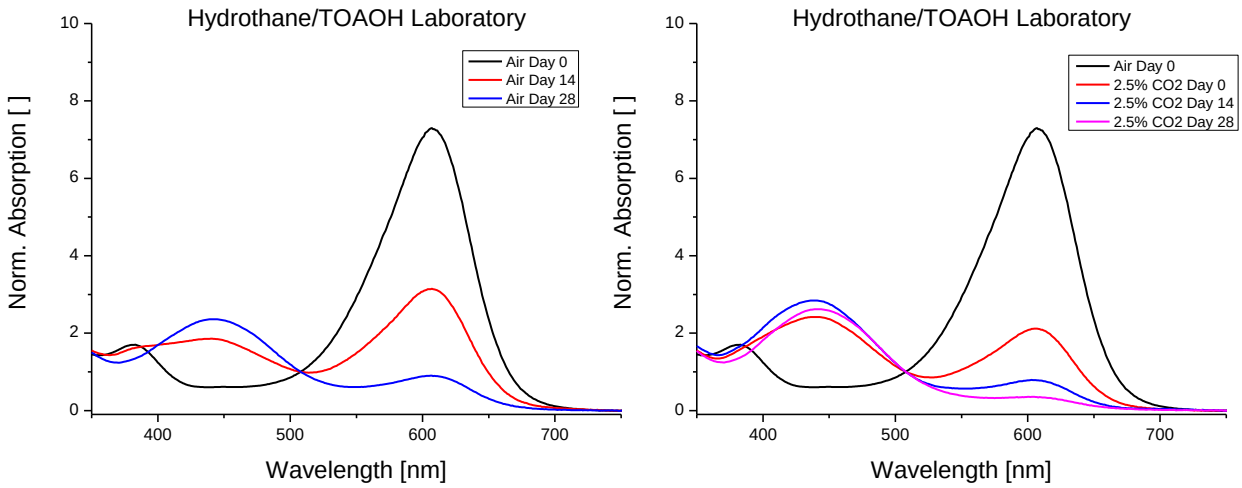

Figure 5.2.1.9: HydroThane in combination with TOAOH kept under laboratory storage conditions

To sum up the data depicted in figures 5.2.1.1 to 5.2.1.9 the maxima of the deprotonated peaks are shown in figures 5.2.1.11 and 5.2.1.12. This summary will be found at the end of each section describing the long-term stability test's results in different storage conditions.

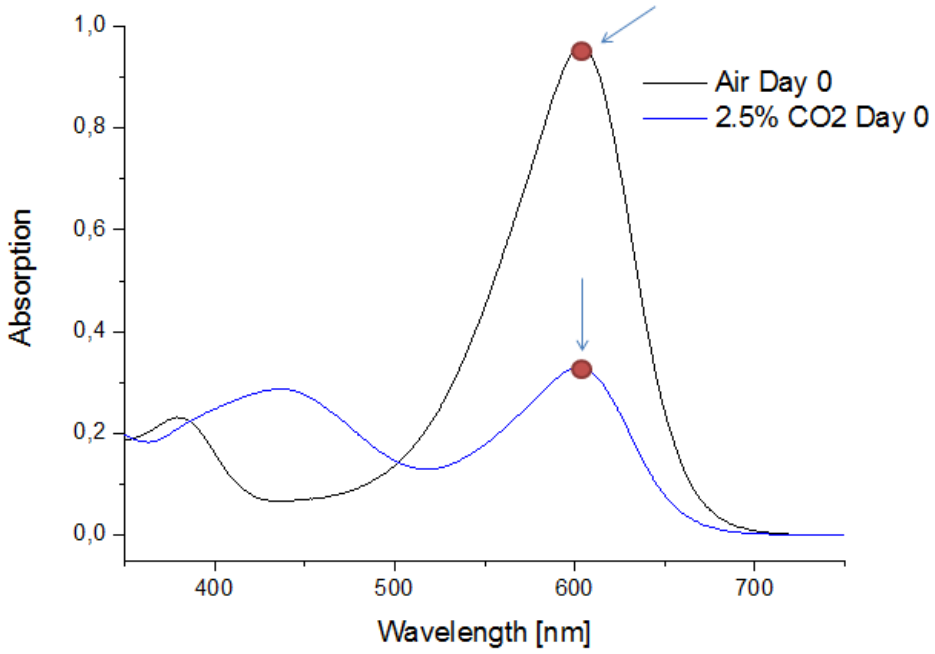

Figure 5.2.1.10: Data points used to allow comparison between bases and polymers

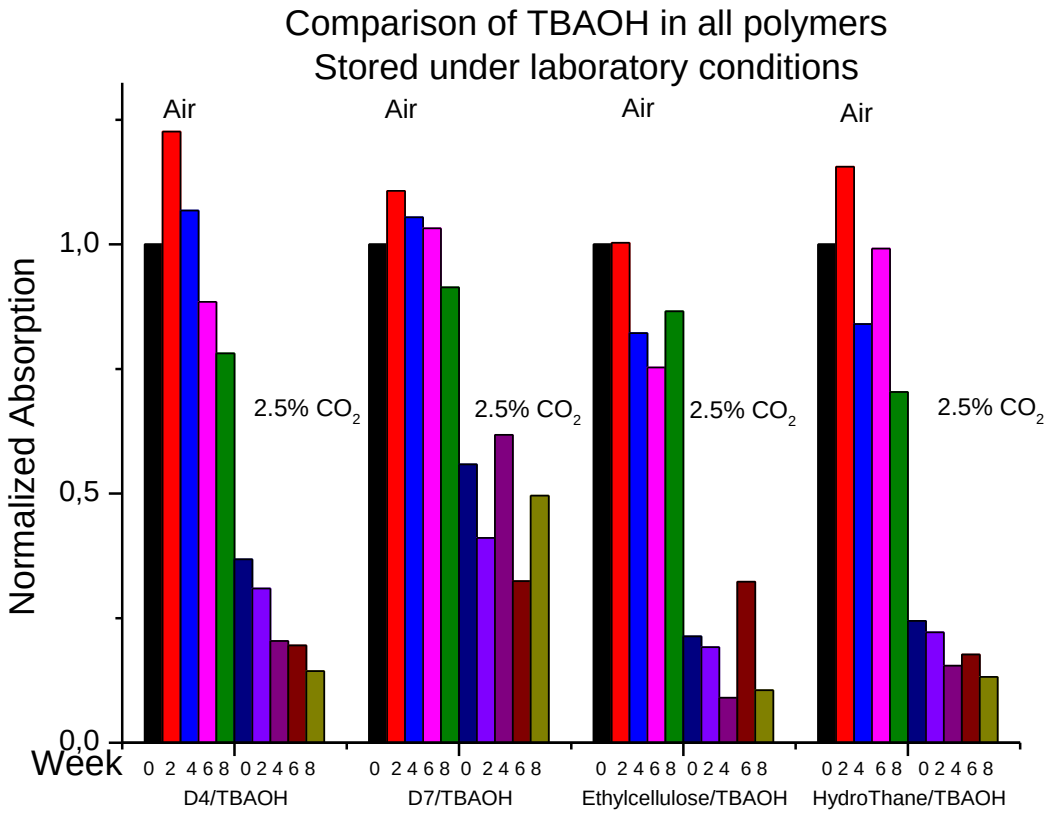

Figure 5.2.1.11: Comparison of the base TBAOH (0.15 mmol/100 mg polymer) in all the polymers stored under laboratory conditions

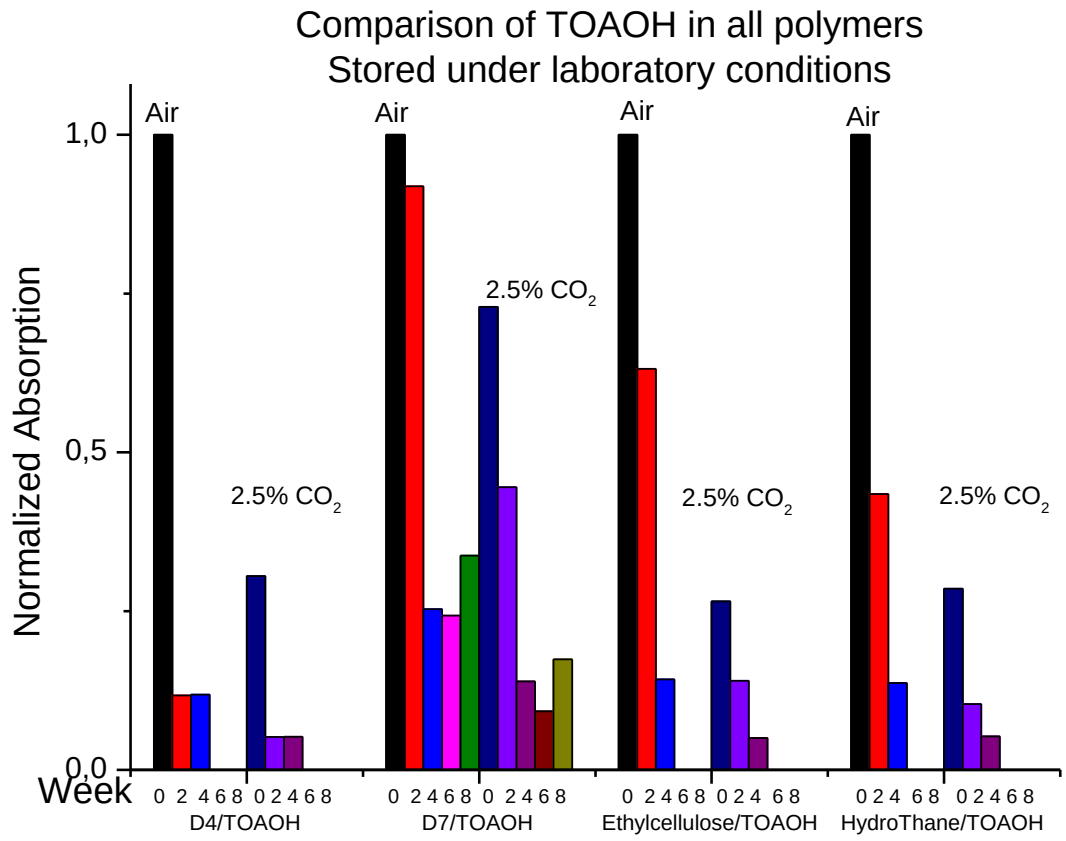

Figure 5.2.1.12: Comparison of the base TOAOH (0.04 mmol/100 mg polymer) in all the polymers stored under laboratory conditions

A comparison between the sensors with different base concentrations shows that the base concentration strongly effects the long term-stability of the sensors. The D4/TBAOH and D7/TBAOH sensors show a slight increase in sensitivity during the first month of storage, while their TOAOH equivalents are permanently protonated after less than four weeks.
D7/TOAOH in comparison to its D4 equivalent retains some degree of usability in the first two weeks, even though the edges of the pre-cut strips show permanent protonation just as quickly. CTAOH foils are contaminated slightly slower than their TOAOH equivalent. This can be explained by the concentration difference of the bases. CTAOH was used in a concentration of concentration of 0.08 mmol per 100 mg polymer, which is twice as much as TOAOH. The excess base acts as a buffer for any acidic components that may otherwise affect the sensor earlier.
The large pieces of sensor foil age slower than the pre-cut strips. They too are protonated from the edges towards the middle, as can be seen in figure 5.2.1.13:

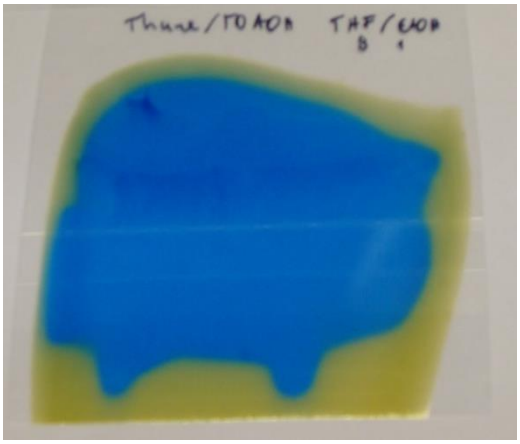

Figure 5.2.1.13: Large piece of a HydroThane sensor with TOAOH as base after 28 days of storage under laboratory conditions.

5.2.2. Office storage conditions

The office storage conditions were the most detrimental conditions in this aging test. This is presumably due to the temperature in the office being slightly higher than in any of the other storage places. Due to this fact, these conditions will be used to discuss the effect a protective layer of silicone rubber had in the aging of the sensors. The spectra of the silicone protected sensors stored under the other conditions can be found in the appendix.

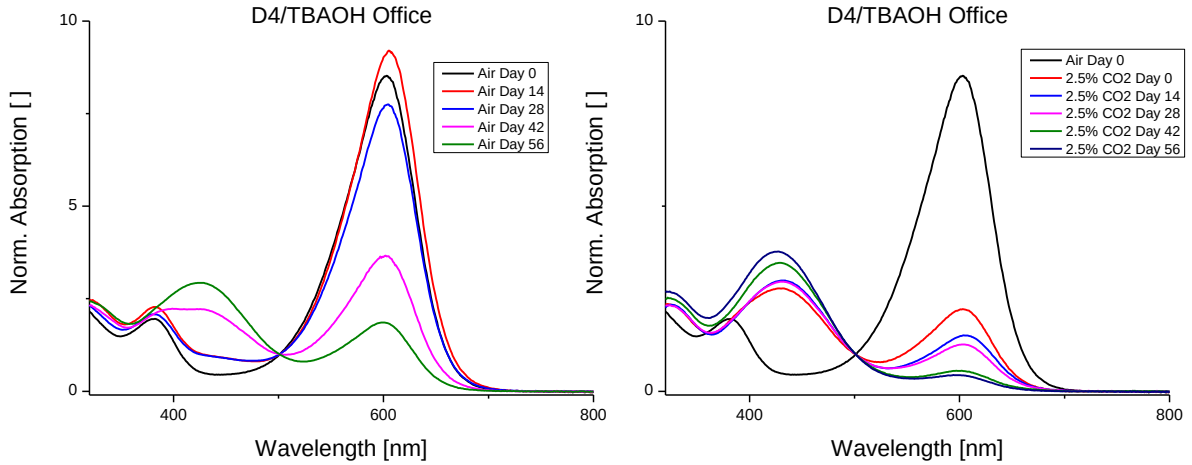

Figure 5.2.2.1: Hydromed D4 in combination with TBAOH kept under office conditions

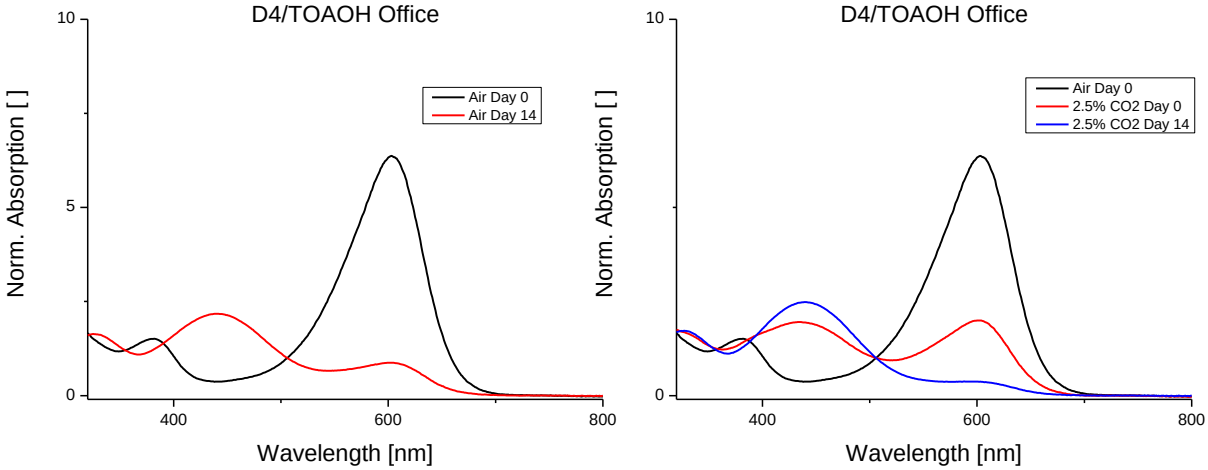

Figure 5.2.2.2: Hydromed D4 in combination with TOAOH kept under office conditions

The silicone rubber layer does not dry on top of a D4 sensor layer, probably due to the polymer's large water absorption capacity.

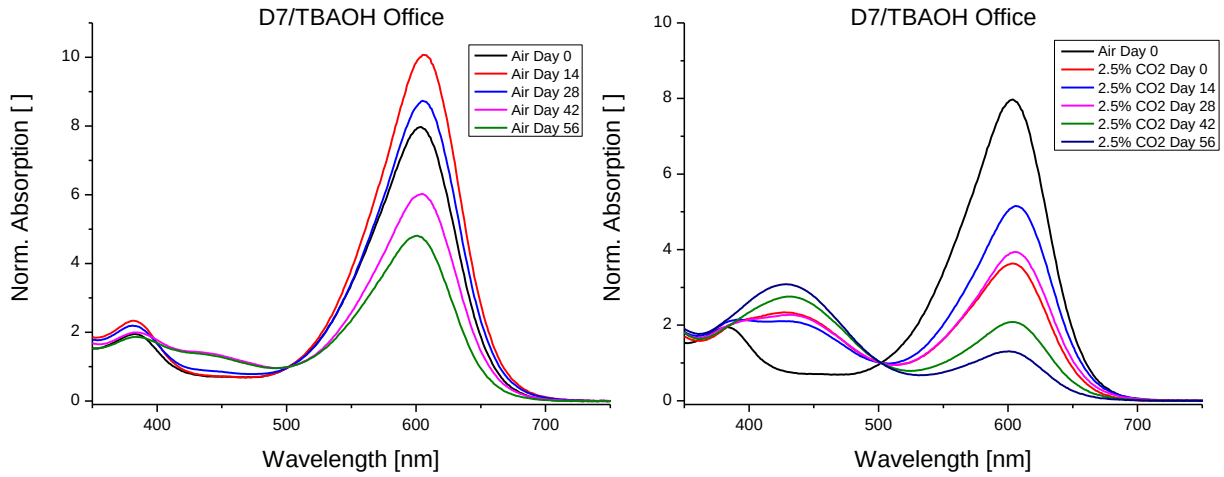

Figure 5.2.2.3: Hydromed D7 in combination with TBAOH kept under office conditions

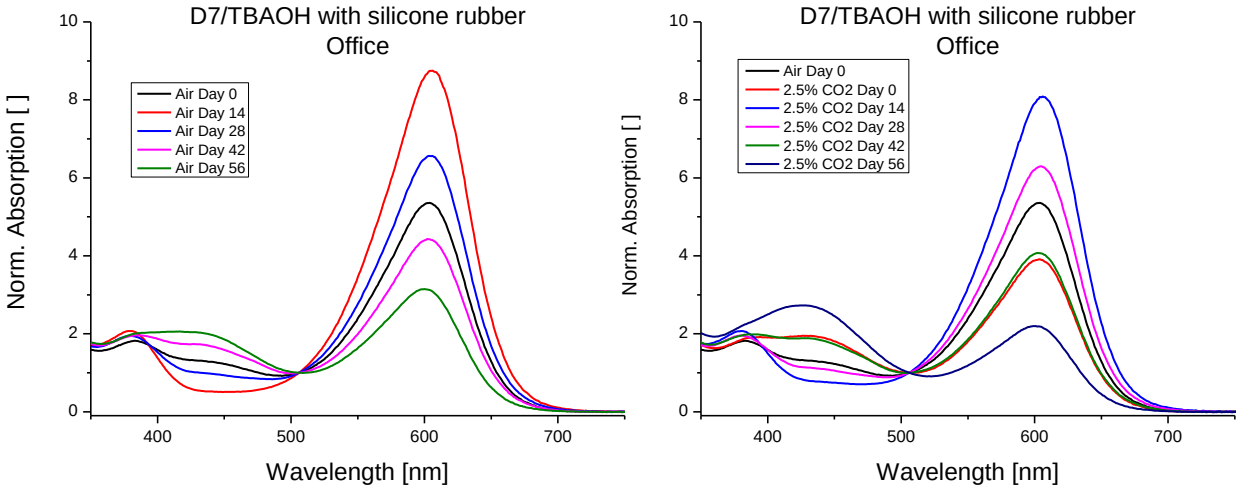

Figure 5.2.2.4: Hydromed D7 in combination with TBAOH kept under office conditions with a protective layer of silicone rubber

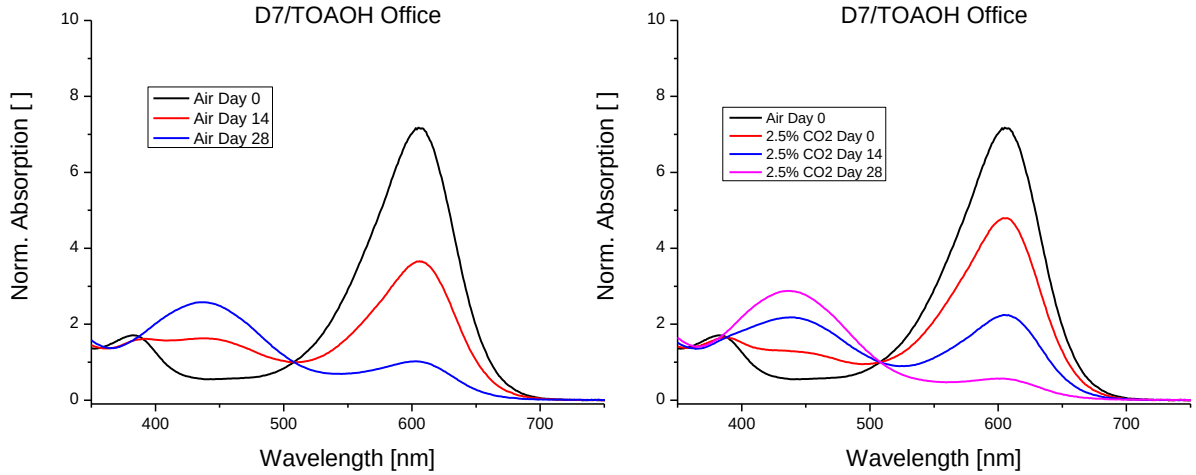

Figure 5.2.2.5: Hydromed D7 in combination with TOAOH kept under office conditions

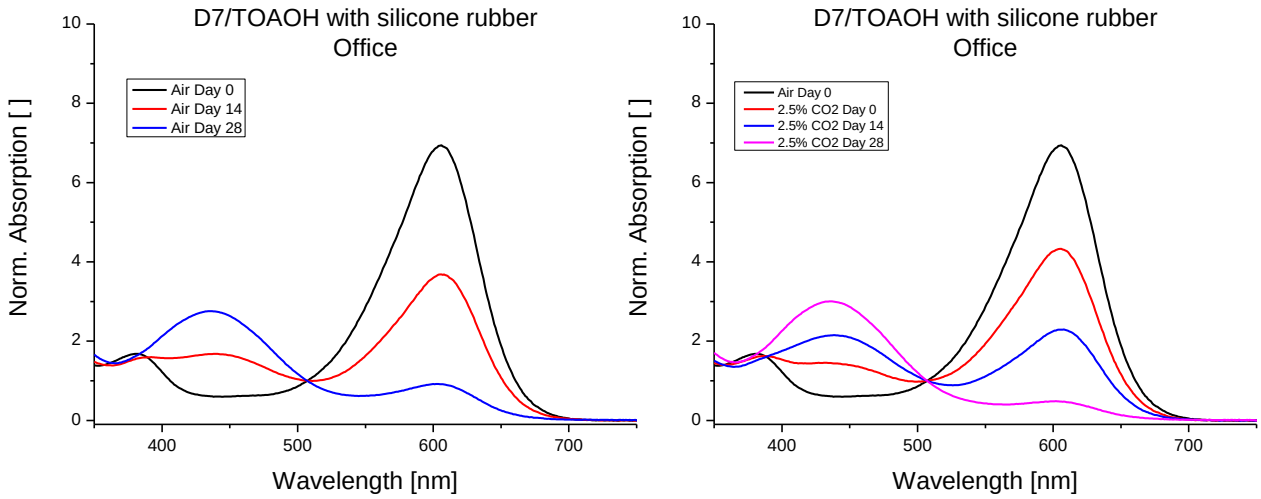

Figure 5.2.2.6: Hydromed D7 in combination with TOAOH kept under office conditions with a protective layer of silicone rubber

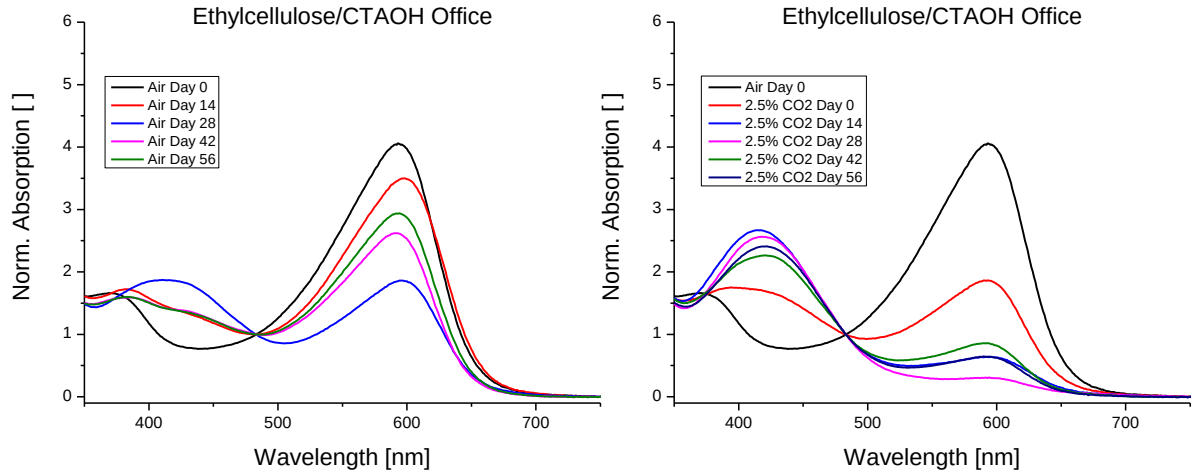

Figure 5.2.2.7: Ethylcellulose in combination with CTAOH kept under office conditions

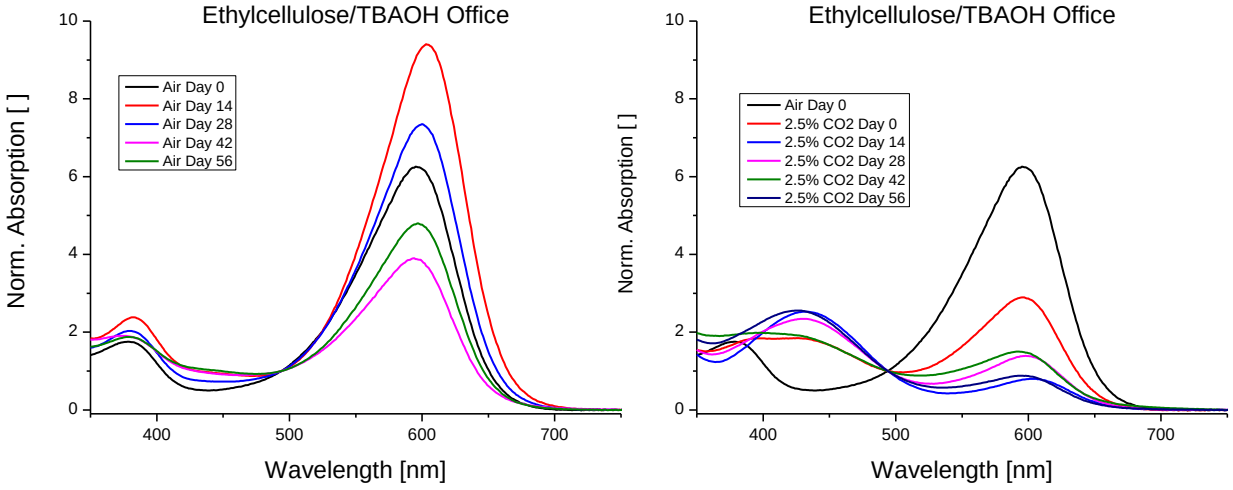

Figure 5.2.2.8: Ethylcellulose in combination with TBAOH kept under office conditions

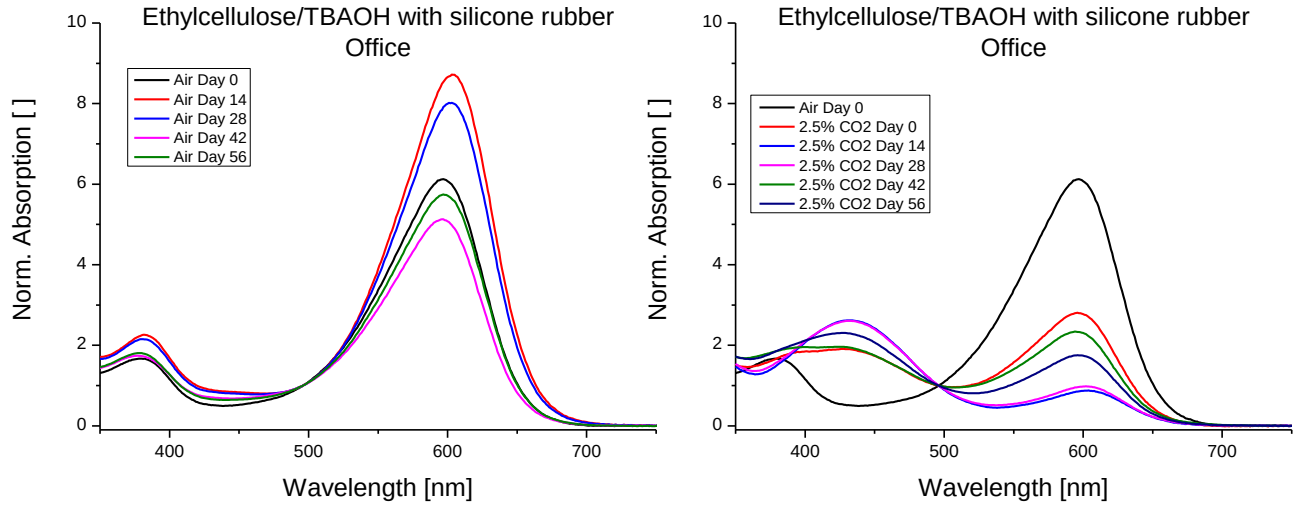

Figure 5.2.2.9: Ethylcellulose in combination with TBAOH kept under office conditions with a protective layer of silicone rubber

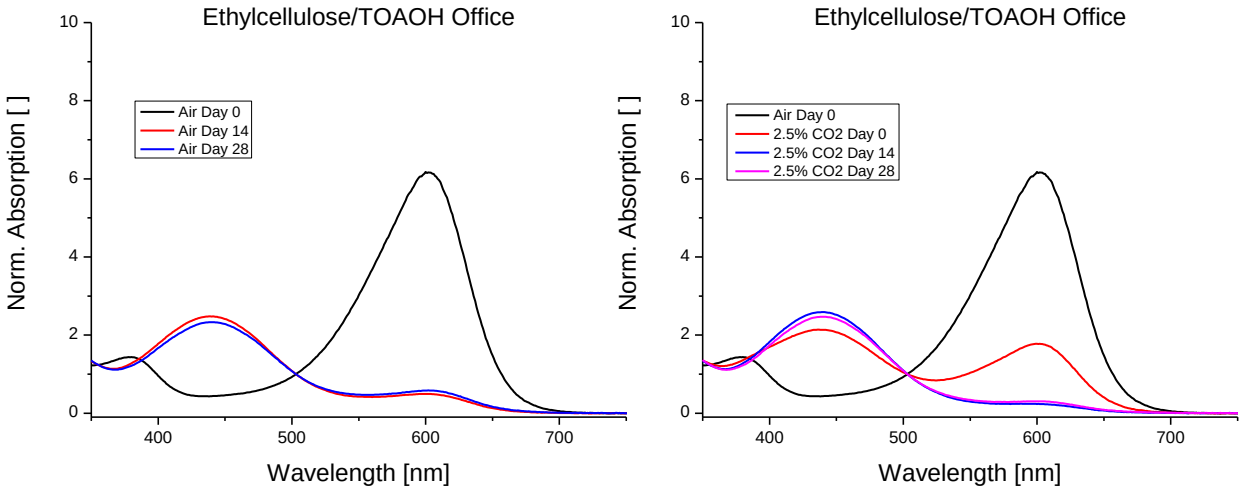

Figure 5.2.2.10: Ethylcellulose in combination with TOAOH kept under office conditions

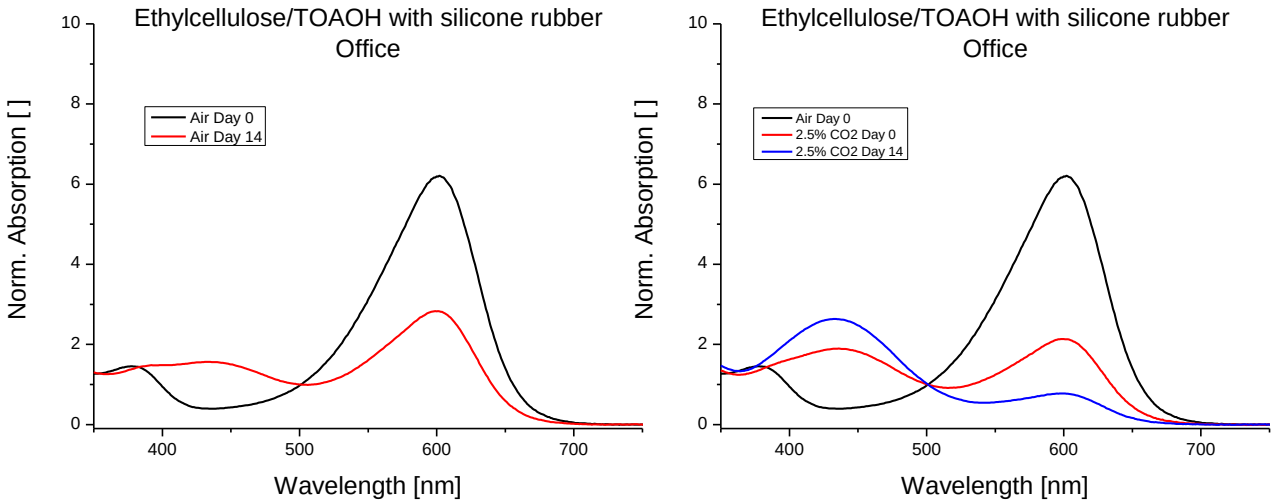

Figure 5.2.2.11: Ethylcellulose in combination with TOAOH kept under office conditions with a protective layer of silicone rubber

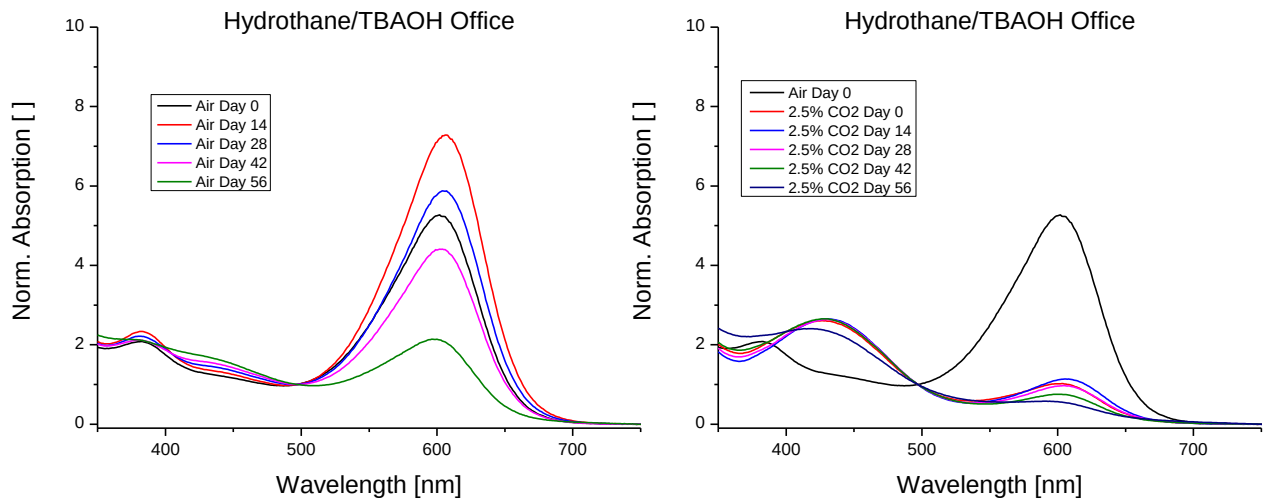

Figure 5.2.2.12: HydroThane in combination with TBAOH kept under office conditions

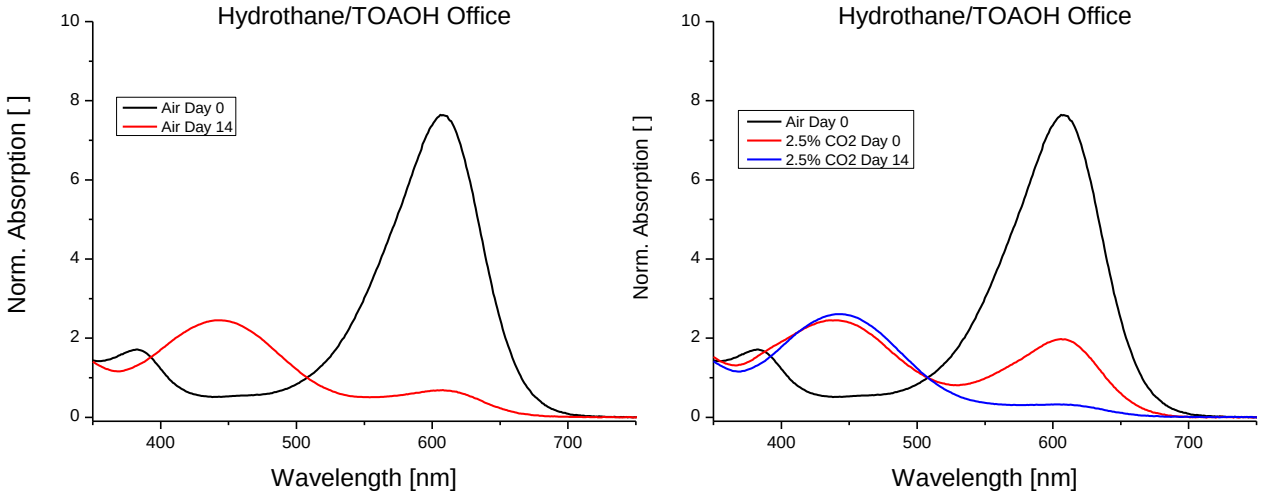

Figure 5.2.2.13: HydroThane in combination with TOAOH kept under office conditions

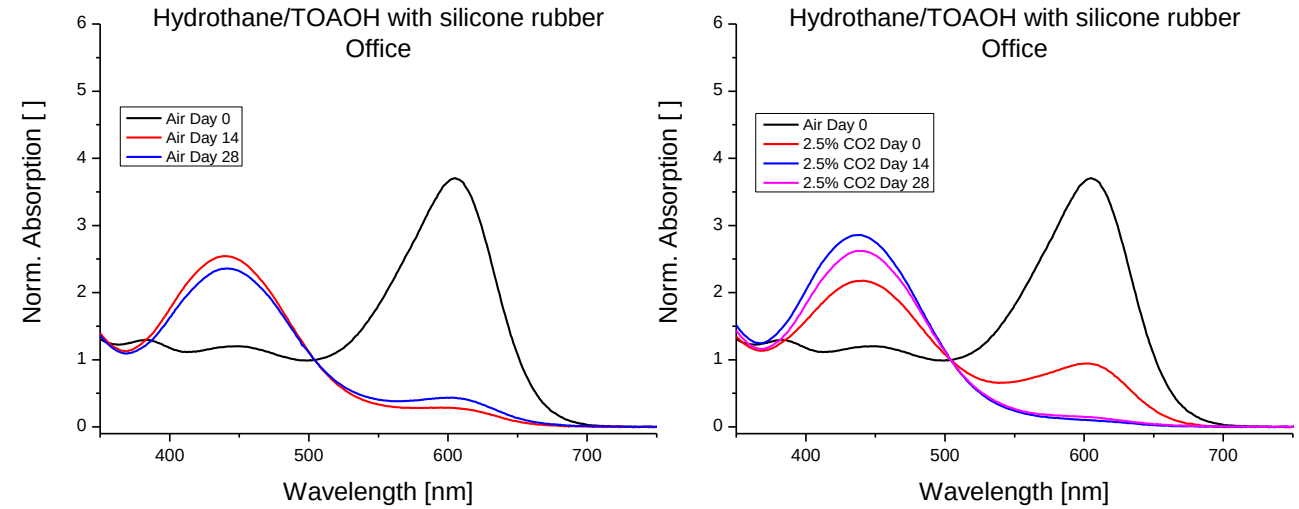

Figure 5.2.2.14: HydroThane in combination with TOAOH kept under office conditions with a protective layer of silicone rubber

As figures 5.2.2.1 to 5.2.2.14 show, the silicone rubber layer only has a minor impact on the sensor's long-term stability. The same trend is noticeable in regard to the silicone rubber protected sensors in the other storage conditions.

Even though it was suspected that the laboratory conditions would be the most extreme and age the sensors the fastest, the long-term stability test suggests that the slight difference in temperature in comparison to the lab made the office conditions the ones that affected the sensors the most. While the laboratory is temperature regulated at 22°C, the office temperatures are not regulated and always fluctuate above that level. This shows in regards to the faster rate at which the sensors with a low base concentration turn yellow under office conditions compared to laboratory conditions.

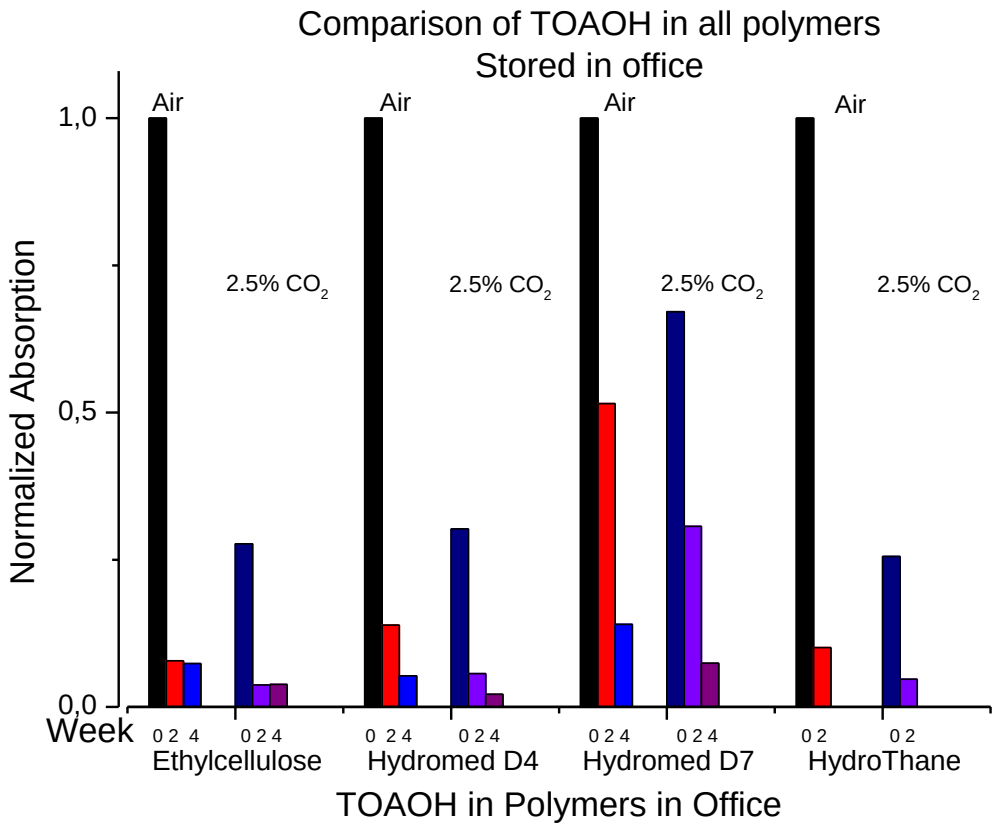

Figure 5.2.2.15: Comparison of TOAOH in the different bases stored under office conditions

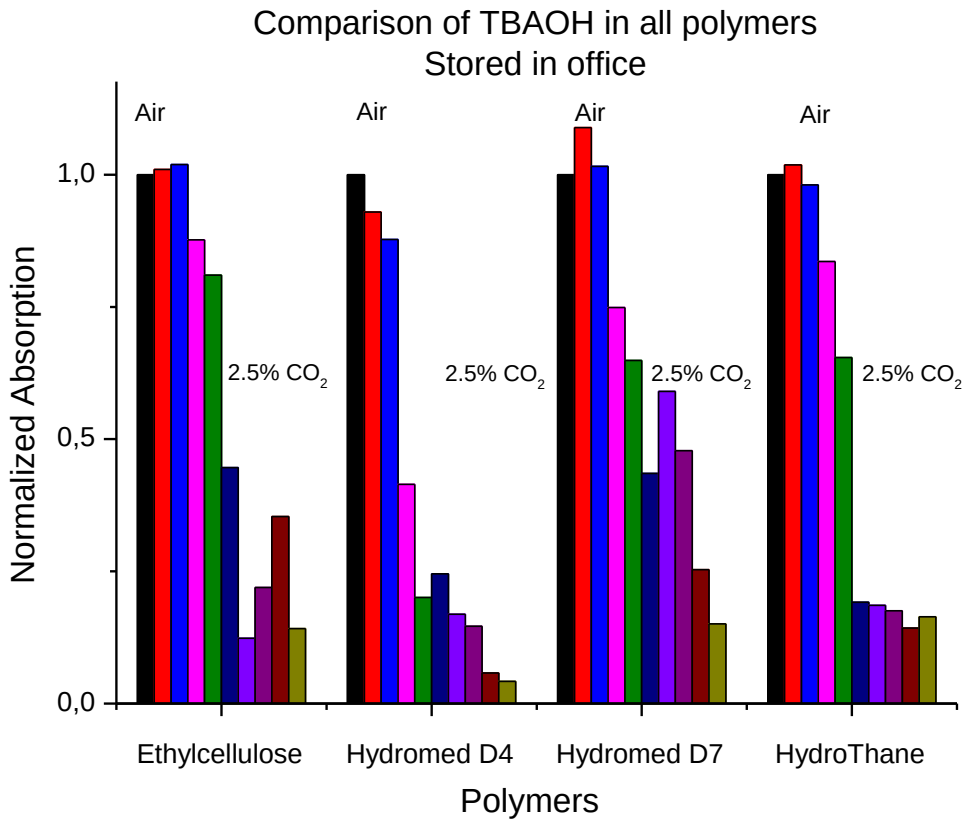

Figure 5.2.2.16: Comparison of TBAOH in the different bases stored under office conditions

Hydrothane stands out in figure 5.2.2.16, as the spectra in this matrix show the least fluctuation over time. A higher base concentration increases the long-term stability under these conditions as well, as was to be expected.

5.2.3. Outside storage conditions

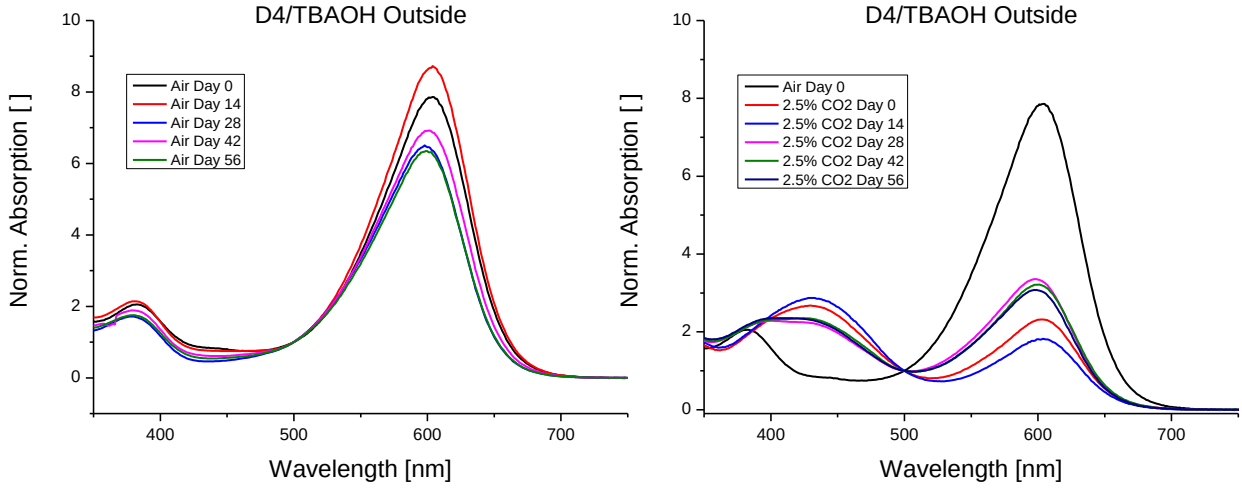

Figure 5.2.3.1: Hydromed D4 in combination with TBAOH kept under outside storage conditions

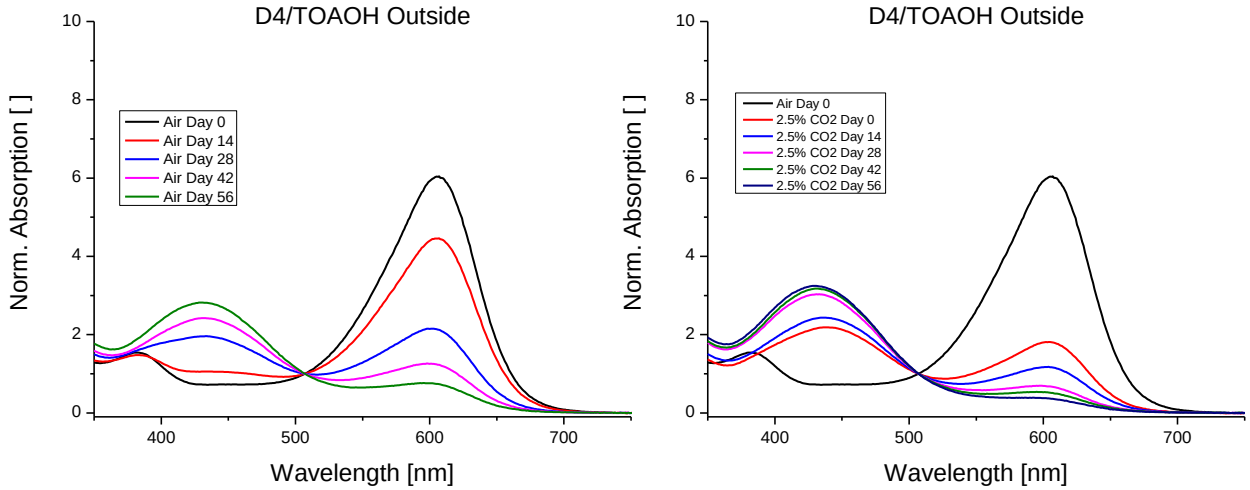

Figure 5.2.3.2: Hydromed D4 in combination with TOAOH kept under outside storage conditions

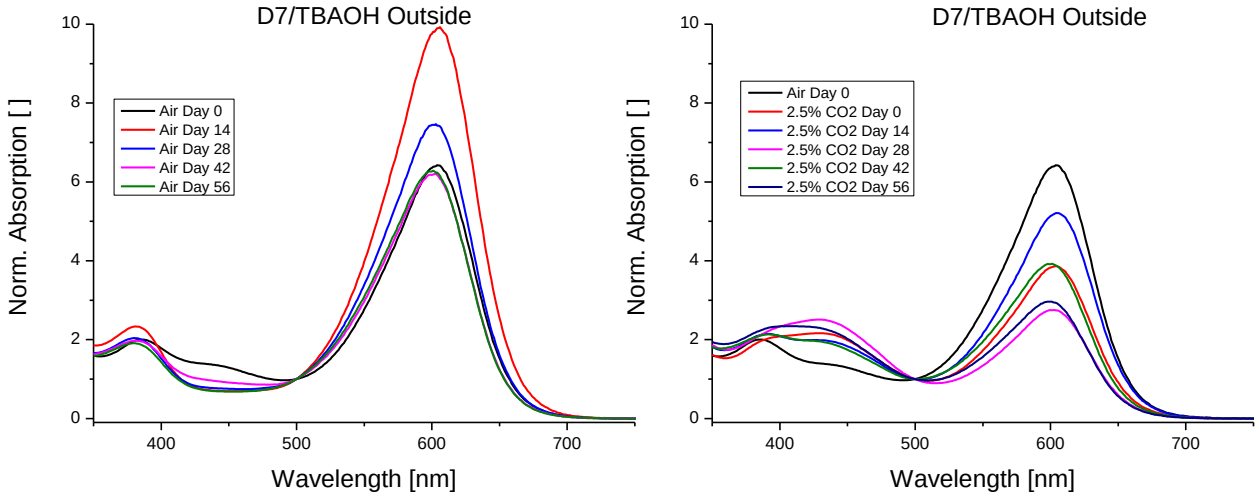

Figure 5.2.3.3: Hydromed D7 in combination with TBAOH kept under outside storage conditions

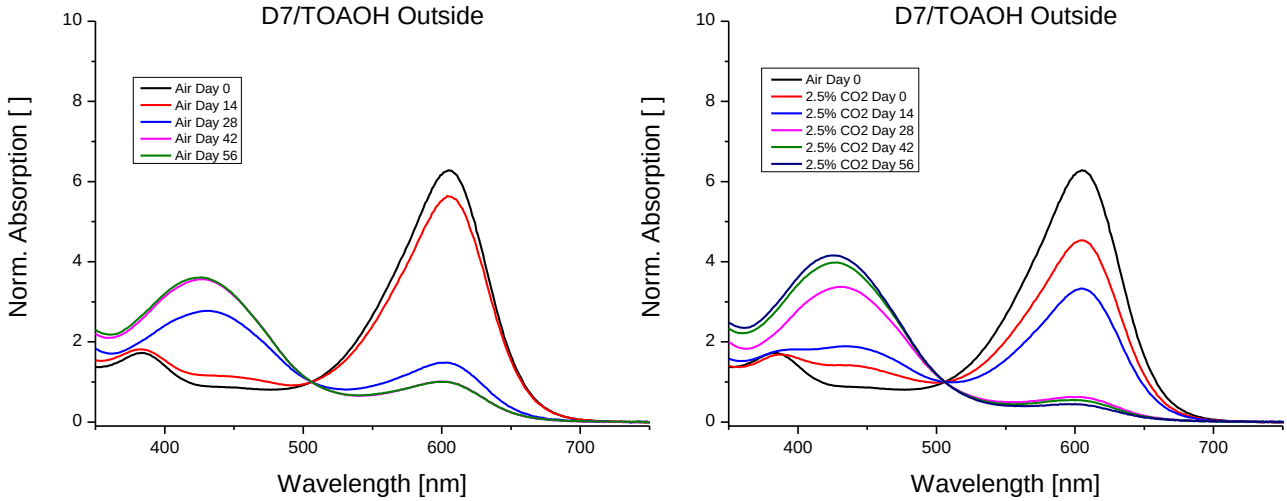

Figure 5.2.3.4: Hydromed D7 in combination with TOAOH kept under outside storage conditions

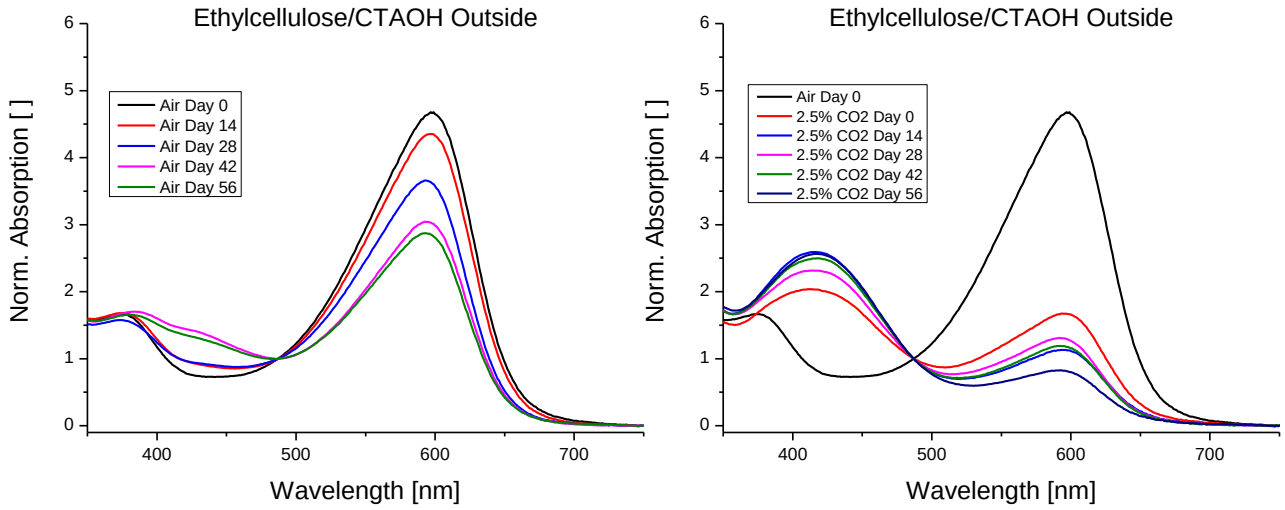

Figure 5.2.3.5: Ethylcellulose in combination with CTAOH kept under outside storage conditions

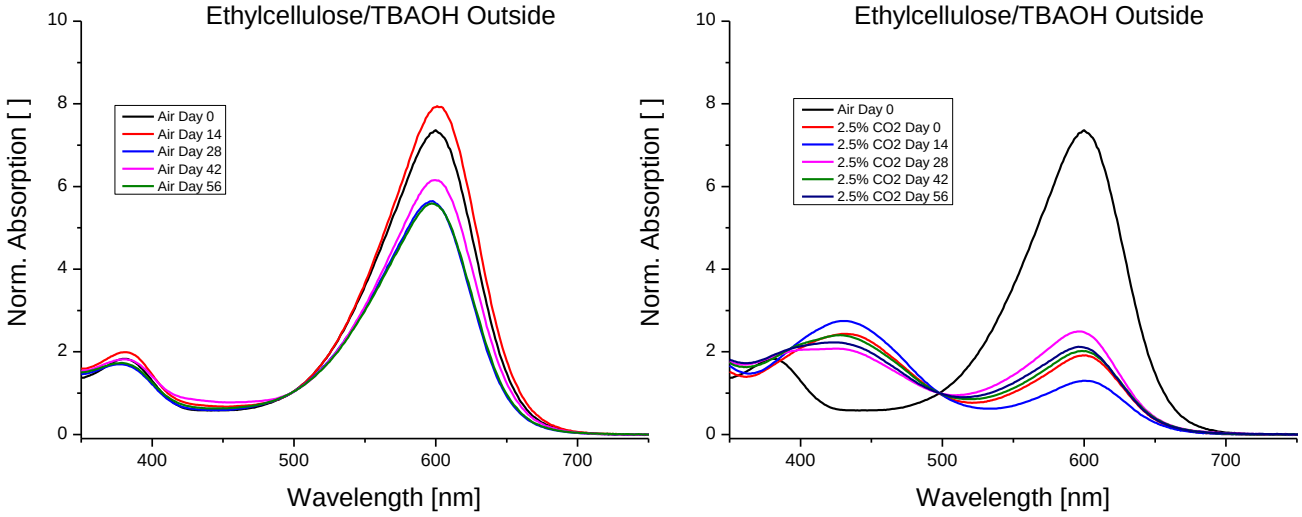

Figure 5.2.3.6: Ethylcellulose in combination with TBAOH kept under outside storage conditions

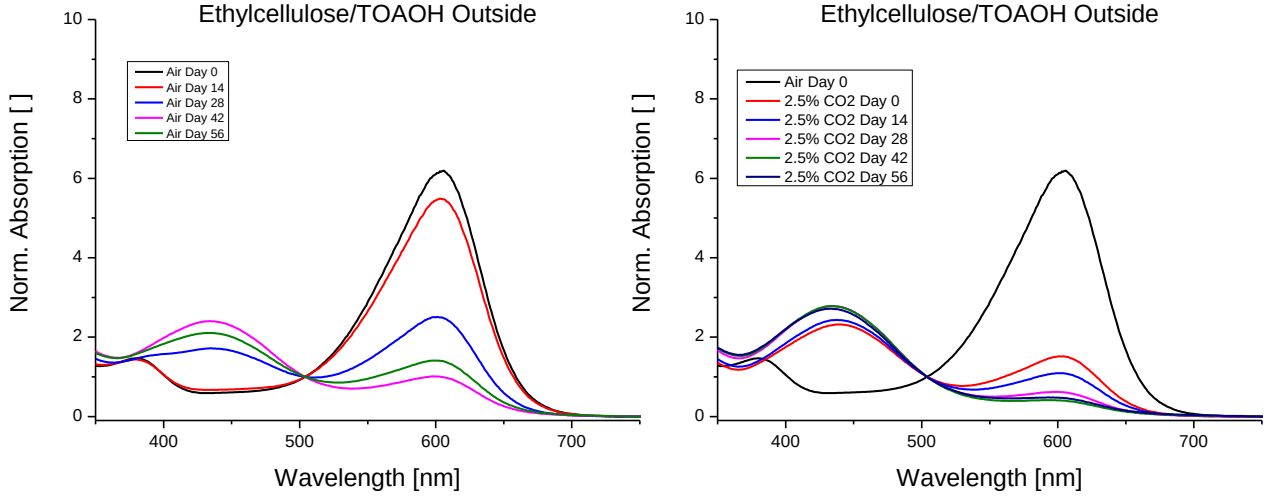

Figure 5.2.3.7: Ethylcellulose in combination with TOAOH kept under outside storage conditions

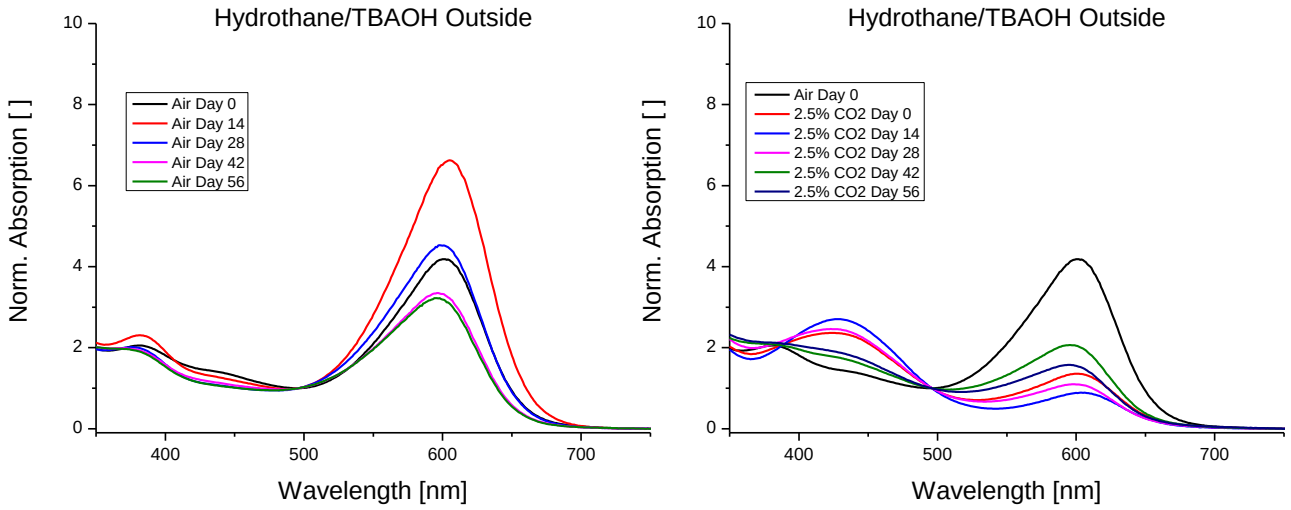

Figure 5.2.3.8: HydroThane in combination with TBAOH kept under outside storage conditions

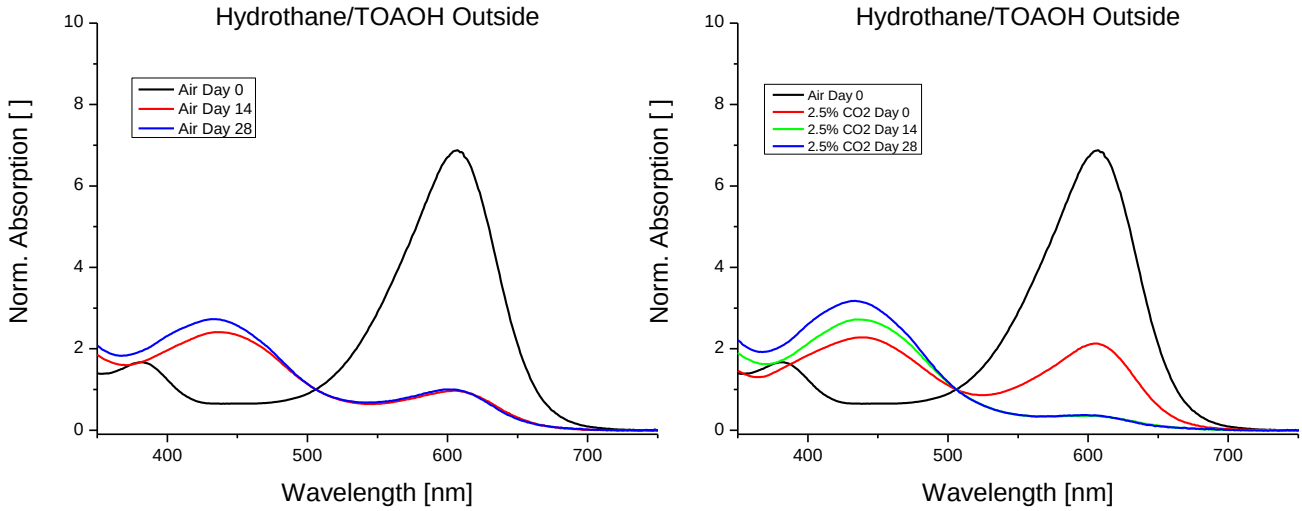

Figure 5.2.3.9: HydroThane in combination with TOAOH kept under outside storage conditions

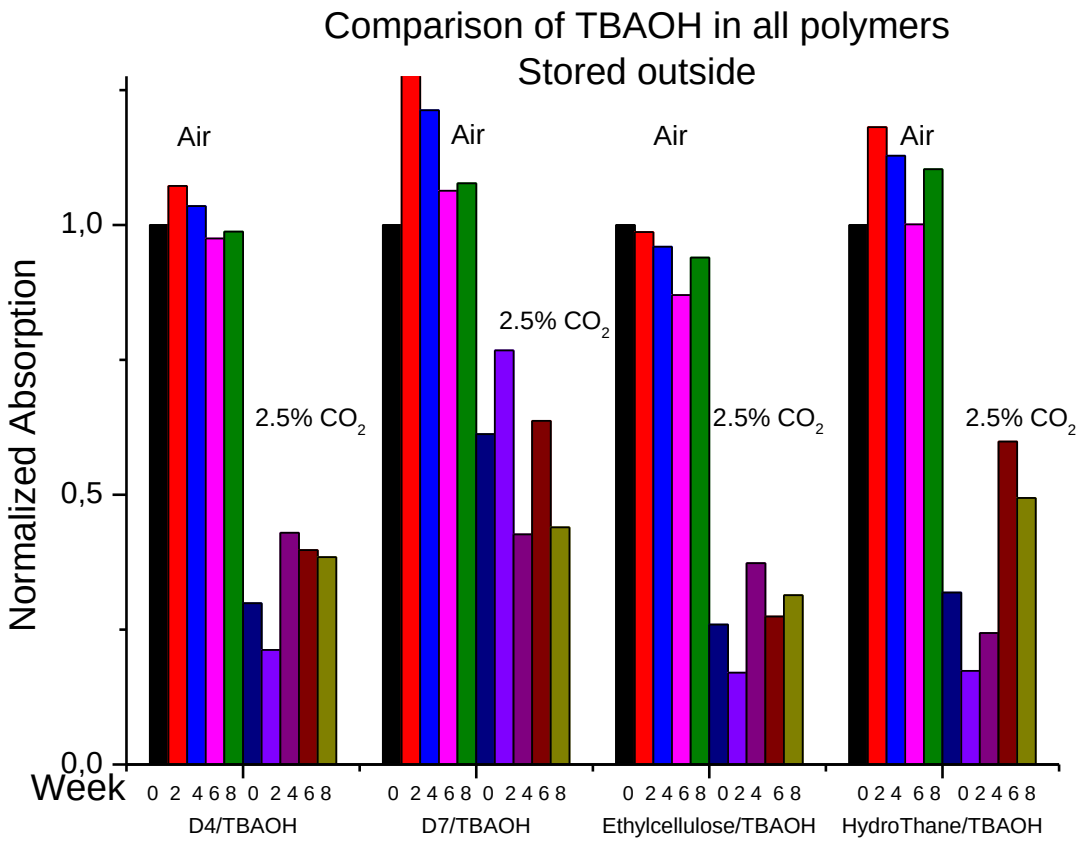

Figure 5.2.3.10: Comparison of TBAOH in the different polymers under outside storage conditions

The outliers in week 6 and 8 are probably due to a constriction of the gas flow during the experiment due to a blockage in the setup.

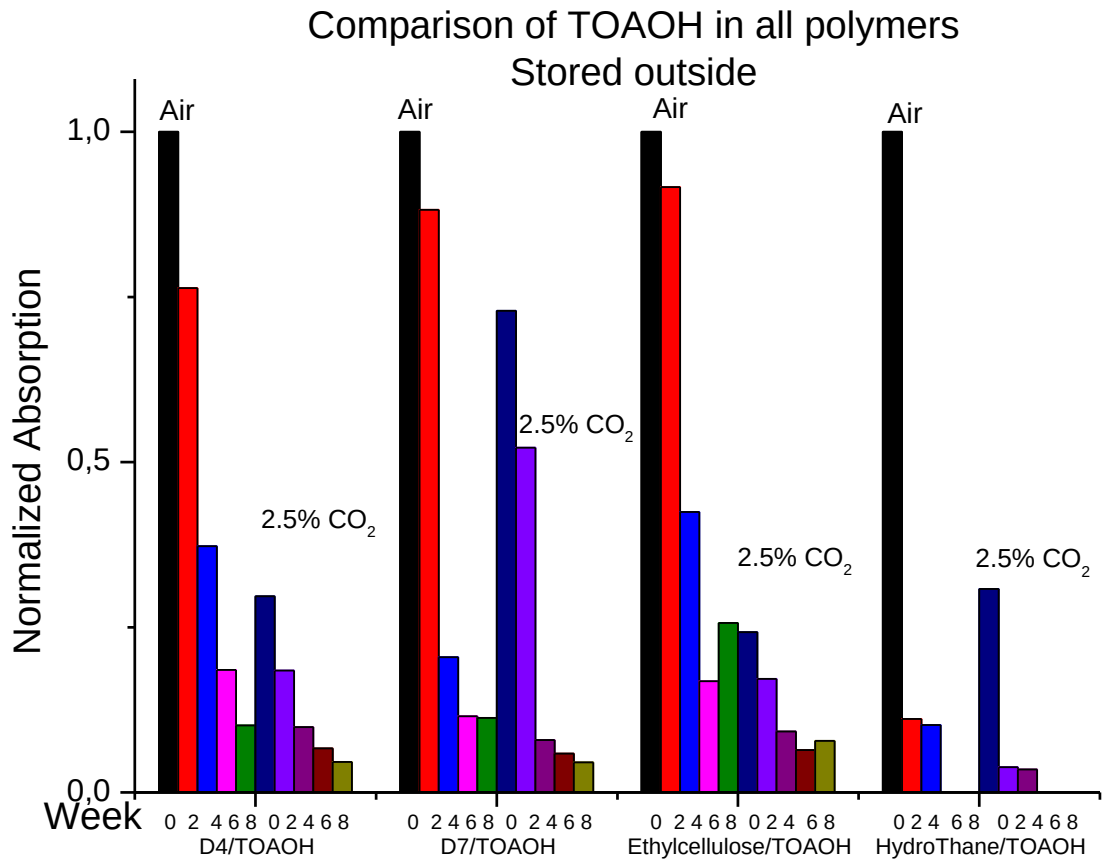

Figure 5.2.3.11: Comparison of TOAOH in the different polymers under outside storage conditions

Overall the sensors that were stored outside show far less drift than the ones in the laboratory or office conditions. This is in all likelihood due to the fact that they were stored outside from the beginning of October to December. During this time the temperatures varied between 20°C and -5°C which conserved the sensors much better. The sensors still showed decay, especially during the first weeks of the stability test, when the temperatures still remained in the 5 to 20°C range.

5.2.4. Ideal storage conditions

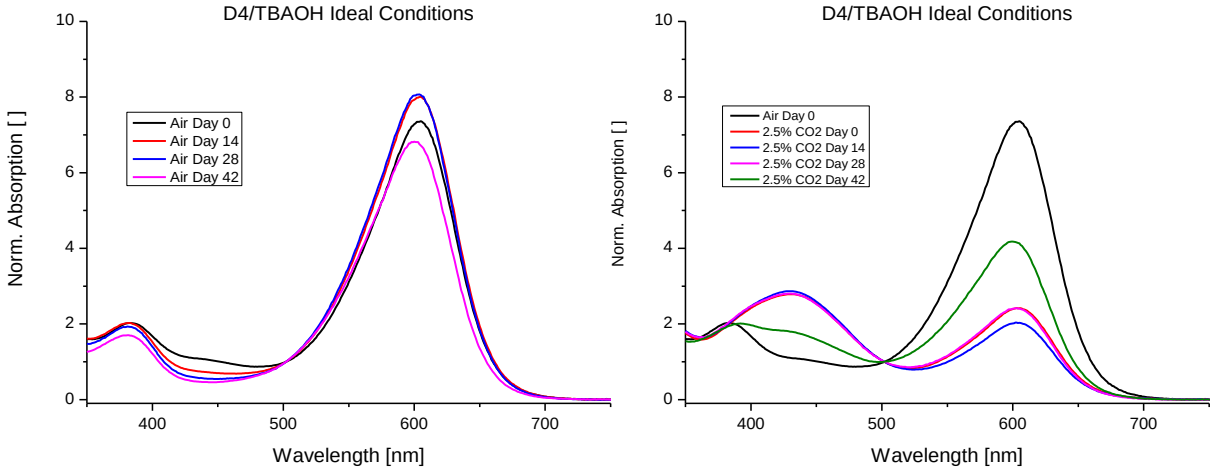

Figure 5.2.4.1: Hydromed D4 in combination with TBAOH kept under ideal storage conditions

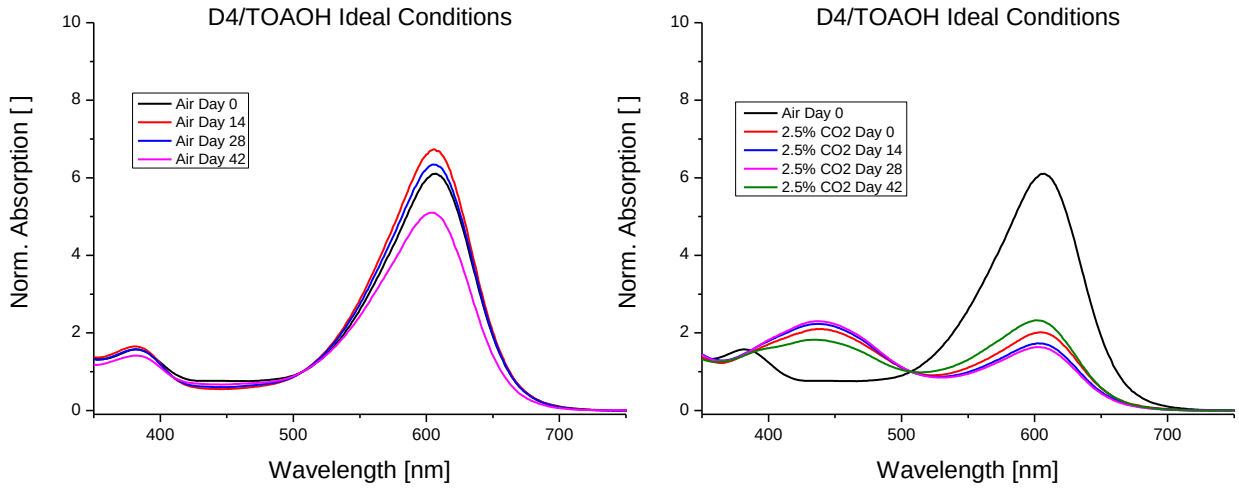

Figure 5.2.4.2: Hydromed D4 in combination with TOAOH kept under ideal storage conditions

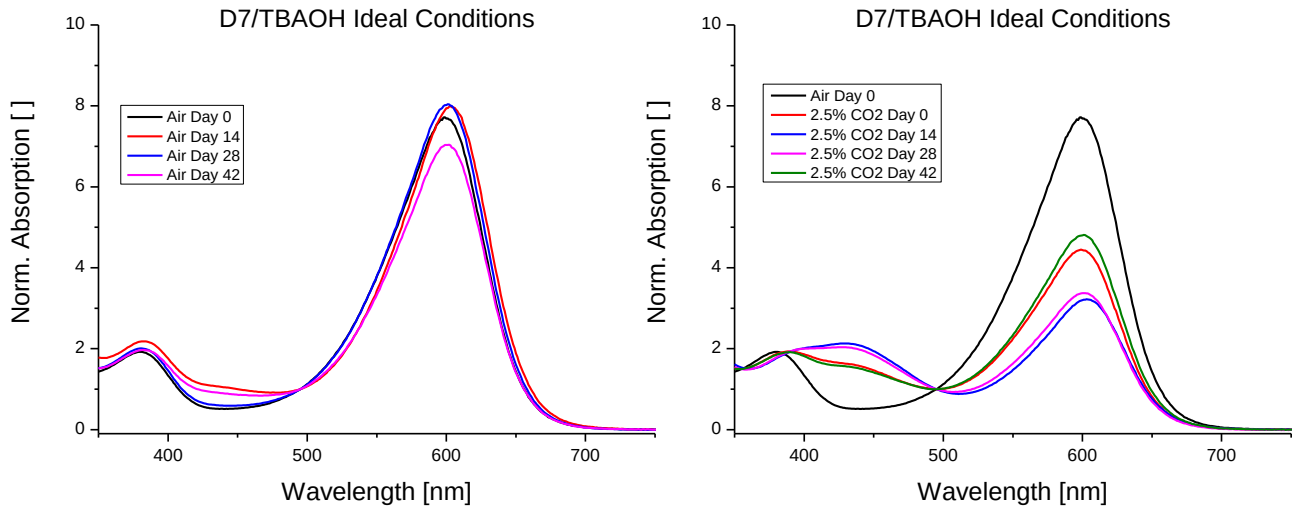

Figure 5.2.4.3: Hydromed D7 in combination with TBAOH kept under ideal storage conditions

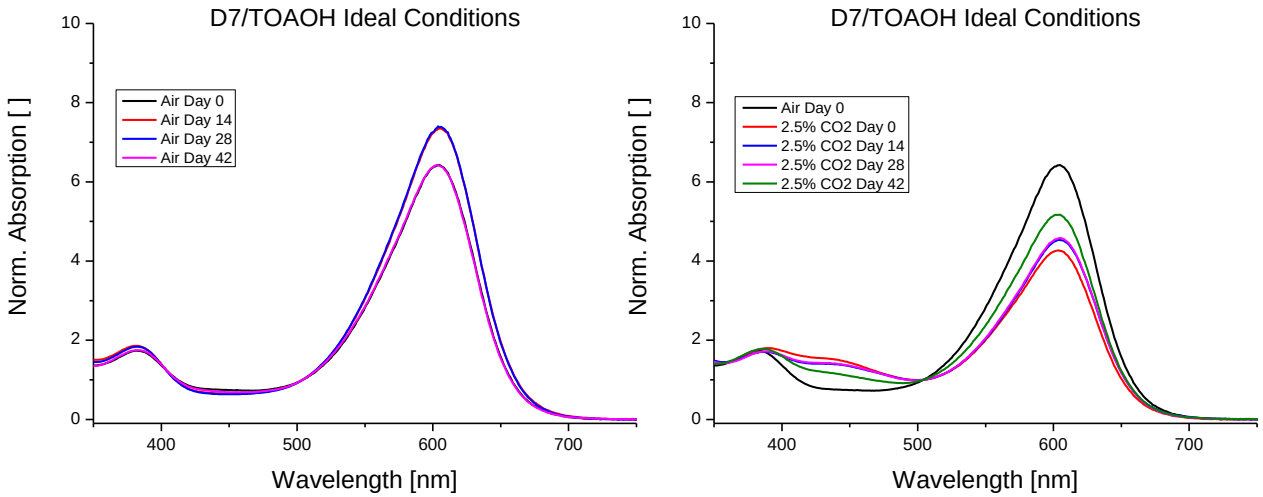

Figure 5.2.4.4: Hydromed D7 in combination with TOAOH kept under ideal storage conditions

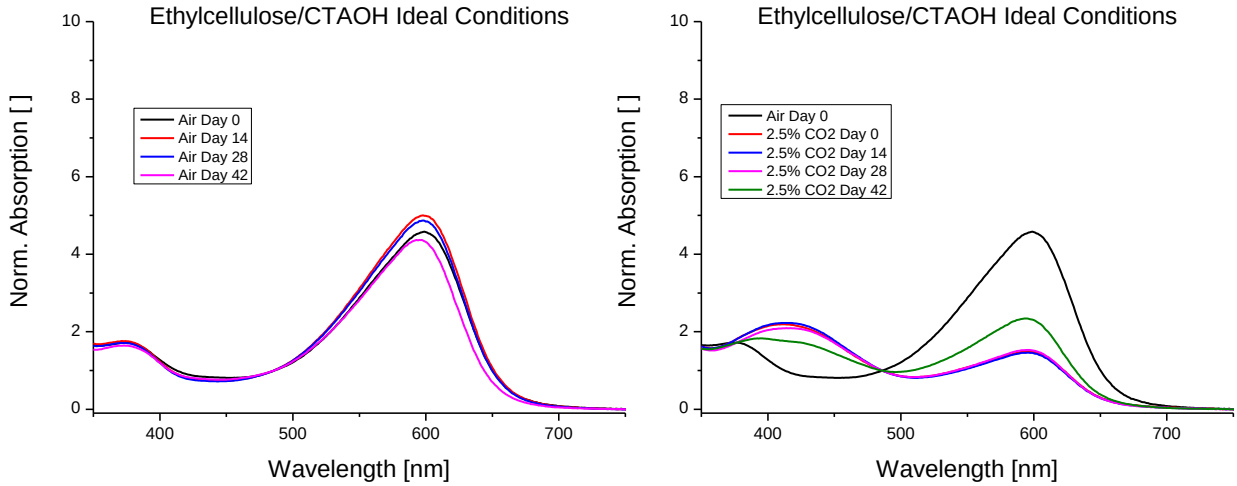

Figure 5.2.4.5: Ethylcellulose in combination with CTAOH kept under ideal storage conditions

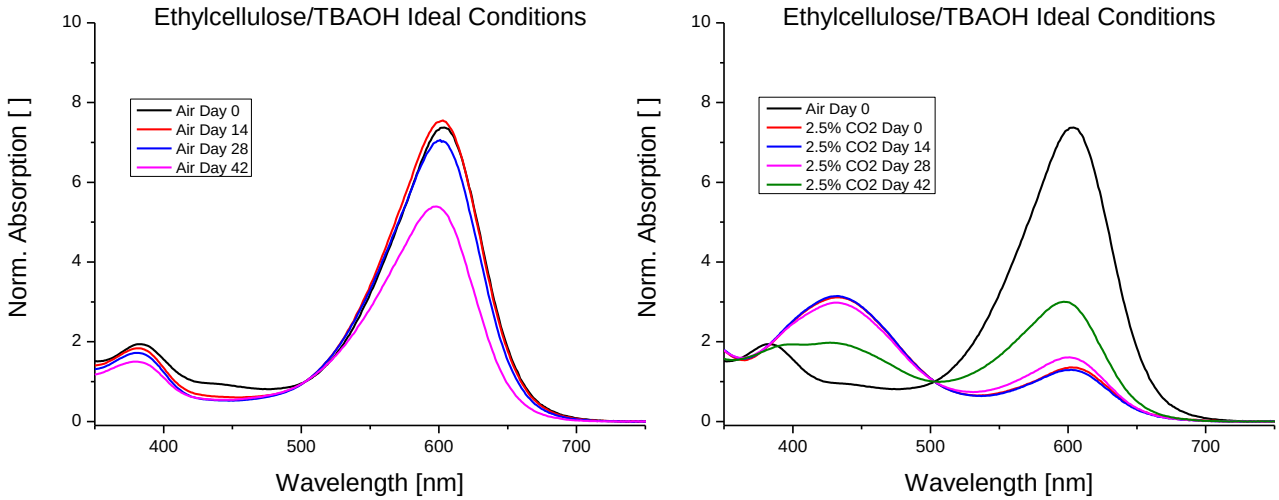

Figure 5.2.4.6: Ethylcellulose in combination with TBAOH kept under ideal storage conditions

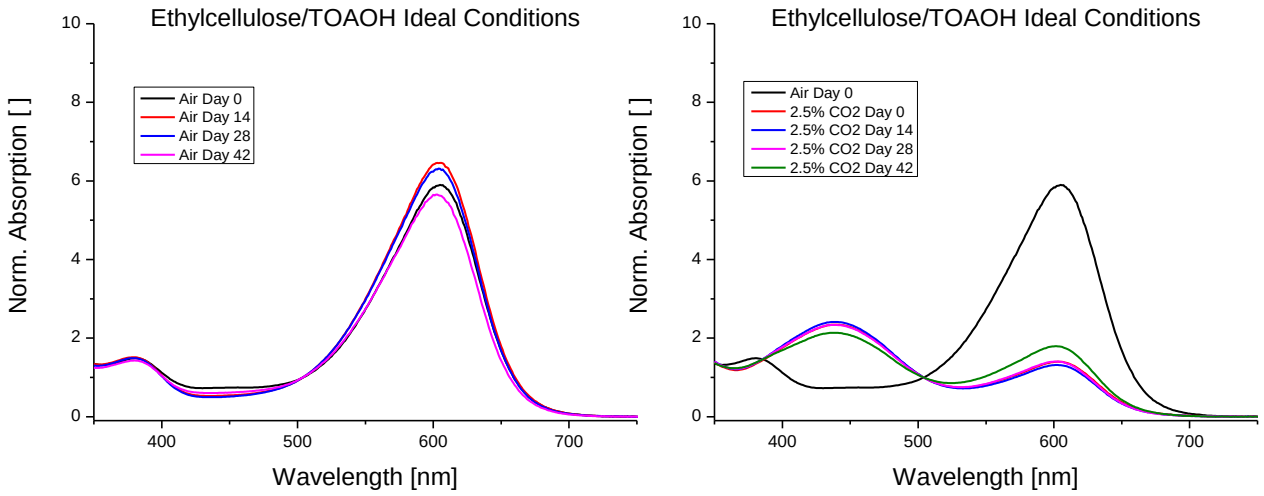

Figure 5.2.4.7: Ethylcellulose in combination with TOAOH kept under ideal storage conditions

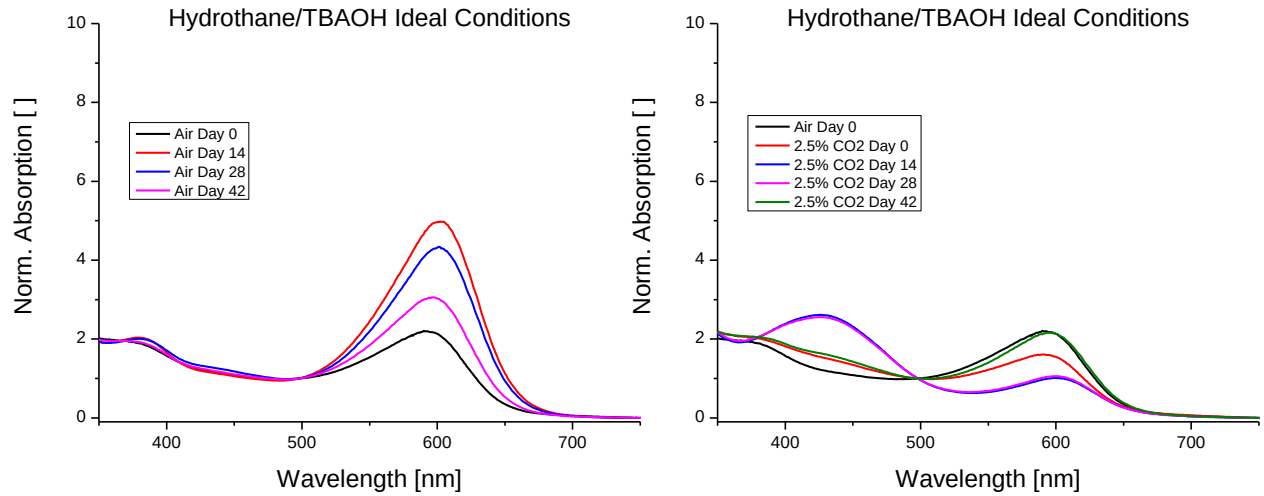

Figure 5.2.4.8: HydroThane in combination with TBAOH kept under ideal storage conditions

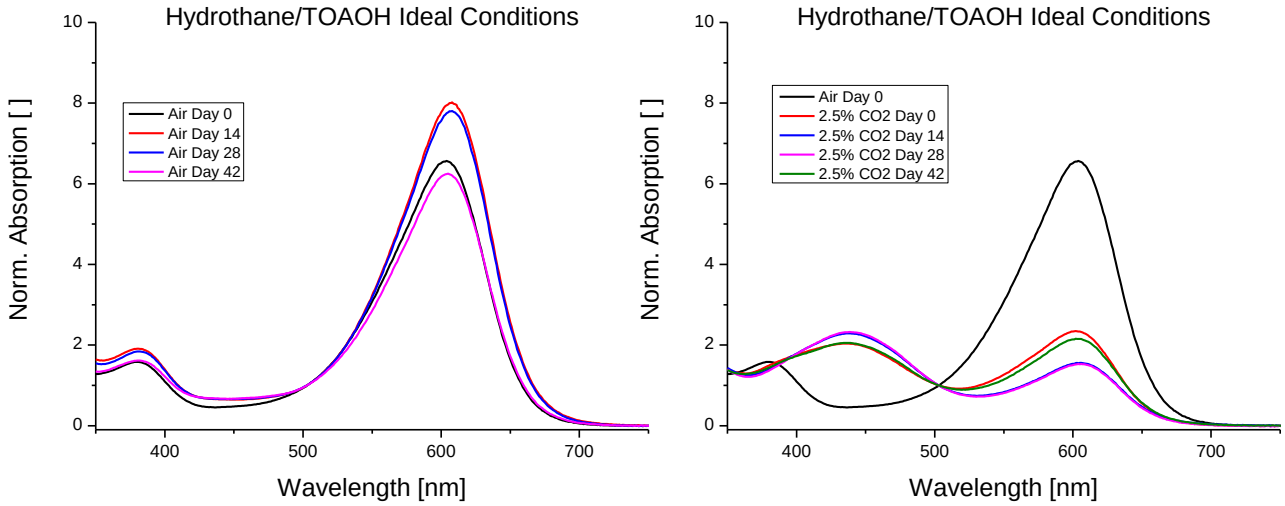

Figure 5.2.4.9: HydroThane in combination with TOAOH kept under ideal storage conditions

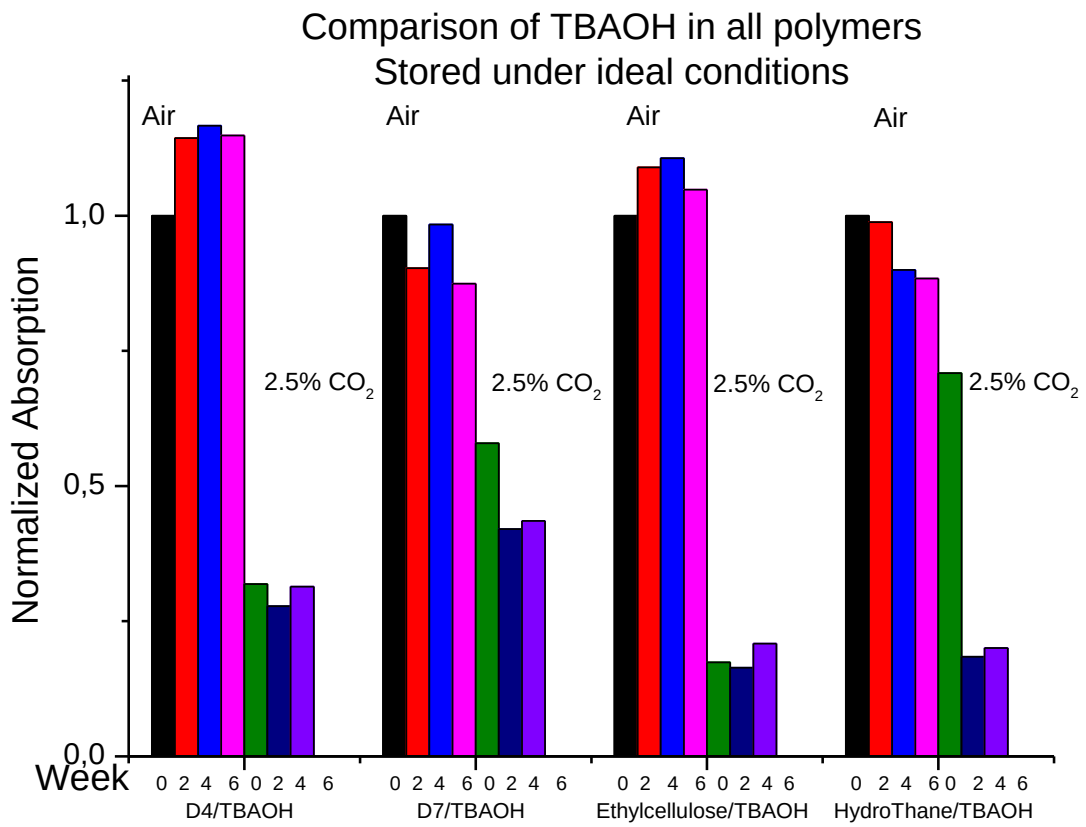

Figure 5.2.4.10: Comparison of TBAOH in the different polymers under ideal storage conditions

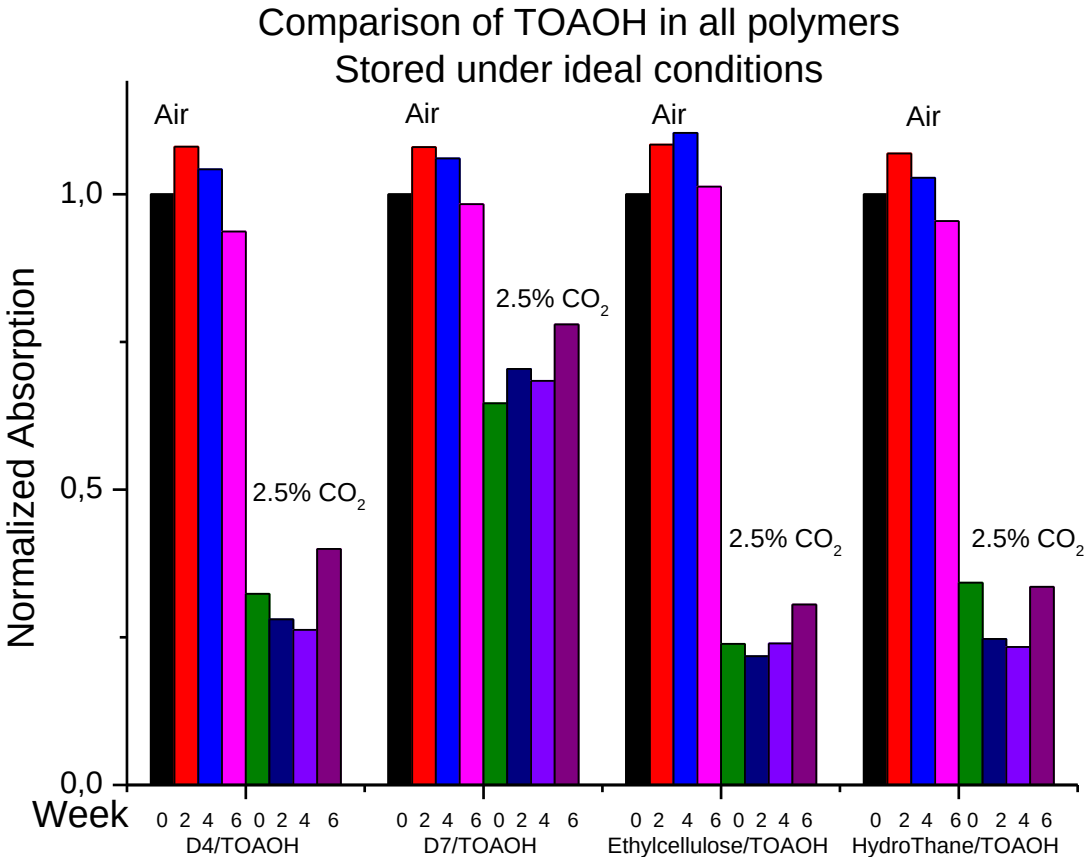

Figure 5.2.4.11: Comparison of TOAOH in the different polymers under ideal storage conditions

The sensors stored under what was referred to as 'the ideal conditions', meaning 5-8°C under CO_2 atmosphere in darkness, showed the least decay as was expected. The CO_2 atmosphere protected the sensors against acidic components found in air. All sensors remained usable throughout the duration of the long-term stability test. However, the response time of HydroMed D7 in combination with silicone rubber as a protective layer increased significantly throughout the test.

The slight sensor drifts displayed in the spectra are due to the fact, that while the ideal conditions were kept as good as practically possible, the sensors were stored between layers of paper, which may be the cause of minor contamination. The sensors also remained under air atmosphere for 2 hours in 14 day intervals as the sensors were measured in the measurement cell to obtain the current spectra, which also poses a chance for contamination.

5.2.5. Comparison of bases in different storage conditions

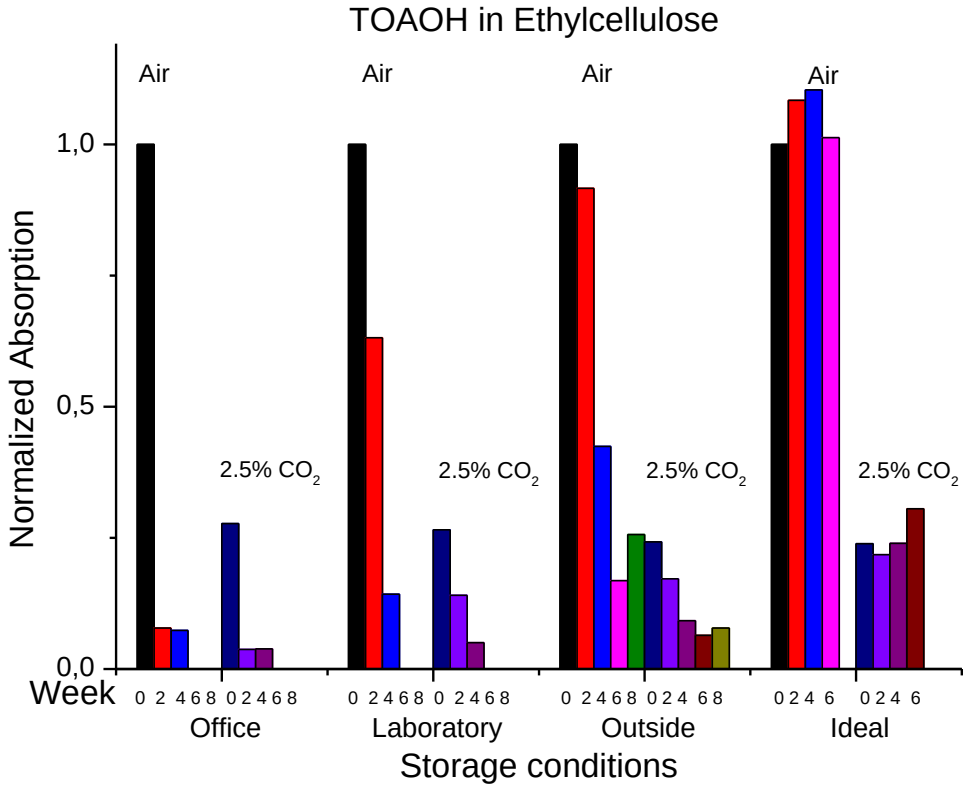

Figure 5.2.5.1: Comparison of TOAOH in ethylcellulose under different storage conditions

Figure 5.2.5.1 shows that while the sensors with 0.04 mmol base/100 mg polymer are contaminated very quickly, the storage under ideal condition insures that the sensors barely drift and remain usable for months.

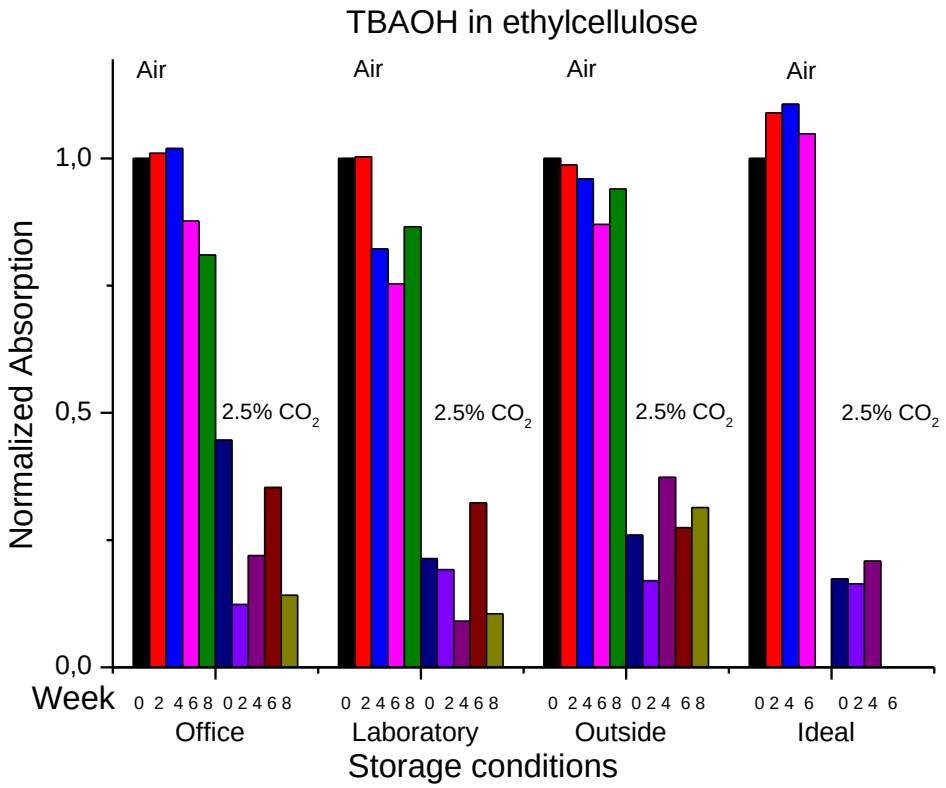

Figure 5.2.5.2: Comparison of TBAOH in ethylcellulose under different storage conditions

With a base concentration as high as 0.15 mmol/100 mg polymer the sensors remain deprotonated and usable for over two months. A higher base concentration as a buffer for acidic substances presents a possibility to increase the long-term stability of a sensor.

5.2.6. Comparison of base stability

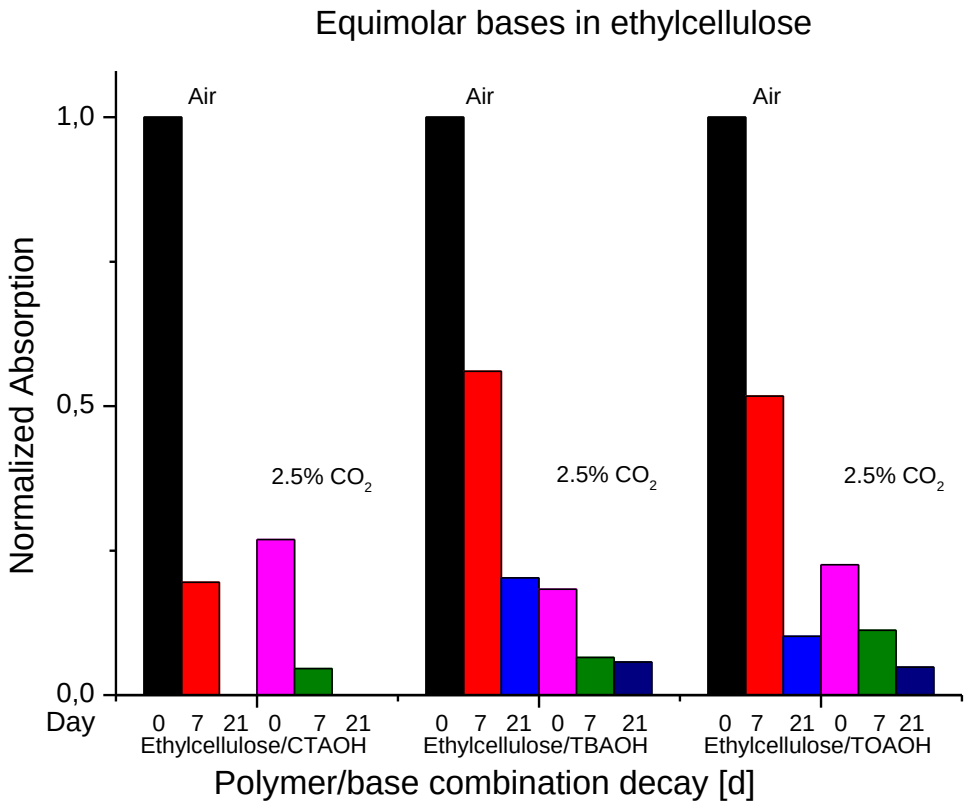

Figure 5.2.6.1: Comparison of the stability of the individual bases in ethylcellulose under office conditions

Since the bases were added in different concentrations it was necessary to determine which of the bases showed the greatest stability when the bases were added to a matrix in equal concentrations. Three sensors were made containing ethylcellulose, m-cresol purple and 0.04 mmol/100 mg of one of the bases. The sensors were stored under office conditions to accelerate their aging process. After only six days the CTAOH sensors were completely protonated, while the TOAOH sensors still showed patches of small deprotonated areas on day 8. After 12 days only one of the pre-cut TBAOH stripes still showed deprotonated areas, leading to the conclusion that at equal concentrations TBAOH shows a minor advantage of TOAOH when it comes to long-term stability.

5.3. Long term stability improvement through protective layers

The protective layers were coated over a 3.75 µm film of an ethylcellulose/tetraoctyl ammonium hydroxide sensor as this is the current state of the art composition for an optical CO_2 sensor. The protective layers were coated with the following thickness:

- Silicone rubber (20 µm)
- Silicone rubber (20µm) /SiO_2/D7 (6.7 µm)
- Silicone rubber (20µm) /SiO_2/PolyHEMA (6.7 µm)
- Hyflon® AD 60 (4.3 µm)
- Hyflon® AD 60 (4.3 µm) + ethylcellulose/TBAOH (10 µm) + Hyflon® AD 60 (7 µm)

It was not possible to produce a sensor foil with silicone rubber and polyvinylalcohol, as the polyvinylalcohol would disperse over the silicone surface even with silicone dioxide particles that were used as surface modifying particles to make the additional protective layers stick to the underlying silicone rubber layer.

The figures 5.3.1 to 5.3.7 show the normalized spectra obtained during the weeks in which the sensors were measured.

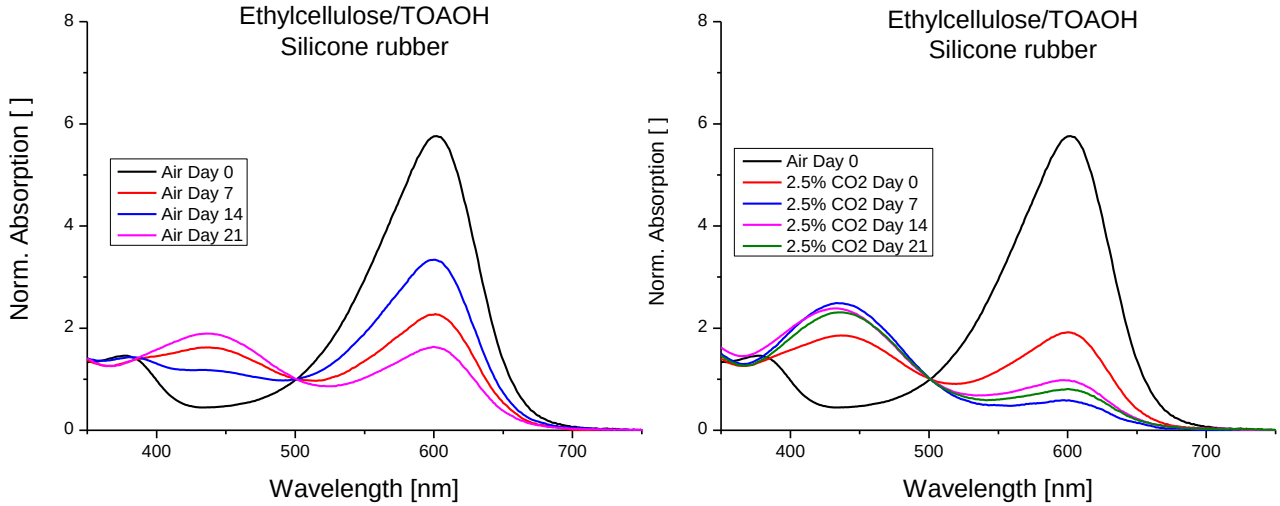

Figure 5.3.1: Spectrophotometric determination of the aging process in ethylcellulose/TOAOH sensors with a silicone rubber protective layer

The spectra show the same rapid decay they showed in the previous long term stability test for this combination.

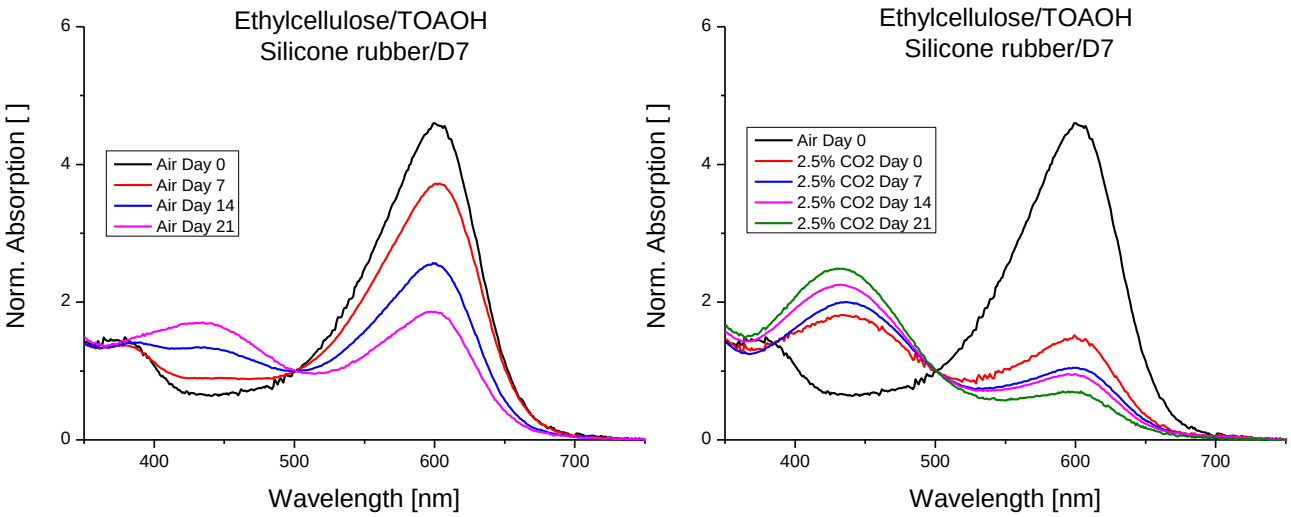

Figure 5.3.2: Spectrophotometric determination of the aging process in ethylcellulose/TOAOH sensors with a silicone rubber protective layer and an additional layer of Hydromed D7

The SiO_2 nanoparticles produce a slight light-scattering effect in the spectra. In addition to that the sensors show approximately the same stability as the sensors with a plain silicone rubber layer for protection.

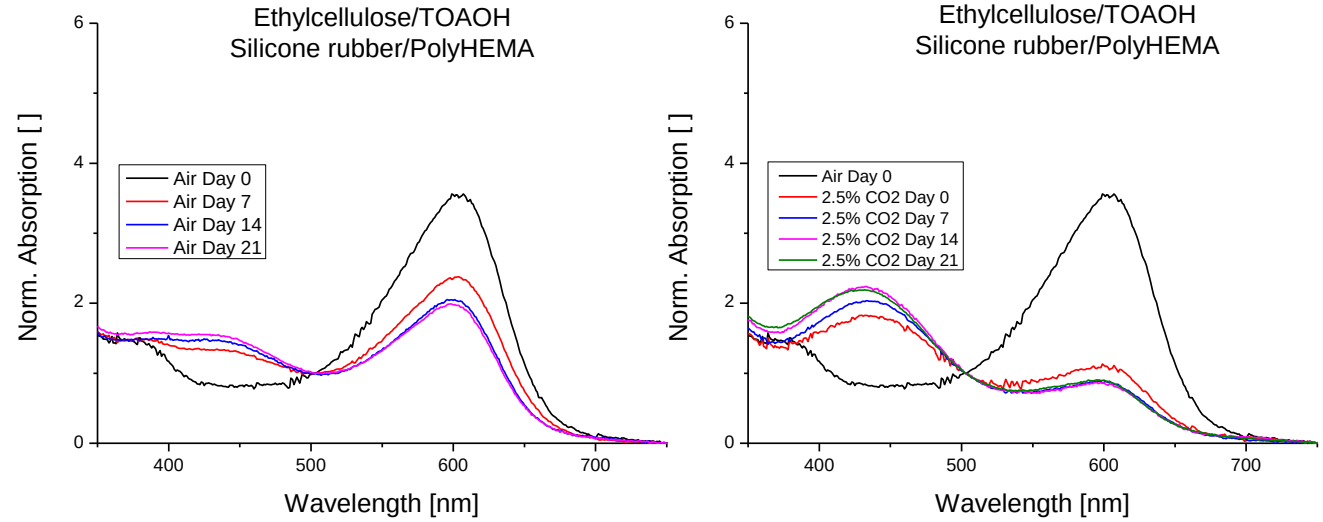

Figure 5.3.3: Spectrophotometric determination of the aging process in ethylcellulose/TOAOH sensors with a silicone rubber protective layer and an additional layer of PolyHEMA

The rapid decay in this sensor is due to the fact that the silicone rubber/SiO_2/PolyHEMA layer peeled off the sensor layer of the stripes only 2 hours after they were cut. The layer on the bulk piece remained intact. However the sensor started showing cracks and decay after only three days as can be seen in figure 5.3.4.

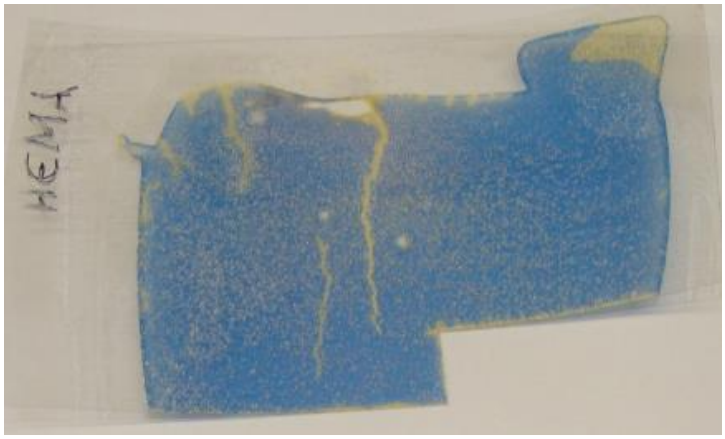

Figure 5.3.4: Ethylcellulose/TOAOH sensor with silicone rubber/SiO_2/PolyHEMA protective layer in bulk after only three days of the stability test

The sensor film shows a brittle quality that promoted decay throughout the sensor rather than just on the edges of the film where decay usually starts.

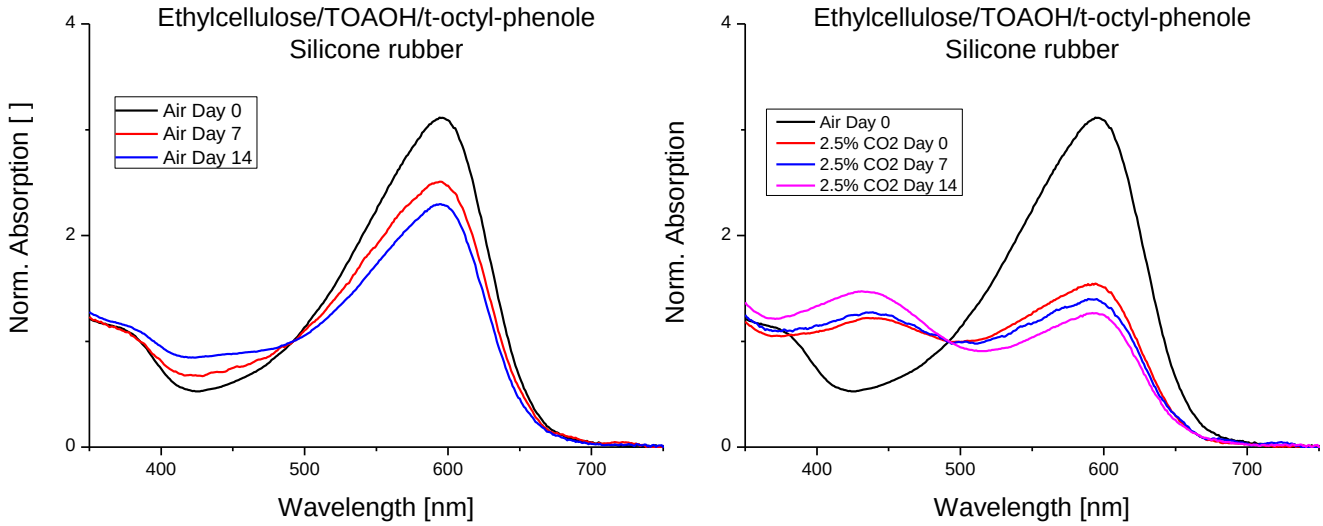

Figure 5.3.5: Spectrophotometric determination of the aging process in ethylcellulose/TOAOH sensors with t-octyl phenol as counter ion and a silicone rubber protective layer

As the effects of a change in counter ions in the sensor were tested, the impact a different counter ion has on the long term stability of the sensor was also to be determined. The test shows that the ion doesn't seem to make a big difference to the aging process of the sensor.

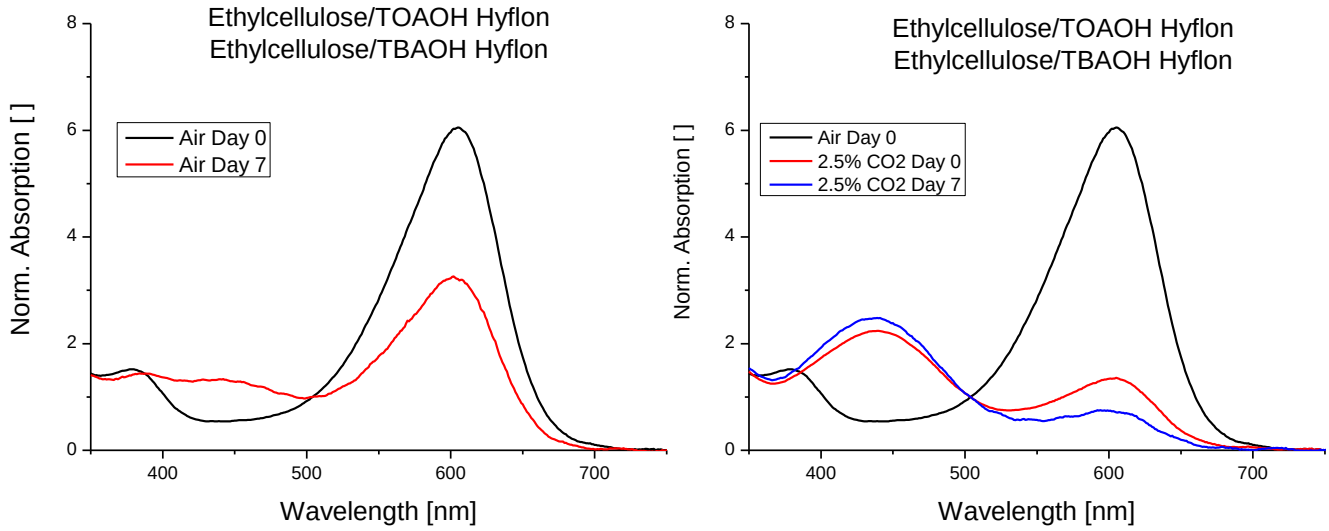

Figure 5.3.6: Spectrophotometric determination of the aging process in ethylcellulose/TOAOH sensors with Hyflon® AD 60, ethylcellulose/TBAOH, Hyflon® AD 60 protective multilayer system

Much like the silicone rubber/silicone dioxide/polyHEMA system this multilayer system peeled off the initial sensor layer in a matter of hours. In this case the layers also peeled off the big piece of sensor foil. Accordingly, the aging of the sensor was rapid.

The Hyflon® AD 60 layer showed remarkable protective properties when coated on the sensor film. The sensor remained deprotonated throughout the duration of the stability test and showed very little drift as shown in the spectra in Fig. 5.3.7. A visual comparison shows the difference between the Hyflon® AD 60 layer and the silicone rubber layer vividly, as depicted in Fig. 5.3.8.

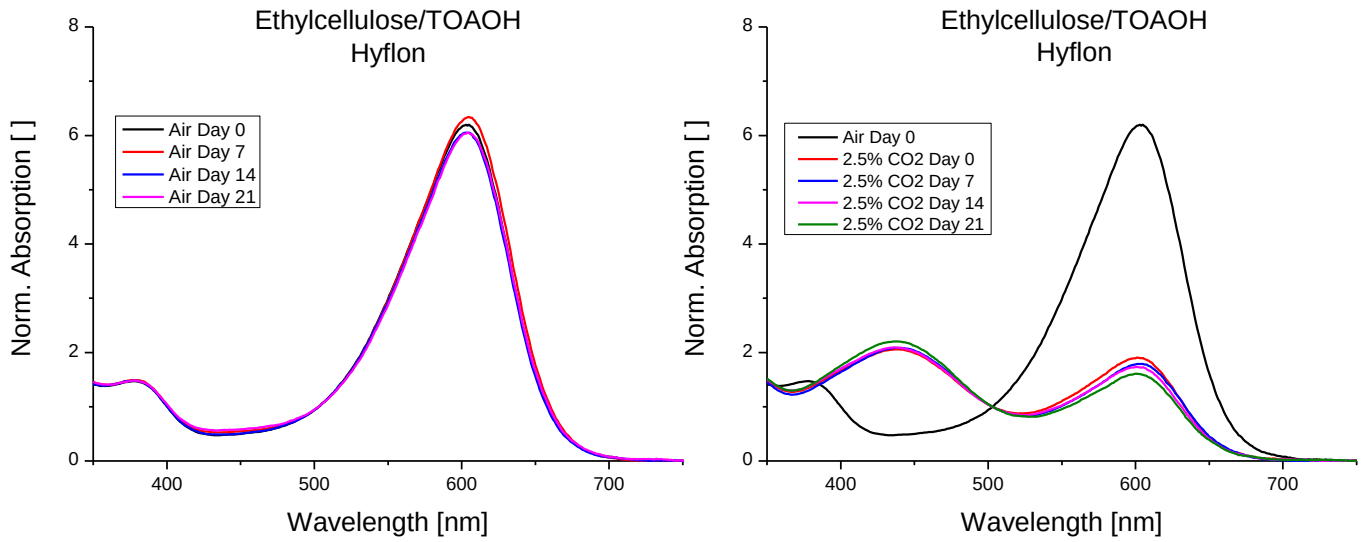

Figure 5.3.7: Spectrophotometric determination of the aging process in ethylcellulose/TOAOH sensors with Hyflon® AD 60 protective layer

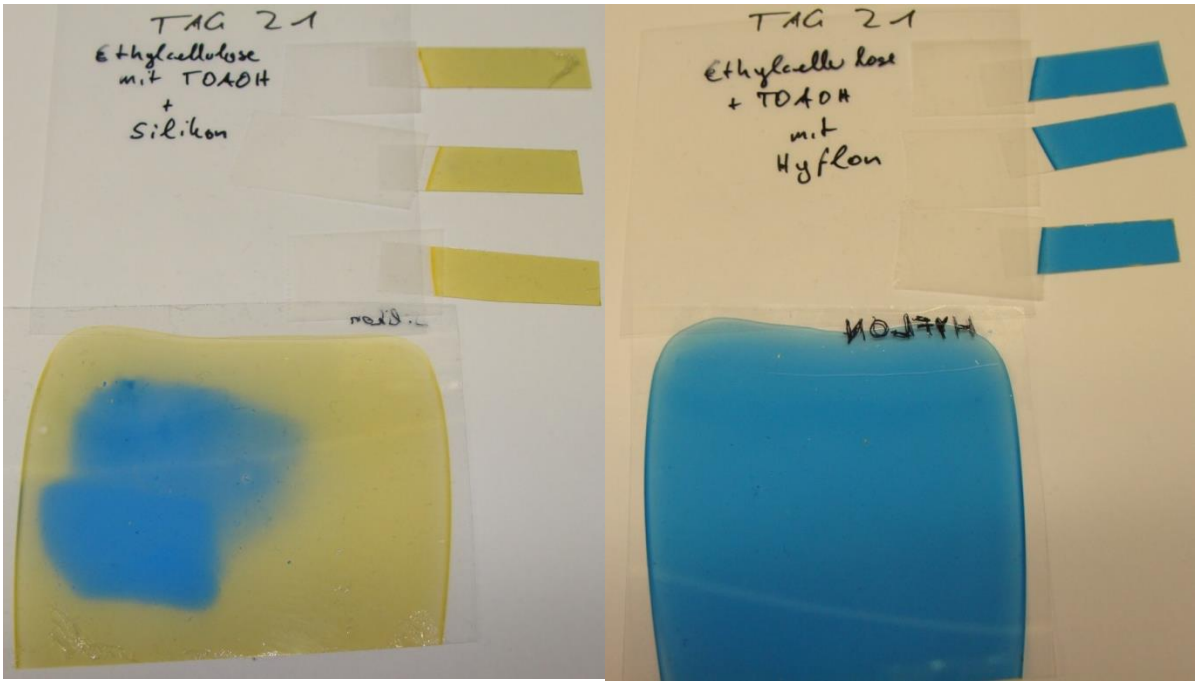

Figure 5.3.8: Comparison of the silicone rubber protected sensor with the Hyflon® AD 60 protected sensor after a three week storage period at room temperature in the office

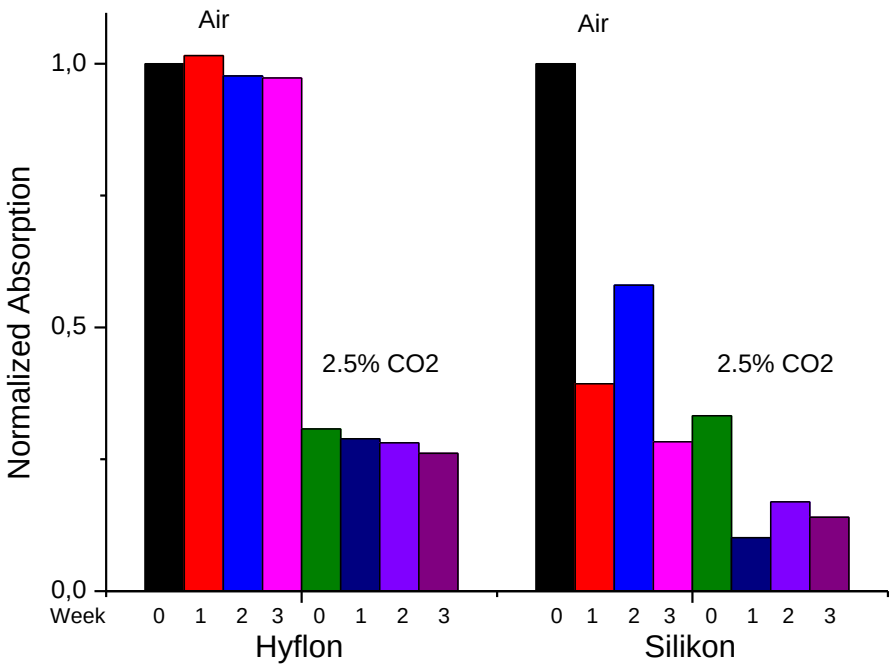

Figure 5.3.9: Comparison of the Hyflon® AD 60 layer and the silicone rubber layer of 3 weeks of storage under office conditions

Another notable advantage of Hyflon® AD 60 is that the layer is almost impossible to peel off of the initial sensor layer while silicone rubber peels off immediately when minor friction is applied. Hyflon® AD 60 also shows a lower affinity to dust as it is completely solid after it dries while silicone rubber always retains a slight sticky quality. This sticky quality results in the sensors attaching themselves to any surface they are stored in, be it a paper bag or a slide tray, as was used in this stability test. This can further compromise the stability of the sensor as parts of the silicone layer get worn off when being detached from the surface they are sticking to, which results in a thinner protective layer and a less smooth sensor surface which can show as noise in the spectra.

5.4. Comparison of response times

As Hyflon® AD 60 proved to be a promising alternative for the silicone rubber layer the response time of a 20 µm ethylcellulose/TOAOH/silicone rubber sensor was compared to a 4.3 µm ethylcellulose/TOAOH/Hyflon® AD 60 sensor. Since the permeability of Hyflon® AD 60 is 15.3 10^{-6} cm^3 (STP)/cm^2 sec cm Hg at 1 bar[45] for CO_2 the sensor with the thinner film showed approximately the same response time as the sensor with the five times thicker silicone rubber layer.

The response time measurement as described in part four of this thesis revealed that Hyflon® AD 60 and silicone rubber show a very similar response time at both 5°C and 25°C. The response time was measured between 1% and 3% CO_2. The change the increasing CO_2 concentration had on the sensor was monitored via the deprotonated maximum at 600 nm. The resulting curve was fitted with the following equation where a, b and c are independent coefficients and A is the measured absorption:

$$A = \frac{a + c * p(CO_2)}{1 + b * p(CO_2)}$$

The response times were calculated with the resulting $p(CO_2)$ values of

$$p(CO_2) = \frac{-A + a}{A * b - c}$$

Tables 5.4.1 and 5.4.2 show the resulting response times for both polymers.

Tab 5.4.1: Response times for Hyflon® AD 60 and silicone rubber protected sensors at 5°C

Protective layer	t_{63} protonated	t_{90} protonated	t_{63} deprotonated	t_{90} deprotonated
Hyflon	29	49	34	67
Silicone rubber	25	40	44	75

Tab 5.4.2: Response times for Hyflon® AD 60 and silicone rubber protected sensors at 25°C

Protective layer	t_{63} protonated	t_{90} protonated	t_{63} deprotonated	t_{90} deprotonated
Hyflon	19	31	25	44
Silicone rubber	16	26	23	40

5.5. Synthesis of 3,6-bis(4-(*tert*-butyl)phenyl)-2- (2,2,3,3,4,4,5,5,6,6,7,7,8,8, 9,9,9-heptadecafluorononyl)-2,5-dihydropyrrolo[3,4-c]pyrrole-1,4-dione

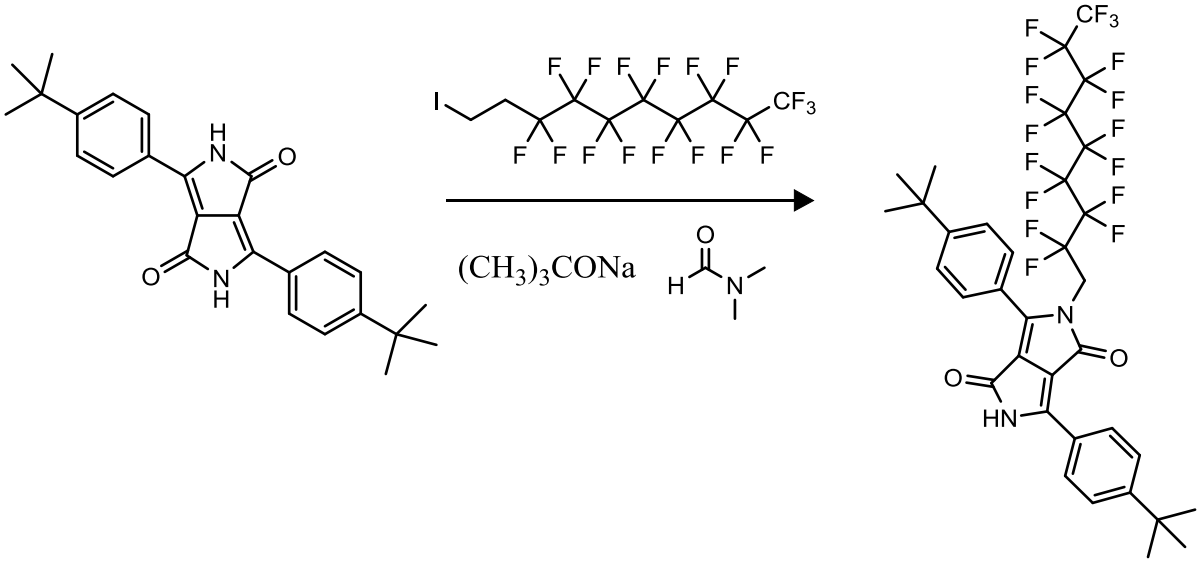

Figure 5.5.1: Reaction scheme for 3,6-bis(4-(*tert*-butyl)phenyl)-2-(2,2,3,3,4,4,5,5,6,6,7,7,8,8,9,9,9-heptadecafluorononyl)-2,5-dihydropyrrolo[3,4-c]pyrrole-1,4-dione

As an interlude the synthesis of the above mentioned dye was attempted. This dye was supposed to be used as part of a CO_2 sensor with a polyfluorinated matrix.

Irgazin Orange (1 g, 2.45 mmol) and sodium *tert*-butoxide (0.48 g, 5 mmol) were dissolved in anhydrous dimethyl formamide (40 mL). 1H, 1H, 2H, 2H- Perfluorodecyliodide (1.72 g, 3 mmol) was added drop wise. After stirring for 16 h at 80 °C the mixture was diluted with deionized water. The dye was extracted with dichloromethane and hydrochloric acid, sodium chloride was added to facilitate the phase separation. The organic phase was collected, dried over anhydrous sodium sulfate and evaporated to dryness under reduced pressure. The crude product was purified via column chromatography on silica gel using dichloromethane/tetrahydrofuran (98:2).

Attempts to produce a functioning sensor with this dye were unsuccessful as the base would crystalize in the matrix during the drying of the sensor layer. In the future attempts will be made to use a polyfluorinated base to counteract this phenomenon.

6 Conclusion and outlook

In this thesis new sensor materials were tested for their temperature dependence and long-term stability. The results show that HydroThane (5%) may present an interesting alternative to the state of the art polymer ethylcellulose, as its temperature dependence is very low, between 25°C and 37°C, and better than ethylcellulose's between the temperatures 5°C and 25°C. HydroThane equals ethylcellulose in response time.

Tetraoctyl ammonium hydroxide is currently used in combination with ethylcellulose as part of the state of the art sensor. Tetrabutyl ammonium hydroxide may increase the long-term stability of the sensor, however at low temperatures the response time of the sensor increases. For both bases a high concentration dramatically increases the sensor's lifetime.
Storage of the sensors in a cool environment also increases their long-term stability.

Multiple protective layers were tested for their application on CO_2 sensors, Hyflon® AD 60 stood out as the most effective polymer by far. Its use on a sensor, that with no protective layer remains functional for less than a week, increased the sensors lifetime to over six weeks at the point at which this chapter is written.

A combination of these results, i.e. a HydroThane sensor with a Hyflon® AD 60 protective layer may prove to be a stable system for long-term CO_2 monitoring for marine research.

While HydroThane shows a better temperature coefficient than ethylcellulose, the temperature change between 5°C and 25°C still produces a notable difference in response for this matrix, therefore further attempts to find a less temperature dependent polymer should be made.

7 References

[1] Mills, A., Lepre, A. & Wild, L. Breath-by-breath measurement of carbon dioxide using a plastic film optical sensor. *Sensors and Actuators B: Chemical* **39,** 419–425 (1997).

[2] Weigl, B. H. *et al.* Optical triple sensor for measuring pH, oxygen and carbon dioxide. *Journal of Biotechnology* **32,** 127–138 (1994).

[3] Harms, P. Kostov, Y. and Rao, G. Bioprocess monitoring, *Biotechnology* 2002, 13:124–127

[4] Von Bültzingslöwen, C. *et al.* Sol-gel based optical carbon dioxide sensor employing dual luminophore referencing for application in food packaging technology. *The Analyst* **127,** 1478–1483 (2002).

[5] Dickson, A.G., Sabine, C.L. and Christian, J.R., (Eds) 2008. Guide to best practices for ocean CO_2 measurements. PICES Special Publications 191 pp.1.

[6] Doney, S. C., Fabry, V. J., Feely, R. A. & Kleypas, J. A. Ocean Acidification: The Other CO_2 Problem. *Annual Review of Marine Science* **1,** 169–192 (2009).

[7] Rost, B., Zondervan, I. & Wolf-Gladrow, D. Sensitivity of phytoplankton to future changes in ocean carbonate chemistry: current knowledge, contradictions and research directions. *Marine Ecology Progress Series* **373,** 227–237 (2008).

[8] Orr, J. C. *et al.* Anthropogenic ocean acidification over the twenty-first century and its impact on calcifying organisms. *Nature* **437,** 681–686 (2005).

[9] Schutting, S., Borisov, S. M. & Klimant, I. Diketo-Pyrrolo-Pyrrole Dyes as New Colorimetric and Fluorescent pH Indicators for Optical Carbon Dioxide Sensors. Analytical Chemistry 85, 3271–3279 (2013).

[10] Mills, A., Chang, Q. & McMurray, N. Equilibrium studies on colorimetric plastic film sensors for carbon dioxide. *Analytical Chemistry* **64,** 1383–1389 (1992).

[11] Apostolidis, A. Combinatorial Approach for Development of Optical Gas Sensors – Concept and Application of High-Throughput Experimentation. Ph.D. Thesis, University of Regensburg, Regensburg, Germany, 2004; http://epub.uni-regensburg.de/10256

[12] Fabry, V. J., Seibel, B. A., Feely, R. A. & Orr, J. C. Impacts of ocean acidification on marine fauna and ecosystem processes. *ICES Journal of Marine Science* **65,** 414–432 (2008).

[13] Segalstad, Tom V. "Carbon cycle modelling and the residence time of natural and anthropogenic atmospheric CO2: on the construction of the" Greenhouse Effect Global Warming" dogma." Global Warming the Continuing Debate. Cambridge, UK. European Science and Environmental Forum. 1998.

[14] Royal Society. 2005. Ocean acidification due to increasing atmospheric carbon dioxide. London: The Royal Society, 223 pp.

[15] Gattuso, J-P., et al. "Effect of calcium carbonate saturation of seawater on coral calcification." *Global and Planetary Change* 18.1 (1998): 37-46.

[16] Bruland KW, Lohan MC. 2004. The control of trace metals in seawater. InThe Oceans and Marine Geochemistry, Treatise on Geochemistry, Vol. 6. ed. H. Elderfield. Elsevier

[17] http://www.oxforddictionaries.com/definition/english/sensor?q=sensor 28.02.14

[18] Göpel, Wolfgang, et al., eds. Sensors, Chemical and Biochemical Sensors. Vol. 2. John Wiley & Sons, 2008.

[19] Mermet, Jean-Michel, Matthias Otto, and Miguel Valcárcel Cases, eds. Analytical Chemistry: A Modern Approach to Analytical Science. 2nd ed. Weinheim ; [Great Britain]: Wiley-VCH, 2004. Print.

[20] Borisov, Sergey M., and Otto S. Wolfbeis. "Optical biosensors." Chemical reviews 108.2 (2008): 423-461.

[21] Wolfbeis, O. S. Materials for fluorescence-based optical chemical sensors. Journal of Materials Chemistry 15, 2657 (2005).

[22] Colette McDonagh, Conor S. Burke, and Brian D. MacCraith. “Optical Chemical Sensors”. In: Chemical Reviews 108.2 (Feb. 1, 2008), pp. 400–422.

[23] Valeur, B. & Berberan-Santos, M. N. Molecular fluorescence. (Wiley-VCH ; John Wiley [distributor], 2013).

[24]http://www.kutztown.edu/acad/chem/chem_images/instrumentation_images/UV_Vis/c50line_text.jpg [07.03.2014]

[25] Luft, Karl Friedrich. "Non-dispersive infrared gas analyzer." U.S. Patent No. 3,968,370. 6 Jul. 1976.

[26] http://www.anton-paar.com/ca-en/products/group/co2-and-oxygen-meter/ [12.04.2014]

[27] Severinghaus, John W., and A. Freeman Bradley. "Electrodes for blood pO2 and pCO2 determination." Journal of applied physiology 13.3 (1958): 515-520.

[28] Hong, W. et al. Full-color CO2 gas sensing by an inverse opal photonic hydrogel. Chemical Communications 49, 8229 (2013).

[29] Su, X., Cunningham, M. F. & Jessop, P. G. Use of a switchable hydrophobic associative polymer to create an aqueous solution of CO2-switchable viscosity. Polymer Chemistry 5, 940 (2014).

[30] Ali, R., Lang, T., Saleh, S. M., Meier, R. J. & Wolfbeis, O. S. Optical Sensing Scheme for Carbon Dioxide Using a Solvatochromic Probe. *Analytical Chemistry* **83,** 2846–2851 (2011).

[31] Liu, Yang, et al. "Fluorescent chemosensor for detection and quantitation of carbon dioxide gas." Journal of the American Chemical Society 132.40 (2010): 13951-13953.

[32] Wolfbeis, O. S., Kovács, B., Goswami, K. & Klainer, S. M. Fiber-optic fluorescence carbon dioxide sensor for environmental monitoring. Mikrochimica Acta 129, 181–188 (1998).

[33] Mills, A. & Monaf, L. Thin plastic film colorimetric sensors for carbon dioxide: effect of plasticizer on response. The Analyst 121, 535 (1996).

[34] Kwon, Tae-Hwan, and Seong Huh. "Bimodal Mesoporous Carbons for CO2 Sorption Application." Bull. Korean Chem. Soc 31.3 (2010): 507-3.

[35] Burke, Conor S., et al. "Development of an optical sensor probe for the detection of dissolved carbon dioxide." Sensors and Actuators B: Chemical 119.1 (2006): 288-294.

[36] Borisov, Sergey M., et al. "Optical carbon dioxide sensors based on silicone-encapsulated room-temperature ionic liquids." *Chemistry of materials* 19.25 (2007): 6187-6194.

[37] Schröder, Claudia R., and Ingo Klimant. "The influence of the lipophilic base in solid state optical pCO2 sensors." *Sensors & Actuators: B. Chemical* 107.2 (2005): 572-579.

[38] Klimant, Ingo, Marco Jean-Pierre Leiner, and James Tusa. "Dry optical-chemical carbon-dioxide sensor." U.S. Patent Application 12/038,583.

[39] Mills, A. & Chang, Q. Tuning colourimteric and fluorimetric gas sensors for carbon dioxide. Analytica Chimica Acta 285, 113–123 (1994).

[40] Wolfbeis, O. S., Weis, L. J., Leiner, M. J. P. & Ziegler, W. E. Fiber-optic fluorosensor for oxygen and carbon dioxide. *Analytical Chemistry* **60,** 2028–2030 (1988).

[41] Borisov, Sergey M., Roman Seifner, and Ingo Klimant. "A novel planar optical sensor for simultaneous monitoring of oxygen, carbon dioxide, pH and temperature." Analytical and bioanalytical chemistry 400.8 (2011): 2463-2474.

[42] Stich, M. I. J., Fischer, L. H. & Wolfbeis, O. S. Multiple fluorescent chemical sensing and imaging. Chemical Society Reviews 39, 3102 (2010).

[43] http://www.advbiomaterials.com/products/hydrophilic/hydromed.html

[44] http://pyro-science.com/submersible-temperature-sensor.html

[45] Arcella, V., Ghielmi, A. & Tommasi, G. High Performance Perfluoropolymer Films and Membranes. Annals of the New York Academy of Sciences 984, 226–244 (2003).

8 Abbreviations

CTAOH	Cetyltrimethylammonium hydroxide (also: Hexadecyltrimethyl ammonium hydroxide)
EC 49	Ethylcellulose with 49% ethoxyl
EtOH	Ethanol
IR	Infrared
NIR	Near infrared
THF	Tetrahydrofuran
TBAOH	Tetrabutylammonium hydroxide
TOAOH	Tetraoctylammonium hydroxide
UV	Ultraviolet

9 Appendix

9.1. List of Chemicals

Chemical	Supplier	Art.-Nr.	CAS-Nr.	Batch-Nr.
Acetone	Brenntag		67-64-1	-
Dichloromethane	VWR		75-09-2	-
Ethanol	Brenntag		64-17-5	-
Hexane				
Tetrahydrofuran	VWR		109-99-9	-
Toluene	VWR		108-88-3	-
Silica Gel				
m-Cresol purple	Sigma Aldrich	857890-1G		
Tetraoctylammoniumhydroxid solution – 20% in Methanol	Sigma Aldrich	87993-50ML		Lot# BCBG9279V
Tetrabutylammoniumhydroxid solution	Sigma Aldrich	178780 50 mL		
Hexadecyltrimethyl ammonium hydroxide solution 25% in methanol	Aldrich Chemistry	52387-50ML		Lot# BCBK6763V
Ethyl cellulose (Ethoxyl content 49%)	Aldrich Chemistry			Batch #: 16998PJ
Hydromed D4	AdvanSource Biomaterials			11-03-0034
Hydromed D7	AdvanSource Biomaterials			
HydroThane 5-93A	CT Biomaterials			Lot# HT 917 SLD
Polydimethylsiloxane, vinyldimethylsiloxyl terminated, viscosity 1000cSt.	ABCR	AB109358	68083-19-2	Lot 1077069
(25-35% Methylhydrosiloxane)-dimethylsiloxane copolymer; viscosity 25-35 cSt	ABCR	AB109380	68037-59-2	Lot 1038911
1,3,5,7-Tetravinyl-1,3,5,7-tetramethylcyclotetrasiloxane 97%	ABCR	AB109175	2554-06-5	Lot 1024448
Platinum-divinyltetramethyldisiloxane complex; 3-3,5% Platinum in vinyl terminated Polydimethylsiloxane	ABCR	AB134321	68478-92-2	Lot 1095009

9.2.1. Silicone layered sensors under laboratory storage conditions

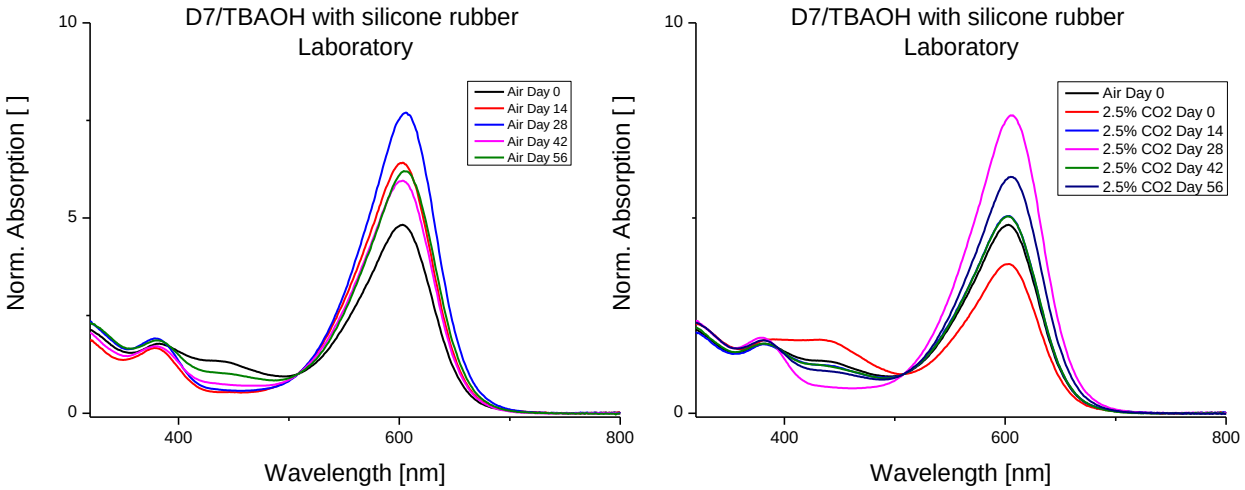

Figure 9.2.1.1: Hydromed D7 in combination with TBAOH kept under laboratory conditions with a protective layer of silicone rubber

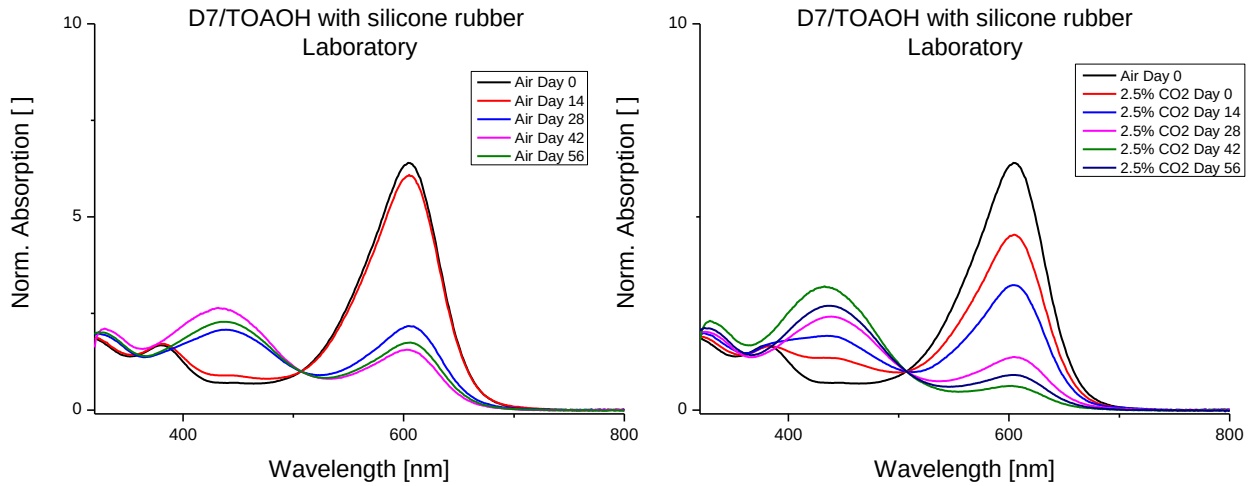

Figure 9.2.1.2: Hydromed D7 in combination with TOAOH kept under laboratory conditions with a protective layer of silicone rubber

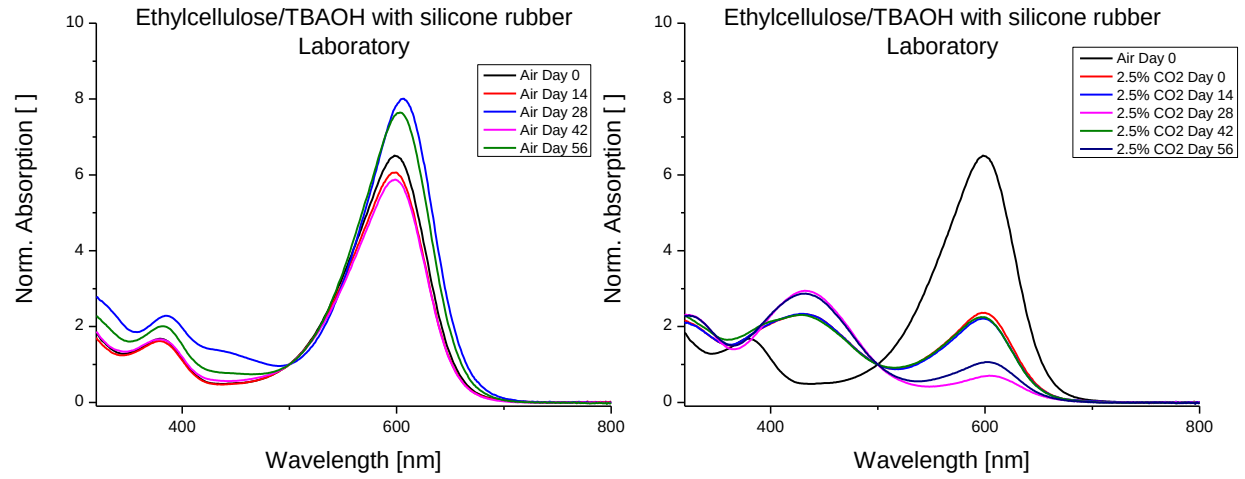

Figure 9.2.1.3: Ethylcellulose in combination with TBAOH kept under laboratory conditions with a protective layer of silicone rubber

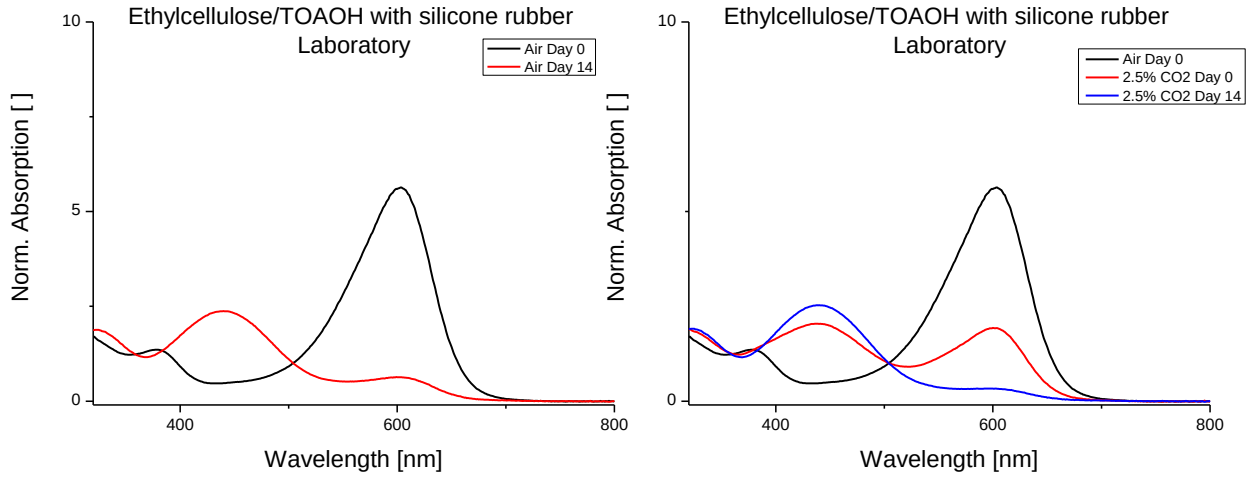

Figure 9.2.1.4: Ethylcellulose in combination with TOAOH kept under laboratory conditions with a protective layer of silicone rubber

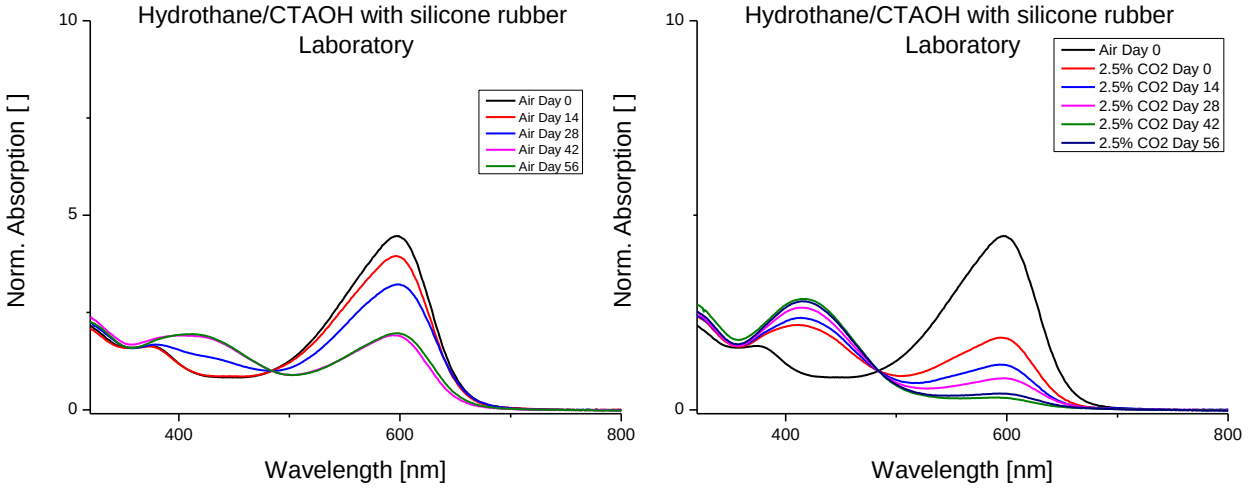

Figure 9.2.1.5: HydroThane in combination with CTAOH kept under laboratory conditions with a protective layer of silicone rubber

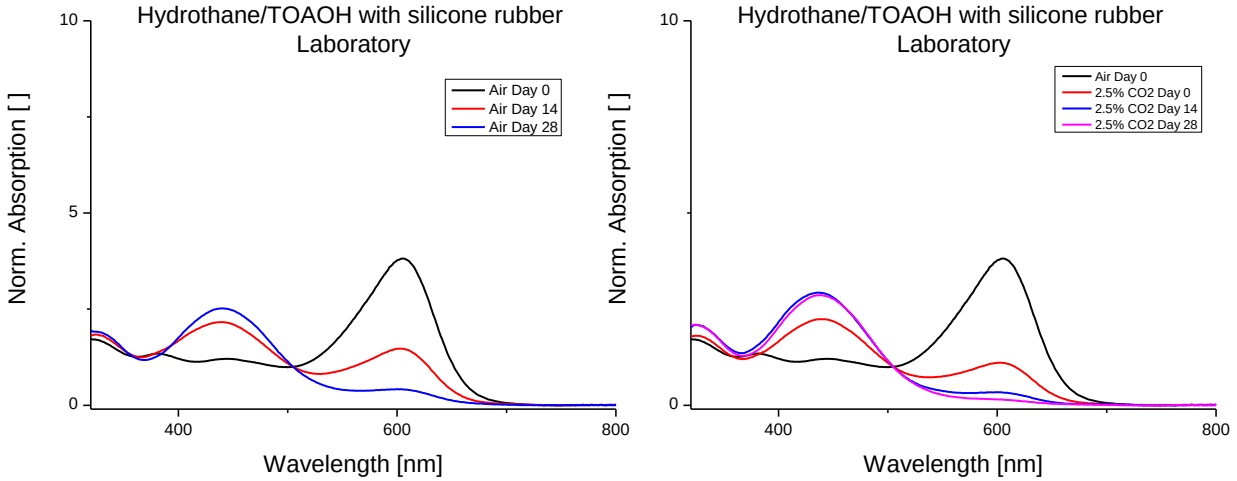

Figure 9.2.1.6: HydroThane in combination with TOAOH kept under laboratory conditions with a protective layer of silicone rubber

9.2.2. Silicone layered sensors under office storage conditions

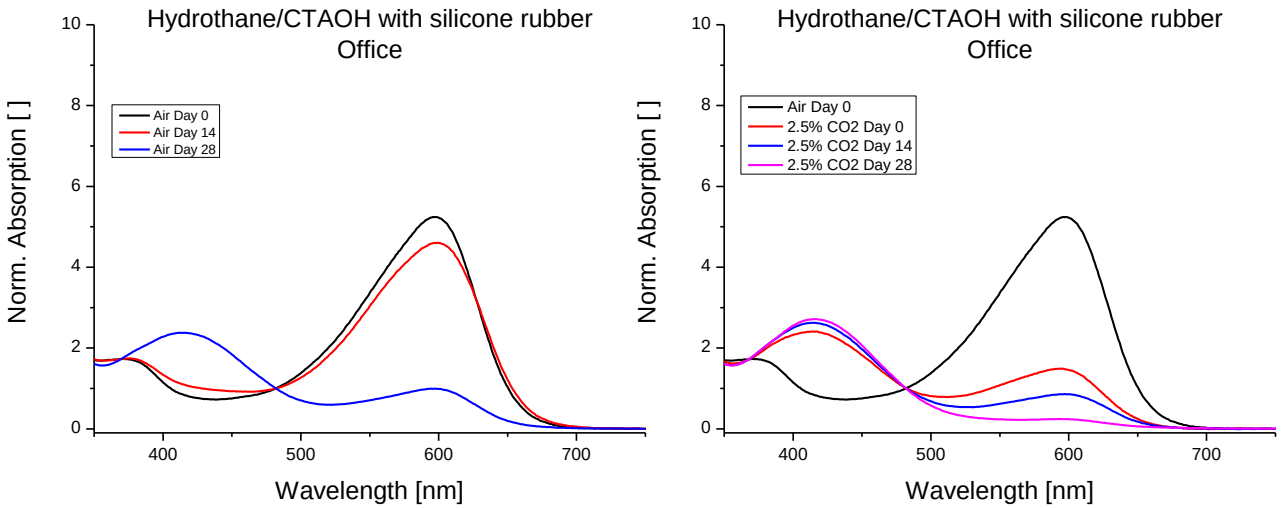

Figure 9.2.2.1: HydroThane in combination with CTAOH kept under office conditions with a protective layer of silicone rubber

9.2.3. Silicone layered sensors under outside storage conditions

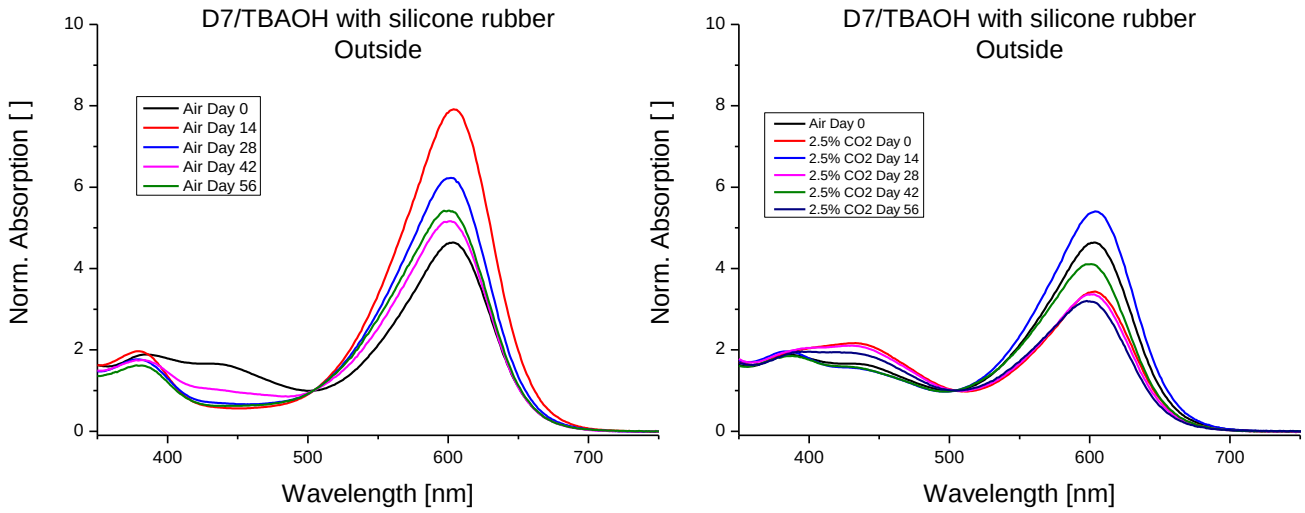

Figure 9.2.3.1: Hydromed D7 in combination with TBAOH kept under outside conditions with a protective layer of silicone rubber

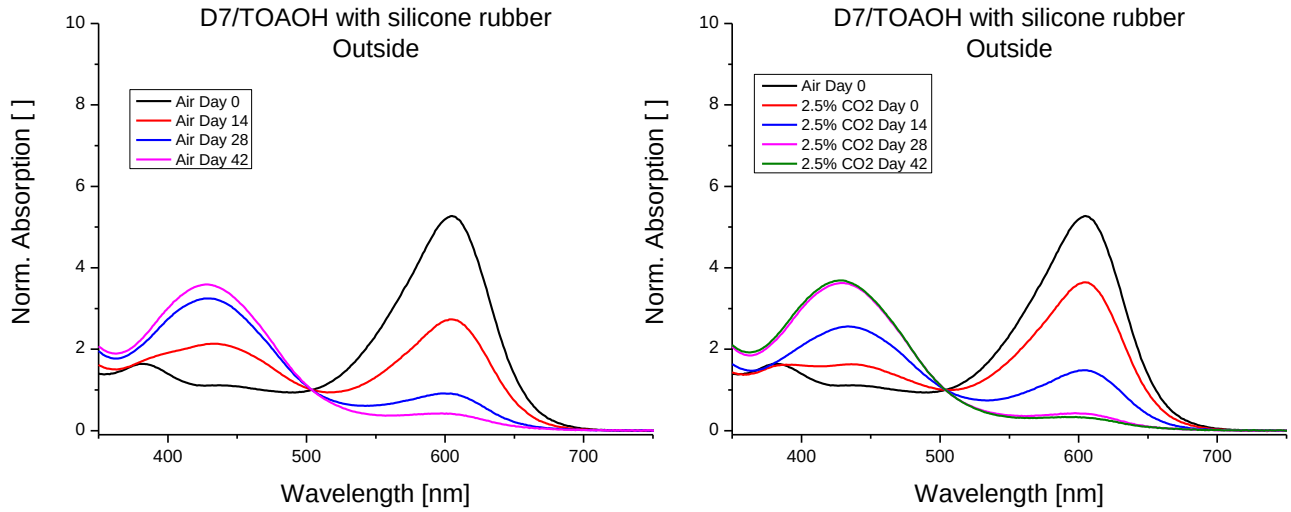

Figure 9.2.3.2: Hydromed D7 in combination with TOAOH kept under outside conditions with a protective layer of silicone rubber

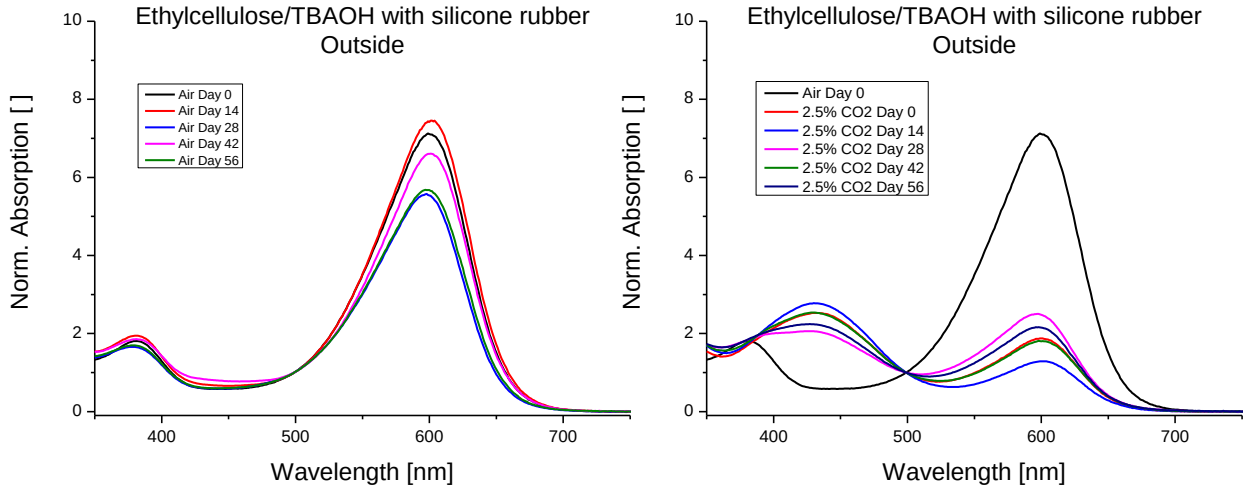

Figure 9.2.3.3: Ethylcellulose in combination with TBAOH kept under outside conditions with a protective layer of silicone rubber

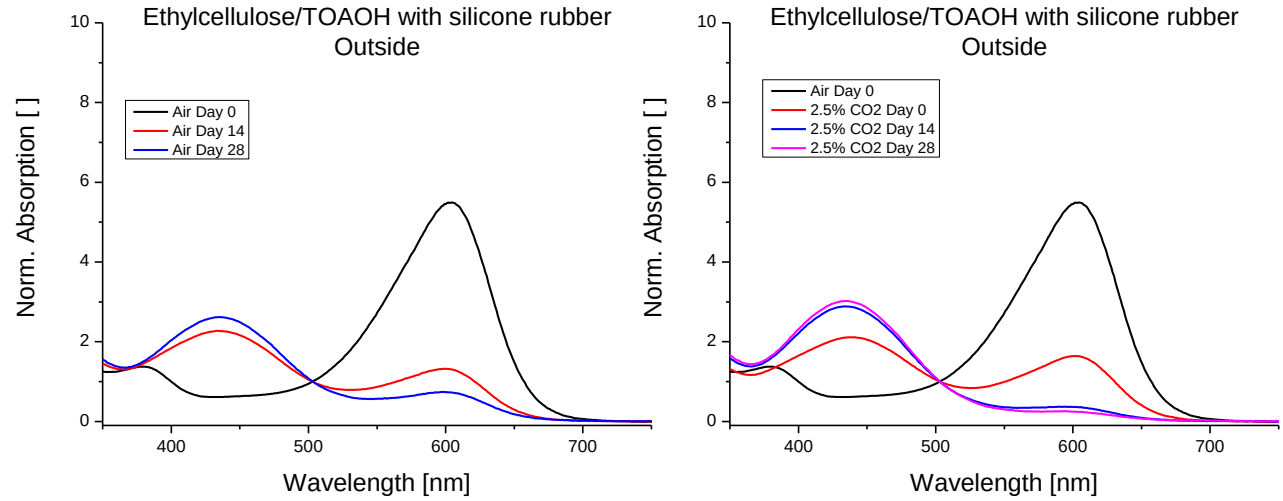

Figure 9.2.3.4: Ethylcellulose in combination with TOAOH kept under outside conditions with a protective layer of silicone rubber

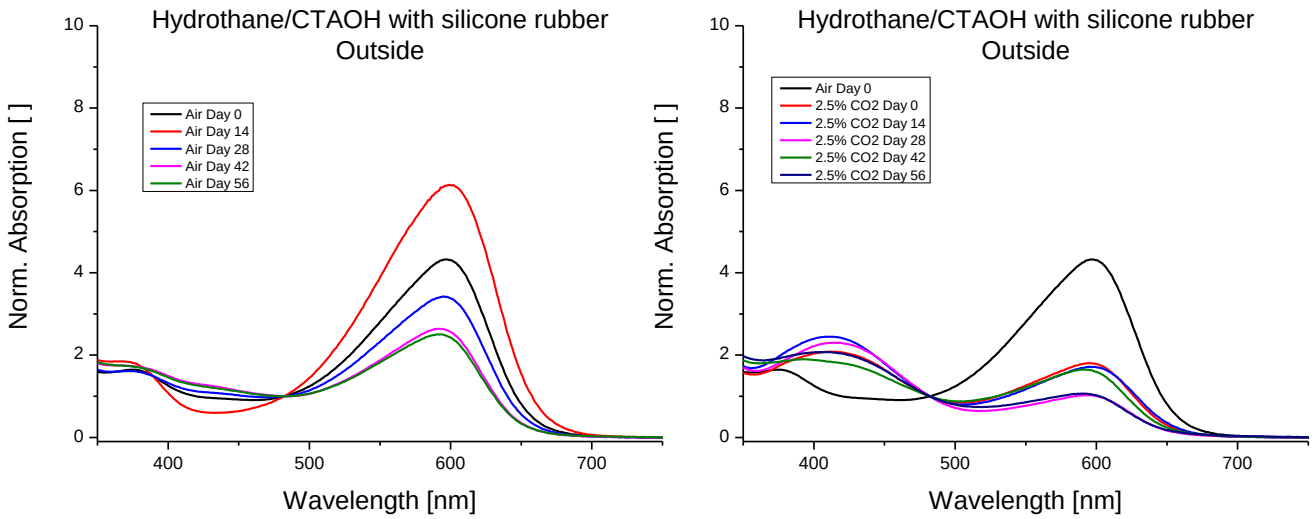

Figure 9.2.3.5: Hydrothane in combination with CTAOH kept under outside conditions with a protective layer of silicone rubber

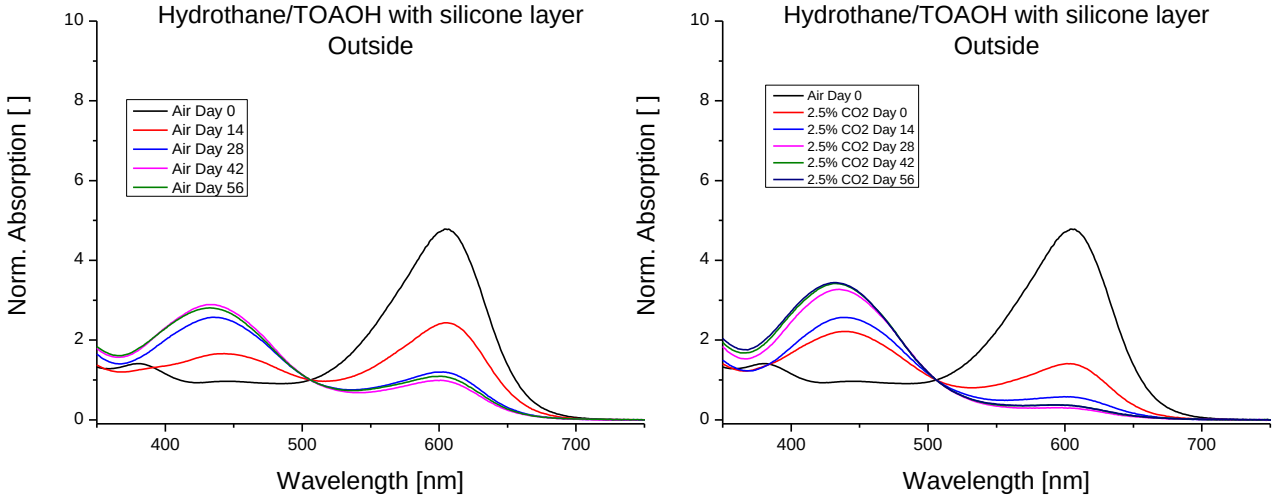

Figure 9.2.3.6: Hydrothane in combination with CTAOH kept under outside conditions with a protective layer of silicone rubber

9.2.4. Ideal storage conditions

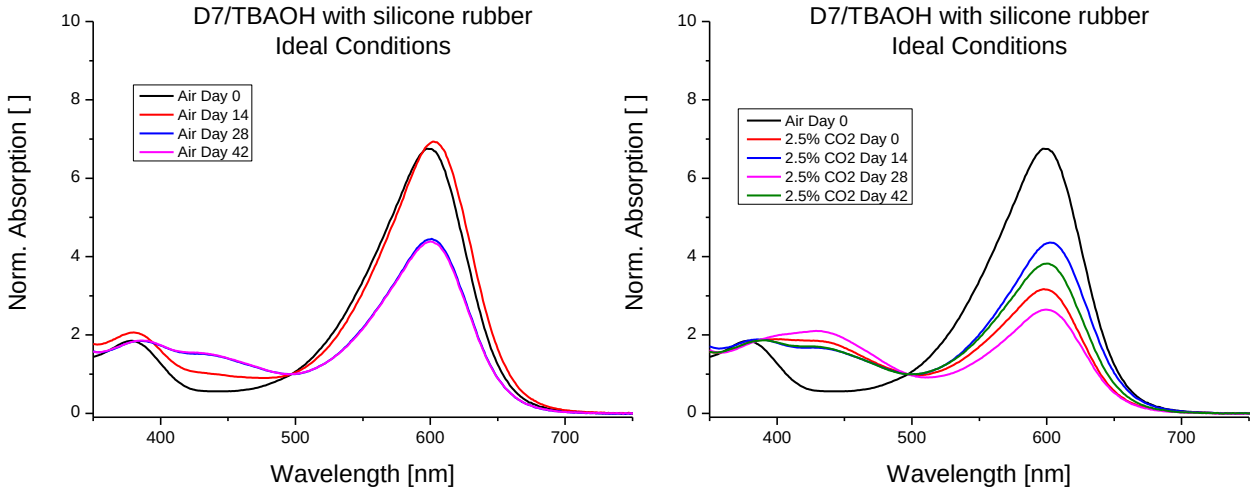

Figure 9.2.4.1: Hydromed D7 in combination with TBAOH kept under ideal conditions with a protective layer of silicone rubber

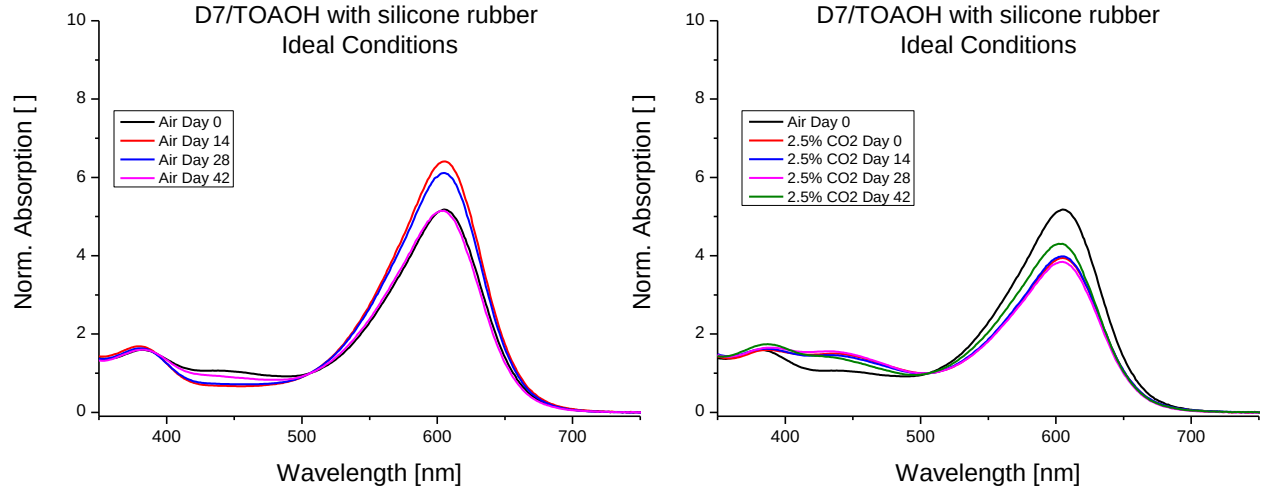

Figure 9.2.4.2: Hydromed D7 in combination with TOAOH kept under ideal conditions with a protective layer of silicone rubber

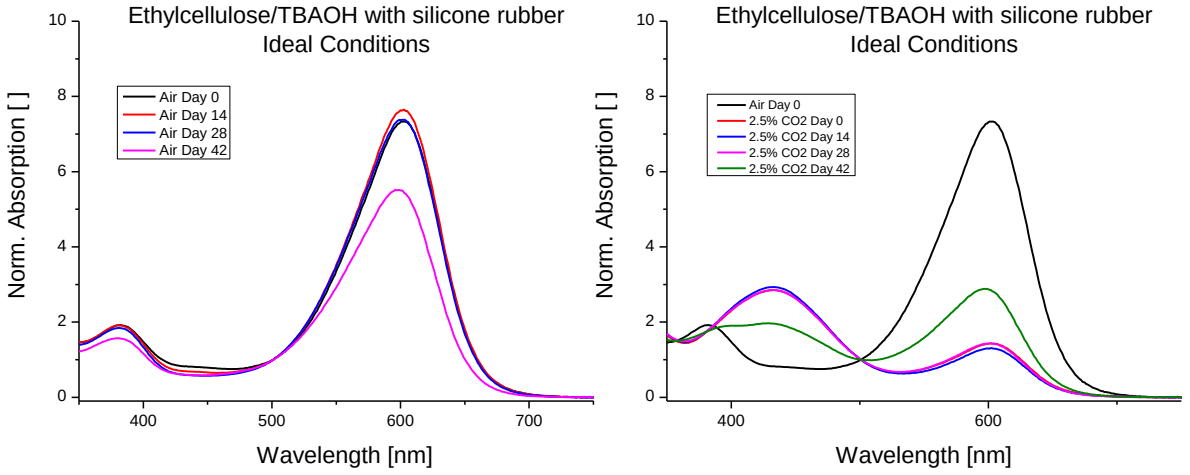

Figure 9.2.4.3: Ethylcellulose in combination with TBAOH kept under ideal conditions with a protective layer of silicone rubber

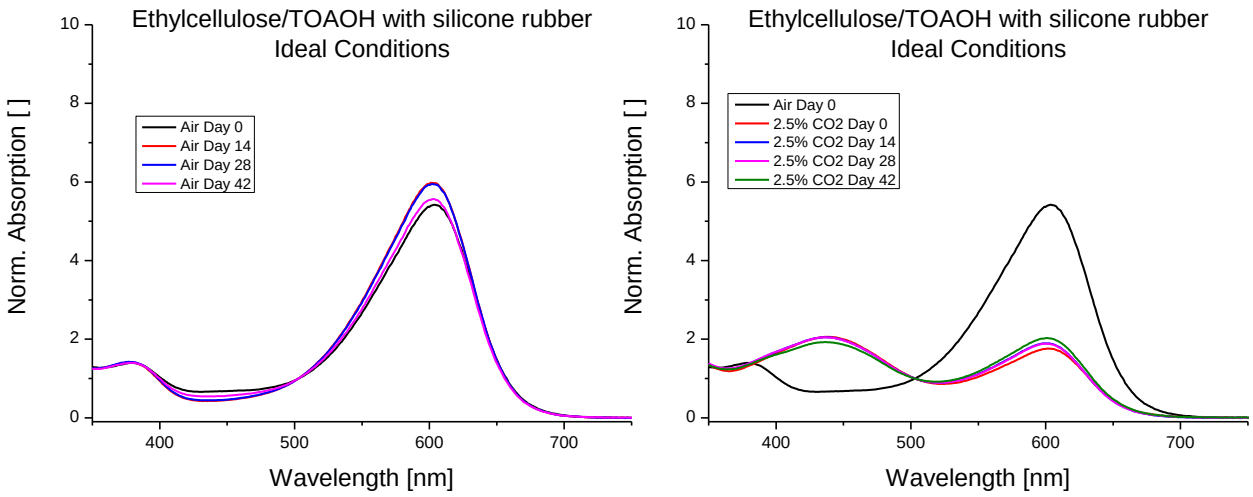

Figure 9.2.4.4: Ethylcellulose in combination with TOAOH kept under ideal conditions with a protective layer of silicone rubber

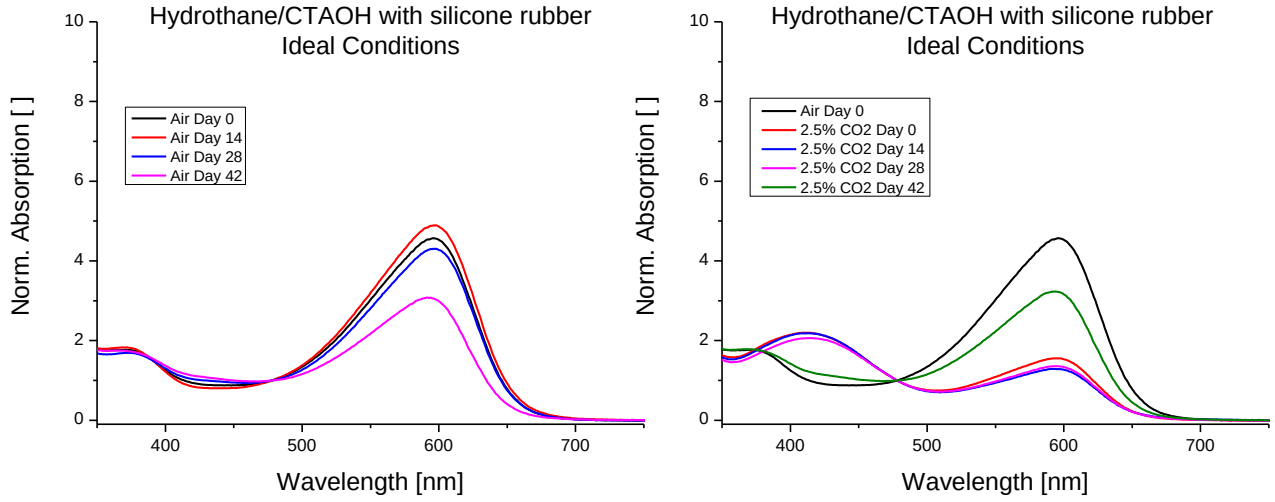

Figure 9.2.4.5: HydroThane in combination with CTAOH kept under ideal conditions with a protective layer of silicone rubber

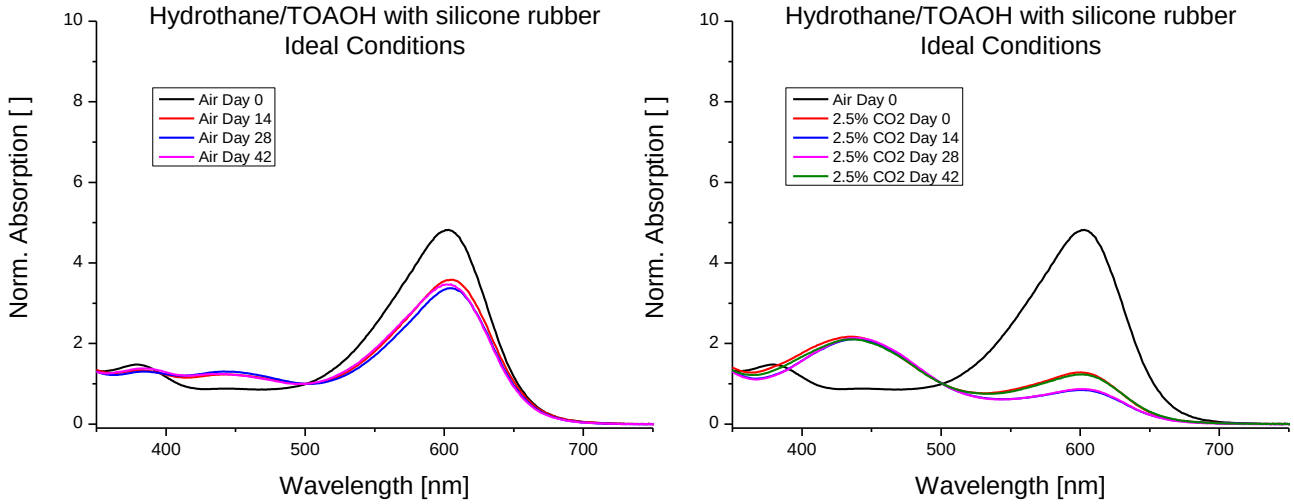

Figure 9.2.4.6: HydroThane in combination with TBAOH kept under ideal conditions with a protective layer of silicone rubber